Lunds universitets naturgeografiska institution

Seminarieuppsatser Nr 28

Kjell B-E Olsson

e a y -i n t i m e a n d s p a c e c a e m i c

based on:

Upward looking sonar,
Satellite images &
a time series of
digital ice charts

Lund 1992

Lunds universitets naturgeografiska institution

Seminarieuppsatser Nr 28

Kjell B-E Olsson

e a y - i n t i m e a n d s p a c e c a e m i c based on:

Upward looking sonar, Satellite images & a time series of digital ice charts

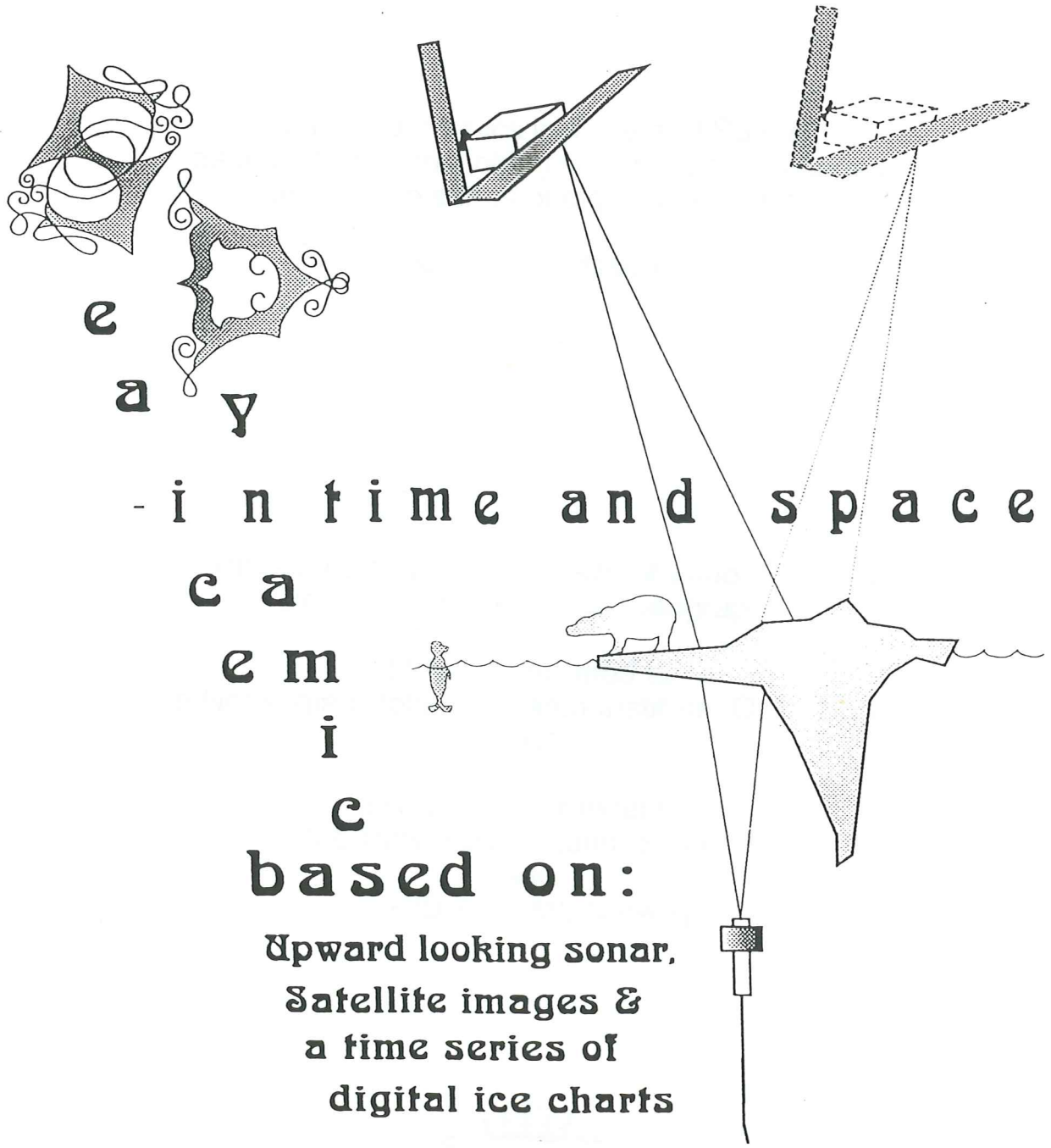

Lund 1992

Sea Ice Dynamics in Time and Space
-based on upward looking sonar, satellite images and a time series of digital ice charts

Kjell B.-E. Olsson

1992

Exams thesis at the University of Lund, Sweden
Department of Physical Geography

Mainly performed at
The Norwegian Polar Research Institute, Oslo, Norway
1991

also to a minor extent at
the University of Lund, Sweden
and
GRID-Arendal, Norway

Dedicated to my cool friend from Kiruna,
who called himself ICE.

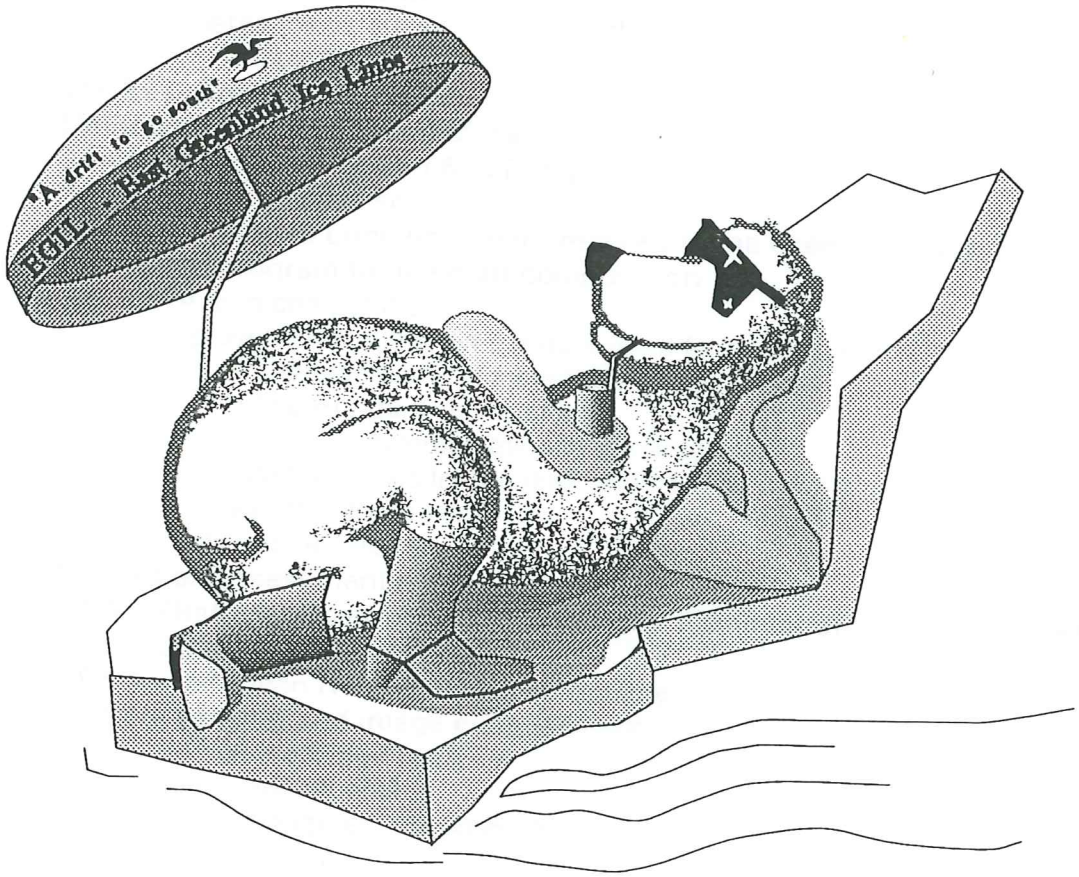

"Perhaps polar bears are white partly in order to keep cool !."
Philip Corbet

Contents

Sea Ice Dynamics in Time and Space
- based on upward looking sonar, satellite images and a time-series of digital ice charts.

Abstract. On a suggestion from the Norwegian Polar Research Institute (NPRI) a moored upward looking sonar (ULS) has been developed by the Christian Michelsen Institute in Bergen, Norway. Ice draft data from this instrument combined with ice drift vector data, normally from a pair of satellite images, can give an estimate of the ice volume transport in a local area.
This report describes the general background, tools and a method for this combination. A computer program for the central task of the method is developed. The program is written in C and tested on an ULS time series from 1987-88 at 75 03.4 degrees N, 12 09.2 degrees W, in the Greenland Sea. The draft data is combined with drift data from NOAA AVHRR images. However, drift vector data can be gathered from many kinds of sources, including ERS-1 SAR data, radar or manual measurements. Different file formats are accepted, for example ARC/INFO. The extracted information can be used in ice modelling, climate monitoring and other purposes.

Zusammenfassung. Auf einen Vorschlag des Norwegischen Polarforschungs Institutes (NPRI) wurde ein stationäres, nach oben gerichtetes Meeressonar (ULS) am Christian Michelsen Institut in Bergen, Norwegen, entwickelt. Von diesem Instrument registierte Eistiefgangdaten können in Kombination mit Eisdriftvektordaten, welche normalerweise aus Satellitenbildpaaren gewonnen werden, eine Abschätsung des transportierten Eisvolumens in einem begrenzten Gebiet erlauben.
Dieser Bericht beschreibt den allgemeinen Hintergrund, die verwendeten Hilfsmittel und eine für die Zusammenstellung verwendete Methode. Ein Computerprogramm wurde für die Hauptaufgabe der Kombinationsmethode entwickelt. Das in C geschriebene Programm wurde anhand einer ULS Zeitserie getestet, welche im Zeitraum 1987-88 bei 75 03.4 Graden N, 12 09.2 Graden W in der Grönlandsee aufgenommen wurde. Diese Messungen wurden mit aus NOAA AVHRR Bildern gewonnenen Eisdriftdaten kombiniert. Derartige Eisdriftvektordaten können jedoch aus einer Vielzahl von Quellen wie zum Beispiel ERS-1 SAR, Radar oder manuellen Messungen abgeleitet werden. Verschiedene Dateiformate, wie z. B. ARC/INFO, werden vom Programm akzeptiert. Die gewonnene Information kann zum Modellieren der Eis, der Klimaüberwachung oder für andere Zwecke benutzt werden.

Sammandrag. Efter ett förslag från Norsk Polarinstitutt (NPRI) utvecklades en ankrad, uppåt-tittande sonar (ULS) av Christian Michelsen Institut i Bergen. Genom att kombinera istjockleksdata från detta instrument med isdriftsdata, vanligtvis från ett par satellitbilder, kan man få en uppskattning av isvolymtransporten, inom ett lokalt område.
Denna rapport beskriver den allmänna bakgrunden, verktyg och en metod för att göra denna kombination. Ett datorprogram har utvecklats för den centrala uppgiften hos metoden. Programmet är skrivet i C och har testats på en tidsserie ULS-data från 1987-88 vid 75 03.4 grader N, 12 09.2 grader V i Grönlandshavet. Tjockleksdata har kombinerats med driftdata från NOAA AVHRR bilder. Driftvektordata kan dock hämtas från många olika källor, inklusive ERS-1 SAR data, radardata eller manuella mätningar. Programmet accepterar olika filformat, t ex ARC/INFO. Den extraherade informationen kan användas inom ismodellering, för klimatövervakning eller för andra syften.

Introduction

Definition

This report is intended as an exams thesis at the University of Lund, Sweden. It is also a report describing ancillary information connected to the computer program described and listed in the technical report (Olsson 1992). The aim has been to be comprehensive, but there is probably some things the reader finds missing.

Objectives

The main project, including this sub-project, is defined as "Long Time Monitoring of Ice Mass Transport (Phase I)" in "ERS-1 application project 3032". The objective of this particular subproject has been to develop a method for the combination of ULS, Upward Looking Sonar, ice draft data with ice drift vector data and to create software to do it. The ice drift vector data should be based on AVHRR (Advanced Very High Resolution Radiometer) or SAR (Synthetic Aperture Radar) data.
It has also been an objective for the author to better understand ice dynamics, particularly in the Greenland Sea, and to arrive at an assessment of the feasibility of the suggested combination. Another personal objective has been to learn C programming.

Structure

The report is divided in three major parts. The first section deals with general characteristics of the ice, with particular emphasis on climatic issues. It touches a theory of selected region ice area sampling. This is however not fully evaluated. The second and third part is devoted to the description of factors involved in the computation of ice draft and ice drift. A general description and overview is followed by a particular description of the developed algorithms. After part three is a suggested method of procedure followed by the discussion for all three major parts. Results are given at the end of each major part.

Performance

The time used is roughly eight weeks for the draft part and two weeks for the drift part. Literature studies have been done continuously. The major part of the project is performed at the Norwegian Polar Research Institute (NPRI) in Oslo. Mainly some computational work, curve plotting and illustration creation has been performed at the Institute of Geography in Lund and at GRID-Arendal.

Hardware and software that has been used

At NPRI mainly Dec work-stations have been used, Decstation 2100 and 3100. A microvax II was used as a server and as host for the image processing system. X-terminal was used sometimes. The ice area computations were made on a Nord 530. In Lund a Macintosh II and a Macintosh classic were used. In Arendal a Sun sparc2 work-station, a PS/2 and a Macintosh powerbook 140 has been used. An HP scanner and some plotters have also been used.

ANSI C under ULTRIX was used for the programming. IIS/IVAS system 600 and BIFF Xshow were used for image processing. Excel, Statview and Lotus-123 for

windows was used for database management and curve plotting on screen. Mainly CorelDraw, Designer and Statview were used for the illustrations. Internally developed software in Fortran was used for ice area extraction and computations. OmniPage has been used for scanner management and text recognition.

Background

The polar sea ice cover has a fundamental influence on the global climate and on the global hydrological system. Its hemispherical and regional influences are even greater. The ice has a noticeable impact on the increasing human activities in the polar regions, making it therefore of interest to monitor, and also forecast, the sea ice extent, movements and general dynamics in time and space.

Previous to the aerial era of Man, the sea ice was monitored from ships on northern routes and from land-based weather stations. With the evolution of aerial photo and satellite image technology new means for ice monitoring over remote and vast areas emerged. In good weather the ice extent and ice conditions can be surveyed.

The major part of the Arctic ice leaves the Arctic Basin via the transpolar current, TC, through the Fram Strait and via the East Greenland Current, EGC. By monitoring the amount of ice transported by the EGC it is possible to get an indicator of the ice conditions in the Arctic, with some time lag. Ice transport can also be used as a more general climatic indicator. The ice transport by TC, takes about four years from the Siberian coast to the Greenland Sea (von Wiese 1922), rendering a good indicator of the climatic conditions in the Arctic Ocean over a period of some years. Earlier, mainly area ice transport, or extension, has been utilized. Several authors, however, point out the importance of volumetric measurements, for example Moritz (1988).

Using repeated satellite coverages with some time lapse, ice displacement can be extracted. Ice drift can be obtained as drift vectors manually, semi-automatically or automatically. These techniques have been utilized by several researchers, using different kinds of images. Computations of the area ice transport have been performed for various time intervals and locations. Assessments of transported ice volume, based on these values, have also been reported (Vinje & Finnekåsa 1986).

Combination of horizontal ice drift with vertical ice draft gives ice volume transport. It is necessary to know the draft of the ice and preferably also the spatial distribution of the draft. This information combined with drift data gives a measure of transported ice volume for a given time interval, normally the period between two images. Draft measurements have thus far been rather sparse and not always readily available. Profiles of the ice bottom topography have been recorded with ULS, on submarines. Local soundings of the ice bottom topography have been performed using a rotated scanning ULS lowered through a hole in the ice (Johnsen 1989).

By combining continuous ULS measurements with ice drift data, one obtains a sequential record of the ice volume transport. This can be of interest in many places, but particularly in the Greenland Sea. NPRI suggested the use of ULS attached to the top of moorings in deep water. The first operational ULS-buoy constructed according to this principle was developed by the Christian Michelsen Institute in Bergen, Norway. A successful deployment was made in 1987-88 in the Greenland sea at 75 03.4 degrees N, 12 09.2 degrees W (Vinje 1989). It was

attached on top of a current meter mooring of the Alfred Wegener Institute for Polar and Marine Research, Bremerhaven, Germany.

Ice and climate

General climatic impact of sea ice

The polar sea ice covers are important factors in the Earths climate (Lamb & Mörth 1978). The regional influence on the hemispheres is, however, somewhat different depending on the physical conditions, giving different types of ice. In Antarctica merely about 15 % of the ice is more than one year old and it is generally smoother and thinner (Kverndal et. al.1990). The enclosure of the Arctic Sea causes more ridging and less storm erosion.

The albedo of the sea ice cover is much higher than for the open sea (Bergdahl 1977) (Hall & Martinec 1985). This results in higher reflection over the ice, (a phenomenon utilized for example by some dark Arctic organisms (Corbet 1972)). The albedo varies with ice growth, ice density and viewing direction (Stringer 1984) (Massom 1991). Ice thickness influence albedo (Thorndike 1980) Reflexion decreases with increased wavelength (Massom 1991). As the difference in albedo is so great, it is often important to consider the fraction of water within the ice covered area, for example in modelling (Thorndike 1980) (Hall & Martinec 1985) (Häkkinen 1990). The effect has been studied for example by LeDrew (Ellsworth LeDrew, UoW, pers. comm.) Most winter ice formation occurs within several relatively small polynyas. Gloersen & Cambell (1990) have found a significant decline in the area of open water within the ice cover over some years.

The ice acts as an insulator between the water and the atmosphere, decrease sea surface heating and influences the radiation balance. Heat loss from open water is 100 times higher than it is from ice (Hall & Martinec 1985). More information on thermal interaction of ice can be gathered for example from (Bergdahl 1977). Lateral and vertical heat and momentum exchange of a deep water ice edge was studied during the MIZEX (Marginal Ice Zone EXperiment) project (Hall & Martinec 1985). The insulation decreases ice underside melting, according to Aagard & Coachman (1968). The ice melt in the central Arctic occurs mainly through top ablation (Häkkinen 1990) The various temperatures over ice areas and water areas creates regional wind and cloud patterns (Lamb & Mörth 1978) (Stewart 1985) (GSP-group 1990).

Freezing of ice releases heat and melting consumes energy. This has a local moderating effect. The ice transport in the north Atlantic influences the energy distribution of the region. The creation of deep sea water when the ice freezes in the Greenland sea is important for the climate. Less deep water production would lead to a more unstable climate (Kverndahl et. al. 1990). The creation of deep sea water in the Greenland sea is also supposed to be a major CO_2 sink.

Helland-Hansen & Nansen (1909) describes the freezing/melting balance. When ice freezes brine is released. One year old ice has just about half the brine content of new-frozen ice and multi year ice has down to a tenth of the brine content of new-frozen ice. Brine release makes the ice sub-surface water heavier. It sinks. The vertical movement normally makes warmer water rise. This neutralizes the freezing more or less and the process slows down or reverses. Aagard & Coachman (1968) has followed vertical movement of denser water in the Greenland Sea.

Ice as an indicator of the climate

The Polar ice caps and their variation has been of scientific interest for many years. Examples of early ventures are the Fram drift in 1893-96, Fig. 23, (Nansen 1897) and the following wellknown investigation of the Norwegian Sea (Helland-Hansen & Nansen 1909). Assessments of the ice volume has been given by several research teams and the general issue is if the ice is decreasing or not, as a response to global change. Walsh (1991) illuminates the basics of this question. Quadfasel (1991) measured ice thicknesses in 1990 20-30 % below the long-time mean and the warmest Arctic deep water temperature recorded, +2.8 C. 1990 was a year of extremely small ice extension, for example around Svalbard. It was the warmest year in the 140 year record of comparable measurements, according to (GECR 1992).

Gloersen & Cambell (1991) have studied time-series from both polar areas, from SMMR data.The series cover 8.8 years, 1978-87. They found a 2.1 % decline of the Arctic ice extent, with a 96 % confidence level significance. No significant trend was found for Antarctica. Vinje (1992) also found a decline when analysing a 24 year time-series over the Nordic Seas. He also studied the trends in minimum and maximum ice extension. This can be used to indicate differences in the annual melt-off, fig. 1.

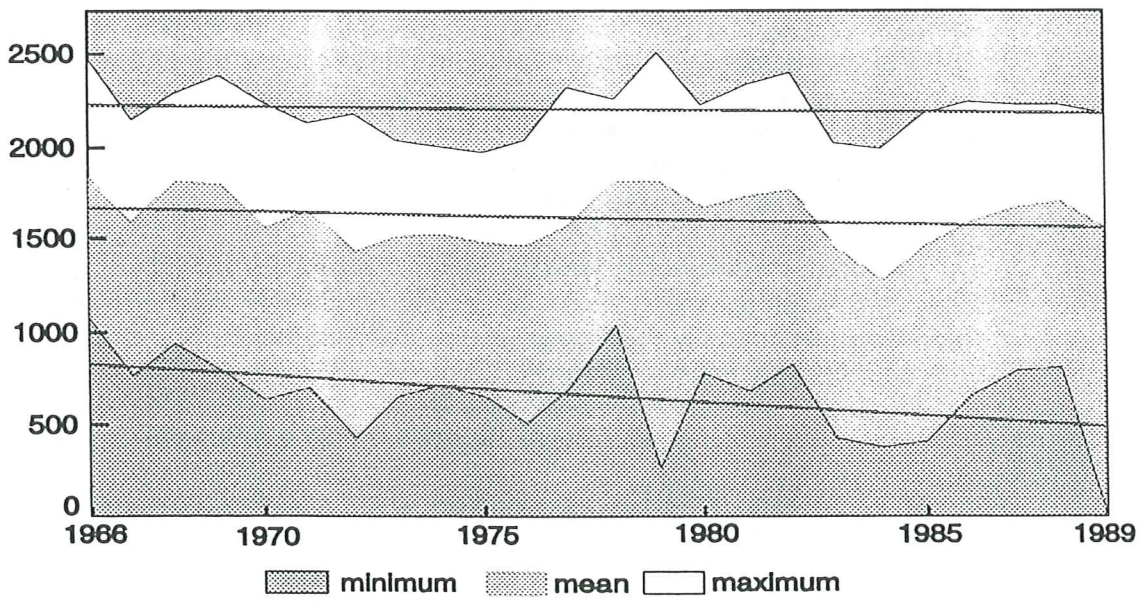

Fig. 1. Maximum, minimum and mean ice extension in the Barents Sea. [1000 km^2]

Arctic ice modelling has been done by several scientists, for example Parkinson & Washington (1979). Häkkinen (1990) gives a good overview. Larsen & Lu (1986), Moritz (1988) and the GSP-group (1990) have modelled the ice in the East Greenland Current area. Effects on the ice of increased atmospheric CO_2 has been modelled. A sudden rise of CO_2 will not influence the sea ice extent (> 0.5 m draft) much, according to Washington & Meehl (1989), referenced in (Kverndal et. al. 1990). A continuous increase of 1 % CO_2 / year will increase the ice extent.

The ice conditions in the north Atlantic influence the climate of northern Europe (von Wiese 1922). The amount of ice affects the hemispherical heat balance and hence the dominating air flow pattern. Persistent ice cover can support static waves in the atmospheric polar front leading to temperature anomalies (Lamb & Mörth 1978) Ahlmann (1970) states that the position and azimuth of the ice edge is influential on the cyclone routes of the Nordic Sea. It is confirmed by LeDrew (Ellsworth LeDrew, UoW, pers. comm), who has studied the cyclone routes also over the Arctic. Similar theories are present concerning the influence of the Antarctic ice on the El Nino phenomenon, on the southern hemisphere. El Nino also influences the Antarctic sea ice (Walsh 1991). The amount of drifting ice determines the influence of the ice at lower latitudes (Ahlmann et. al. 1970) (Bergth'orsson 1970). Bergth'orsson (1972) states that the temperatures at Iceland is strongly correlated to the amount of drift ice. He has also studied the advection of climate by ocean currents.

Sea ice volume is determined directly by radiation balance, ice drift and the sea- and atmosphere temperatures (Bergdahl 1977) (Kverndal et. al. 1990).
Currents and general weather are important factors in the process of creating the ice conditions. Changes in regional ice area have various causes in different seasons (Moritz 1988). Thermodynamic growth dominates in the winter, melt in the summer and advection in the autumn and in the spring.

The ice can act as an indicator of climate fluctuations (Häkkinen 1990). That is one reason the researchers try to model and predict the behaviour of the ice cover. Ice extent is used as a climate indicator for example in State-of-the-Environment-Norway, compiled by GRID-Arendal, in cooperation with NPRI and others. It is also discussed for example by Vinje (1992). The ice reflects the predominant conditions over some time(von Wiese 1922) (Torgny Vinje, NPRI, pers.comm).The ice extent has declined lately and the atmospheric temperatures has grown warmer since about 1970, or been stable, at the Arctic meteorological stations (Hansen-Bauer 1991). Comparison of the two latest normal periods show differing results. Running 30 year mean however indicates that the normal periods, particularly 1931-60, was not so "normal" (Førland & Nordli 1991). There is a tendency that the ice extent follow the solar activity (even if several other causes are superimposed), fig. 2. Supposed climatic effects of solar activity was one reason for the choice of the 30 year mean (Førland & Nordli 1991).

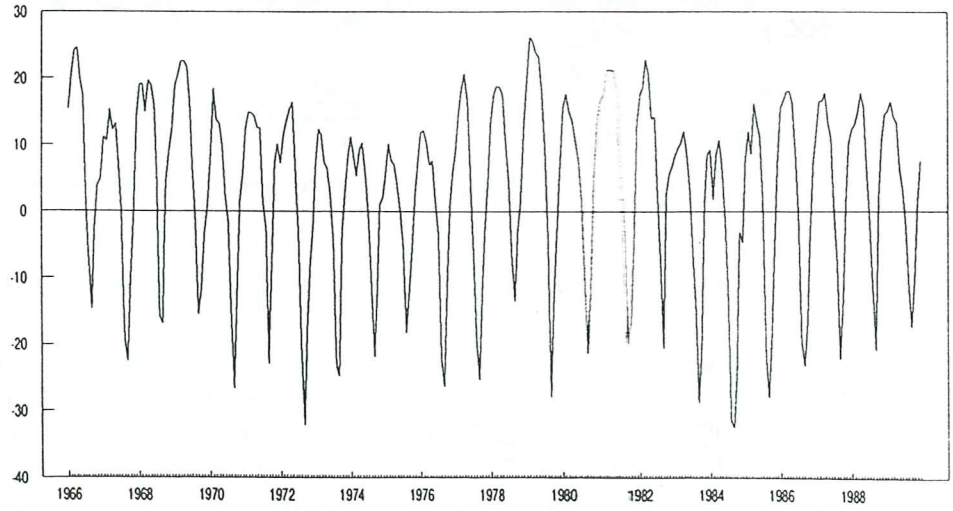

Fig. 2. Weekly ice extent deviation from 24 year average, percent, Barents Sea. A tendency of a period of about ten years can be seen, possibly correlated with the solar activity.

Time series of ice extension

Time-series of ice extension exist in several countries, for example Germany, Denmark and Norway. NPRI has got a continuous digital time series from 1966 to the near present, with weekly resolution. It covers the Greenland Sea, the Barents Sea and parts of the Norwegian and Icelandic Seas, 50 - 85 degrees N, 30 degrees W-80 degrees E. The ground (sea) resolution varies from 2.7 km^2 to 19.9 km^2 per pixel, tab.1. Each pixel is 1/10 of longitude times 1/40 of latitude. The ice is divided into eleven classes, from no ice to very closed pack ice, tab. 2. Each ice chart is controlled against most other available sources, tab. 2.

	At latitude:	Span	Resolution[deg]	Side-length[km]	Area
Latitude-direction,N-S:	All	35 deg.	0.025 = 1/40	2.78	¤lon.=
Longitude-direction, E-W:	85	110 deg.	0.10 = 1/10	0.97	2.7
	80		0.10 = 1/10	1.93	5.4
	70		0.10 = 1/10	3.80	10.6
	60		0.10 = 1/10	5.56	15.5
	50		0.10 = 1/10	7.15	19.9

Tab. 1 : Digital ice data base pixel resolution. After (Vinje 1988).

	Ice classes	Sources
0	No ice at all	Satellite image, NOAA from 1976
1	Fast ice	American ice maps, from 1972
2	Very closed pack ice	British ice maps
3	Closed pack ice	German ice maps (not used in practice)
4	Open pack ice	Aircraft observation, visual
5	Very open pack ice	Aircraft observation, radar
6	Young ice	Ship observation
7	Grease ice	Shore station observation
8	Grease ice and old ice	If source is uncertain:
9	Diverging grease ice	Observation unspecified
10	Open water (some ice floes)	Uncertain ice border
		Assumed ice border
18-40	Sea surface temperature,-2 - 20 C	

Tab. 2 : Characteristics of the digital ice data base at NPRI. After (Vinje 1988).

Software to extract different parameters is developed at NPRI, for example probability, ice extremes, number of days with a certain ice type, the area of some ice type etc. Some kinds of aggregated time-series can be created. The software was originally developed on Nord computers and it is still primarily running on them. Some of the software and all ice data files are converted to UNIX/workstation environment. The database is divided in one western and one eastern part. Digitizing of older hardcopy ice charts is being done to complement the series back to the first part of the eight-teenth century. All existing ice charts are also controlled considering data storage correctness. For example are possible drop-outs filled. The early ice charts are however of lower quality, due to less precise satellite sensors (Ånund Kvambekk, NPRI, pers. comm.) The classical series of monthly ice probability maps published by vinje (1981) is based on the time series and the programs at NPRI, fig. 3.

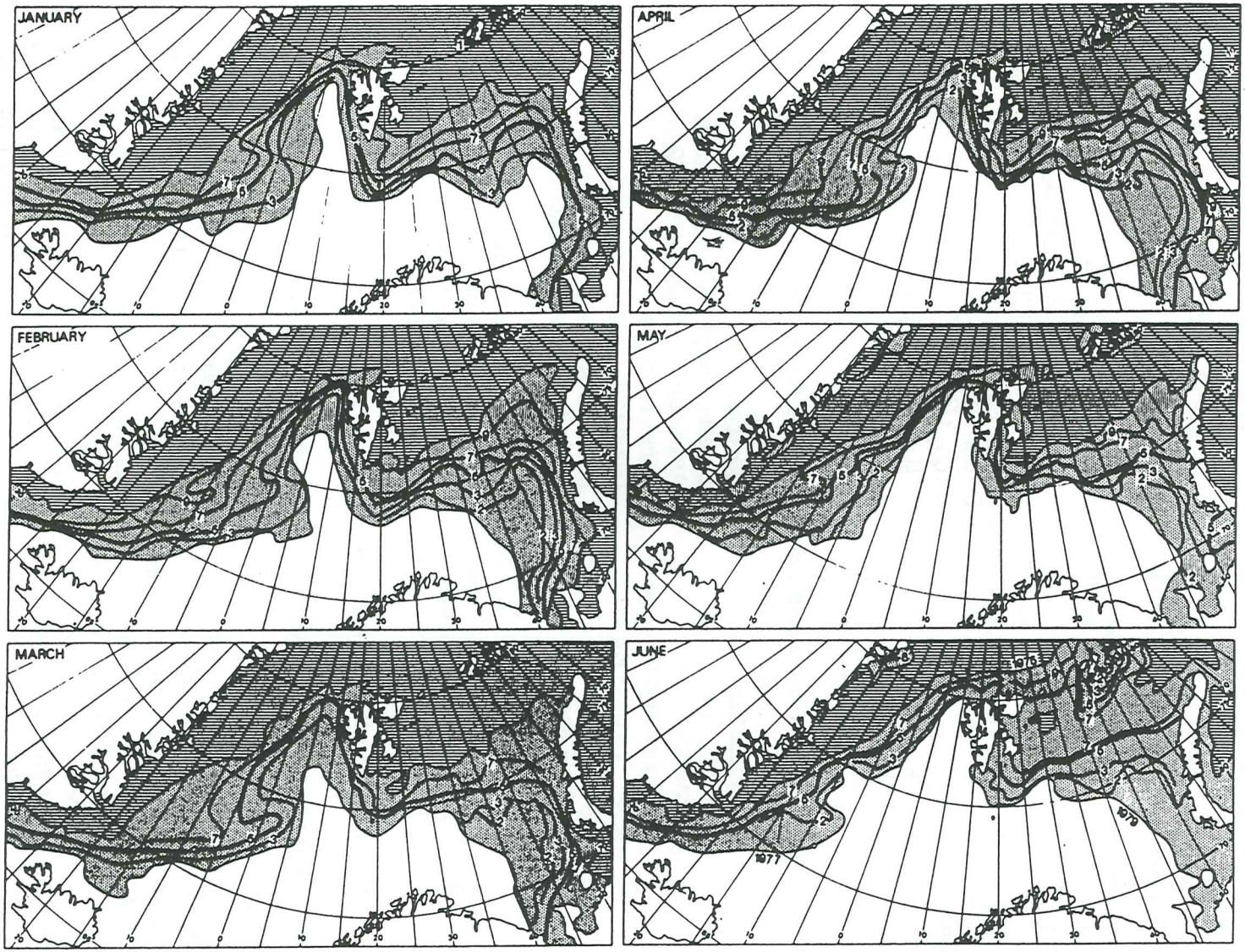

Fig. 3. The more or less classical ice frequency charts from (Vinje 1981). Frequency distribution of sea ice concentrations above 4/10 at the end of each month.

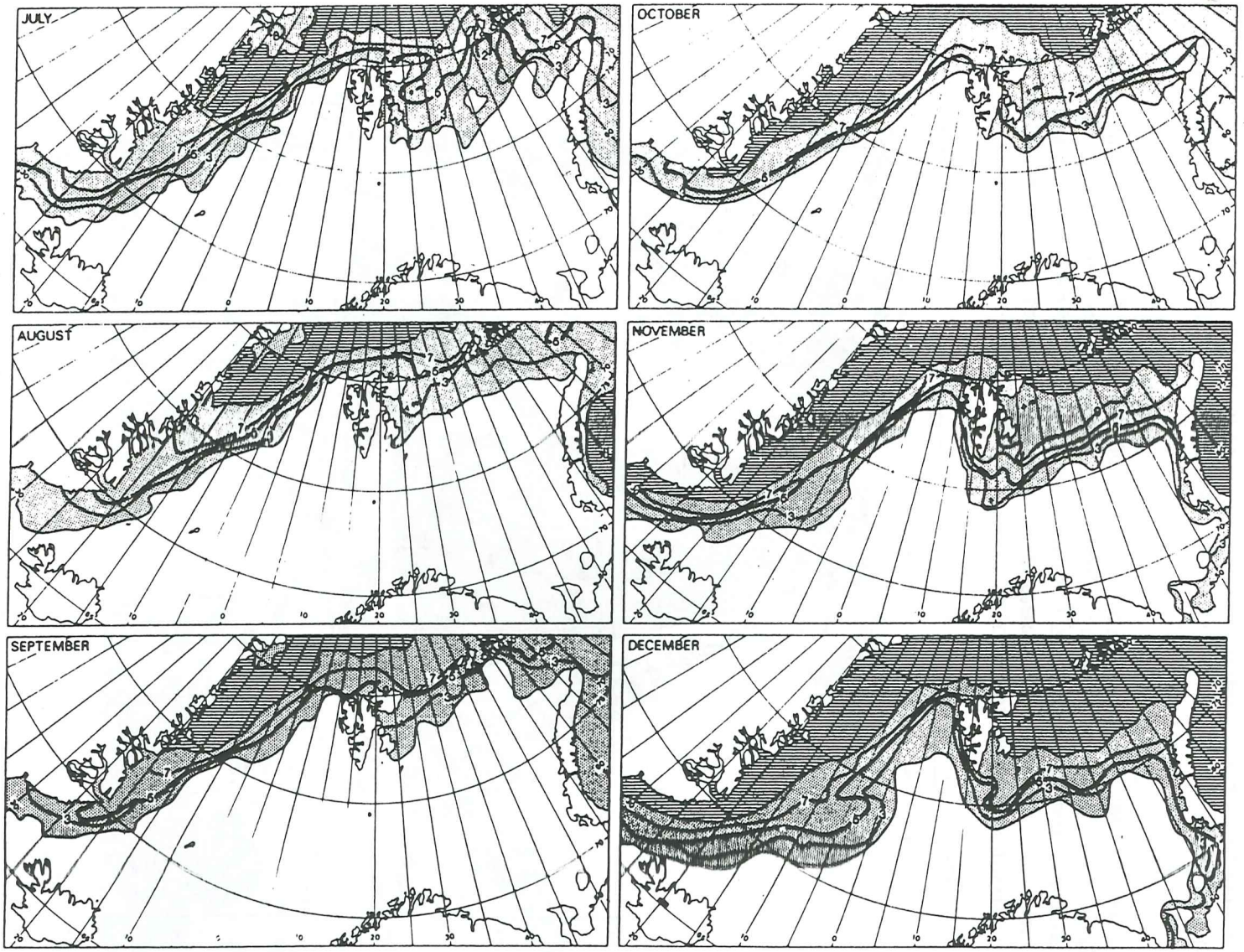

Fig. 3. The more or less classical ice frequency charts from (Vinje 1981). Frequency distribution of sea ice concentrations above 4/10 at the end of each month.

Subarea ice extent sampling hypothesis

A hypothesis is that by using a simple procedure and a simple parameter, ice can be used as a climatic indicator. Ice area trends or deviation from the normal ice condition are used on ocean-wide basis for example by Vinje (1992) and Campbell & Gloersen (1991). By studying the ice conditions in selected subareas over time this may be as possible and maybe even more informative on a regional level. The shape of the subareas should be simple, for example rectangular. Subareas may be used separately or in combination.

To examine this theory nine subareas was delineated in the north Atlantic/Barents Sea, fig. 4. The choice of the subareas is based on investigations of mean ice conditions and ice probability. One important general criteria in the selection has been that there should be a weather station near the area. Land is intended to be sparse within the subareas.

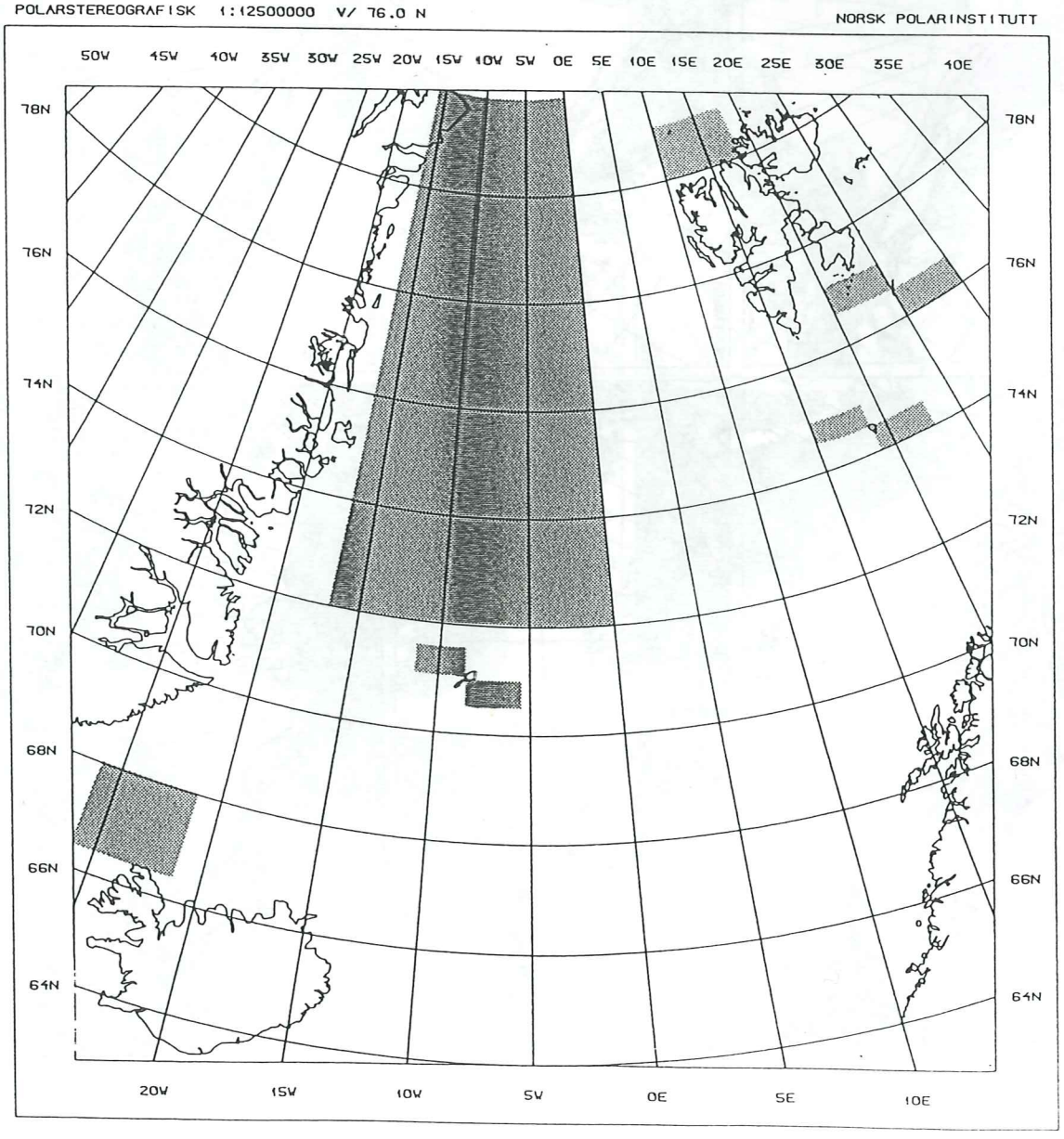

Fig. 4. The test areas selected for the subarea ice extent sampling.

The subareas are somewhat different, i. e. they represent two categories. Six areas are coupled in pairs, located at the major Norwegian Arctic Islands, Jan Mayen, Bear Island and Hope Island. In all three regions surface current branches dominated by Atlantic and Polar water, respectively, meet. They are also close to the polar front, fig. 5.
The remaining three subareas cover more extensive sea areas. The ice conditions in these areas, particularly the Greenland sea and north of Iceland, are supposed to influence Scandinavian weather and climate, mentioned in (Vibe 1978), for example

For each subarea the weekly ice data has been aggregated to monthly mean values. The classes have been combined to represent dense, closed ice, thin, open ice and no ice. This is in good agreement with classes used for climatic studies (Torgny Vinje, NPRI, pers. comm.). "Closed ice" normally represents multi-year ice and "open ice" represents new ice or scattered ice. Dense closed ice often constitutes the major part of the ice cover, particularly in the Barents Sea.

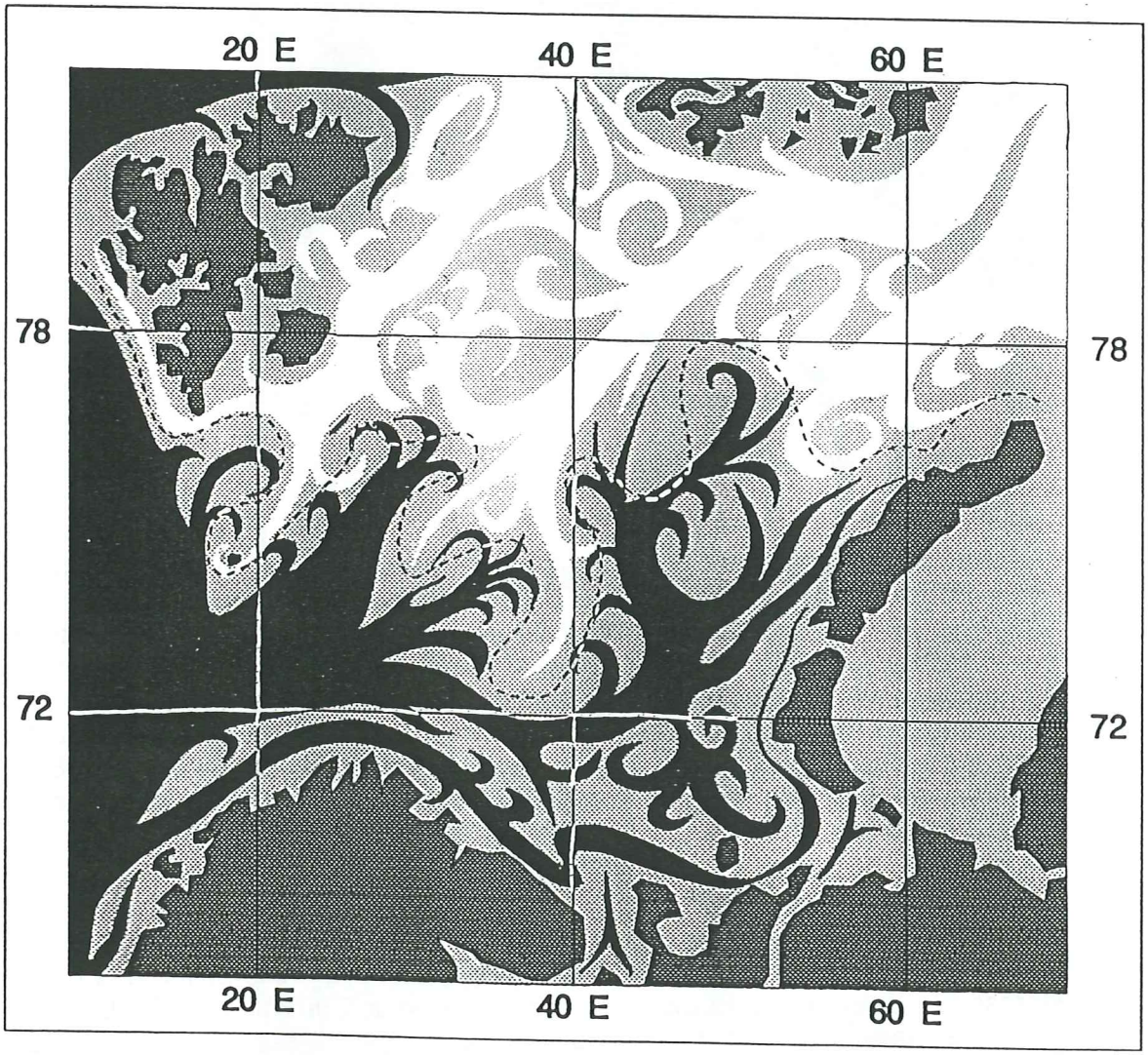

Fig. 5. The currents of the Barents Sea and the average position of the oceanic polar front. North Atlantic Current water - black. Arctic water -white. Dashed line - Polar Front. Based on figures in (Novitskiy 1967) and (Loeng 1983). Tidal currents often dominate the currents in the Barents Sea (Korsnes 1991).

Results

Data from all test-areas have been put into a data base. Diagrams have been plotted, but there has not been any time for statistical analysis yet. The intention is also to perform statistical analysis using the test area ice data together with temperature data from the Arctic Islands and precipitation data from the north and west coast of Norway. Weather data has been received from the Norwegian Meteorological Institute, DMNI, but no analysis has yet been done.

Visual inspection of the diagrams, showing dense ice extension for the test areas, reveal some interesting features. SE of Jan Mayen there is seldom pack ice at all. NW of Hope Island, on the other hand, conditions are opposite. There is seldom free of dense pack ice. The ice conditions in the NW subarea generally differ noticeably from the conditions in the SE subarea, fig. 6.

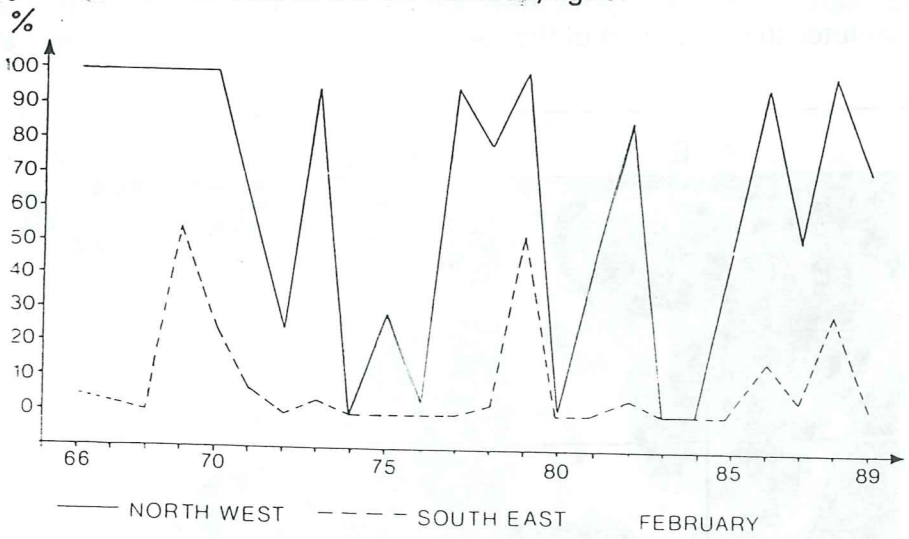

Fig. 6. Comparison of the extent of closed ice in a couple of sub-areas, NW and SE of Jan Mayen.

The area covered by dense ice, probably multi-year Arctic ice, in the Greenland Sea varies considerably from one year to another. Both deviation from the overall mean area and monthly deviation from the 24 year average for the same month, have been studied. Fig. 7. shows the deviation in percent from the overall mean percentual coverage by dense ice in the Greenland Sea.
Accepting ice area as an indicator of climatic conditions ice volume would be an even more significant indicator. This is suggested for example by Moritz(1988). It is of particular interest in the East Greenland Current, as much of the denser ice there have Arctic origin.

The East Greenland Current

The Arctic water and pack ice gyrates clockwise in the Arctic basin. It is conveyed across the basin at the Eurasian side by Transpolar Current, TC. Fig. 8 & Fig. 25. The ice transport from Siberia to the Fram Strait, between Greenland and Spitsbergen takes two to four years. It was also this current that transported Nansen's vessel Fram across the basin from Novosibirskiye Ostrova (New Siberian islands) to Spitsbergen during the expedition 1893 -1896 (Nansen 1897).

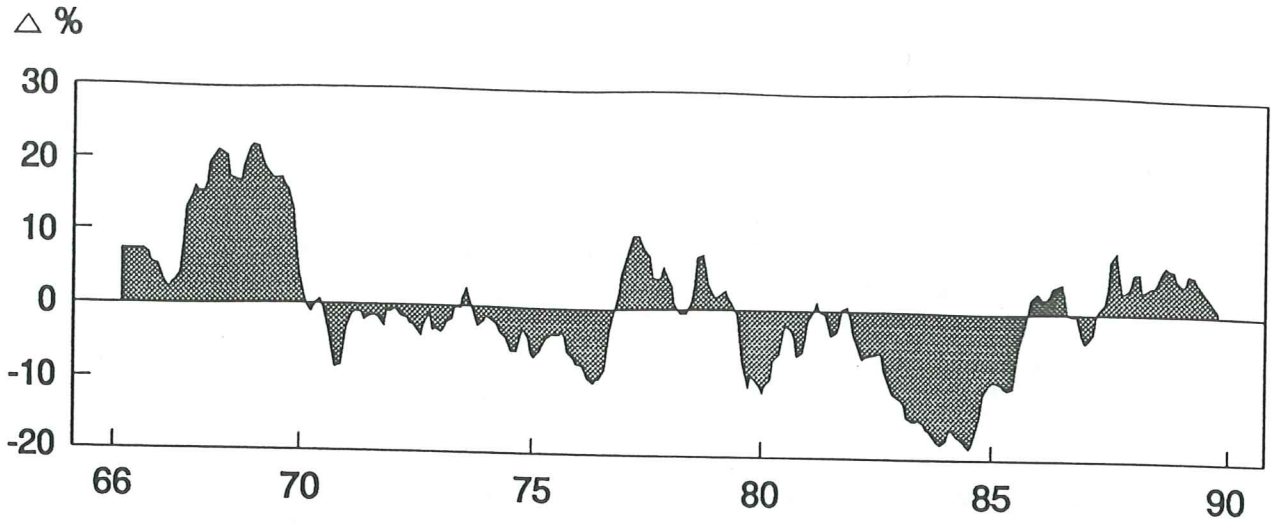

Fig. 7. The deviation in percent of the 12 month running mean from the 24 year mean percentual coverage by closed ice in the Greenland Sea.

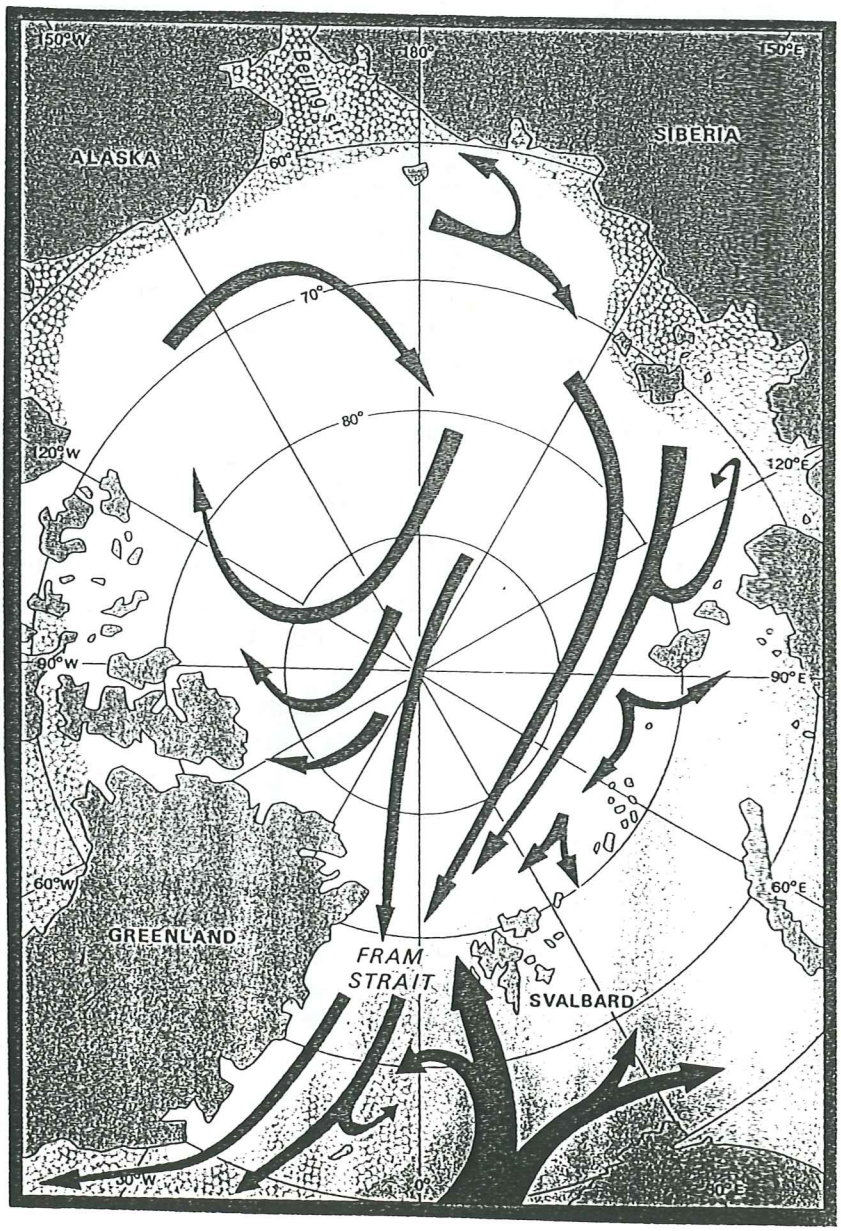

Fig. 8. The general surface circulation in the Arctic Basin. Courtesy T. Vinje. Adopted from figure in (Gordienko 1958).

The ice motion grows more steady towards Fram Strait and meandering decreases (Vinje 1982). When the ice reaches Fram Strait TC meets a contributor from the Arctic, north coast of Greenland. This together with an increasing current speed and divergence south of the strait results in a funnelling effect in the region of Fram Strait, for example mentioned by Kristensen (1983), fig. 9. A particular rhomboid fraction pattern can be seen and there is usually a protrusion at Nordostrundingen. Rhomboid fraction pattern has also been studied between Kvitøya and Nordaustlandet (Vinje 1977). Winds from the north accelerate the ice drift, with maximum acceleration north of Fram Strait and in the marginal ice zone (Vinje 1977). Winds from the south are retarding the ice (Vinje 1982).

The East Greenland Current, EGC, refers to the strong surface current that flows from Fram Strait to the Iceland Sea, along the east coast of Greenland. Speed and divergence increases from Fram Strait and southwards (Moritz 1988) (Zhang 1989). The current is somewhat restricted as it passes the Iceland-Greenland ridge (Helland-Hansen & Nansen 1909). The highest speed is over the Greenland shelf break (Helland-Hansen & Nansen 1909) (Vinje 1977). It may sometimes also be associated with the polar front (Aagaard & Coachman 1968).The underlying, warmer water travels slower than the cold surface current. The current layer is deeper on the landward side than on the outer, owing to the rotation of the Earth (Helland-Hansen & Nansen 1909). Aagard & Coachman (1968) defines it's lower limit as the depth where the temperature has reached 0 C and the salinity 34.5 per mille. The greater part of the water-mass of the current continues along the continental slope of NE Iceland. A second part of the current is diverted towards Jan Mayen, to form the Greenland Sea Gyre. In deeper water layers there is also a counter gyre over the Greenland shelf. A counter gyre is also possible at the surface (Vinje & Finnekåsa 1986). The general circulation is illustrated in fig's 8 and 10.

The vertical temperature and salinity structure reflects that of the Polar Basin, even as far south as Iceland-Jan Mayen (Helland-Hansen & Nansen 1909). There are great seasonal variation in both temperature and salinity, influencing the water column stability. The highest density is often found in the uppermost 10-15 m (Helland-Hansen & Nansen 1909) and the minimum temperature at about 50-60 m. The GSP-group (1990) found weak stratification and a strong barotropic component, leading to correlated transport also of deeper water layers, in the EGC.

Most of the Arctic ice leaves the Arctic through the Fram Strait, 70-90 % (Vinje 1977) or even 95 % (GSP-group 1990). The annual transport is about 1/10 of the average amount of ice present in the Arctic Basin (Kristensen 1983). Several studies have therefore been performed in the Fram Strait area to assess the mass and volume leaving the Arctic. Assessments further south are more sparse. Usually area estimates have been done. Volume is estimated in some studies, for example (Vinje & Finnekåsa, 1986). Ice is also formed and melted in the Greenland Sea (Vinje & Finnekåsa 1986) (Moritz 1988). 30 % loss of ice was found between 75 and 80 degrees N in the Greenland Sea in the melting season (GSP-group 1990). This can have an important influence on the heat exchange and the production of deep water. A production rate of about one million $m^3/_s$ has been estimated by Heinze (1990) (referenced in GSP-group 1990). Deep water production is important for the ocean ventilation and for CO_2 fixation. The deep water of the Greenland Sea is the coldest, freshest and densest deep water mass of the Nordic Seas (GSP-group 1990).

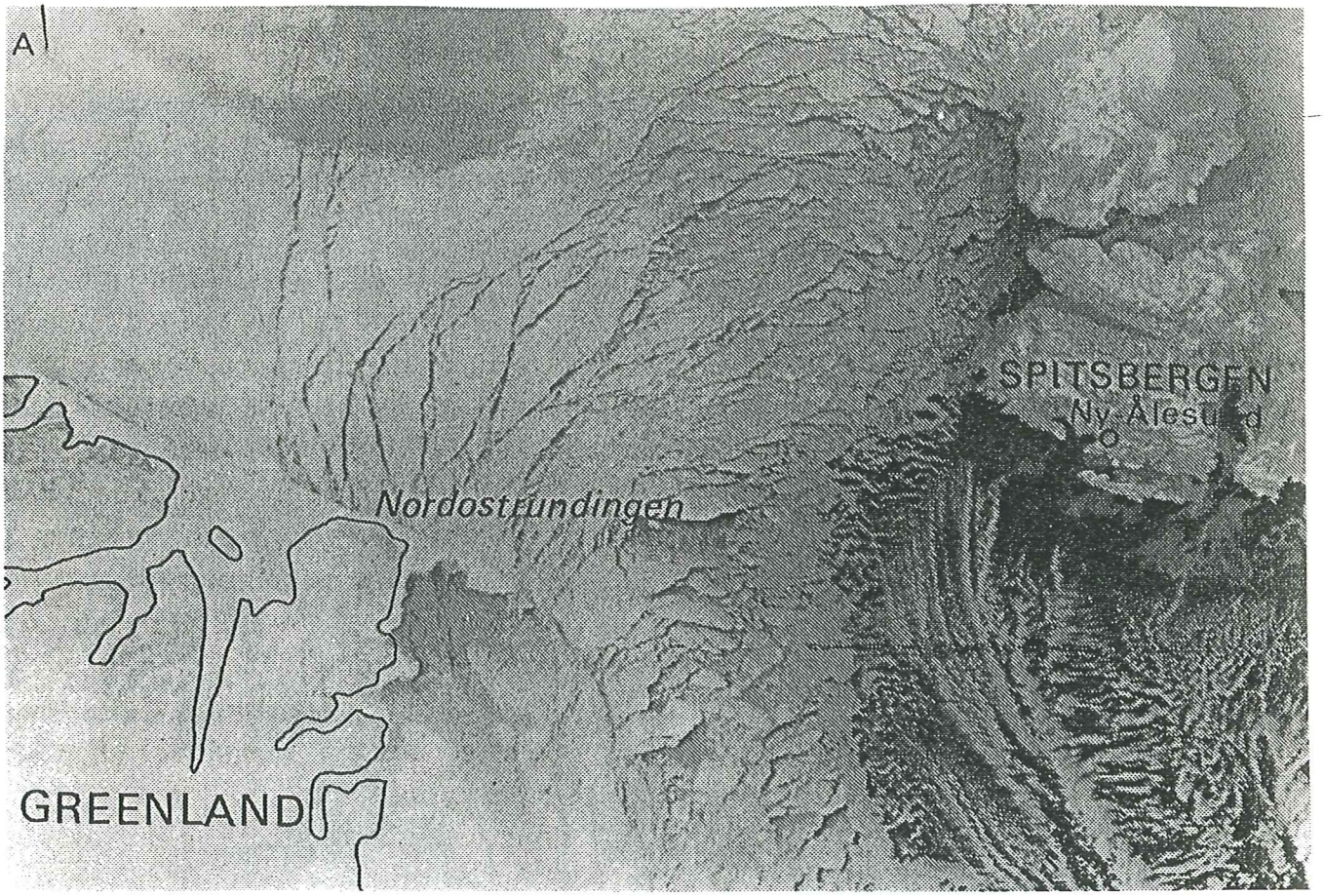

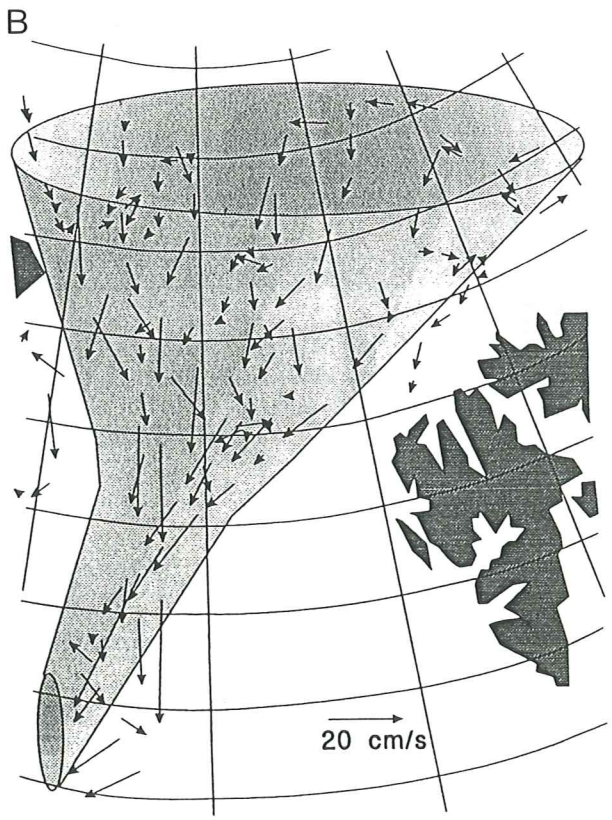

Fig.9. The "funnelling" effect in the Fram Strait area. Funnelling occurs both because of the convergence of the transpolar current and the arctic current from N of Greenland and because of the acceleration and divergence southwards from the Fram Strait. A is a daylight NOAA-6 image from 2/3 1981 during an outbreak of polar air. Note the parallel-epiped shaped ice floes, the protrusion at Nordostrundningen and the polynya south of it. From (Vinje & Finnekåsa 1986a).
B shows the funnelling effect as illustrated by buoy drift vectors, 1976-1980. Based on figure in (Kristensen 1983).

To assess the magnitude of melting and freezing, more thorough measurements are needed, for example along lines perpendicular to the EGC (Torgny Vinje, NPRI, pers. comm.). Melting and freezing has also been modelled. For example Moritz (1988) have made modelling efforts and gives estimates based on most of the known monitorings. He emphasises the need for better measurements, particularly in the southern part of the Greenland Sea. ULS, combined with satellite images can give this information.

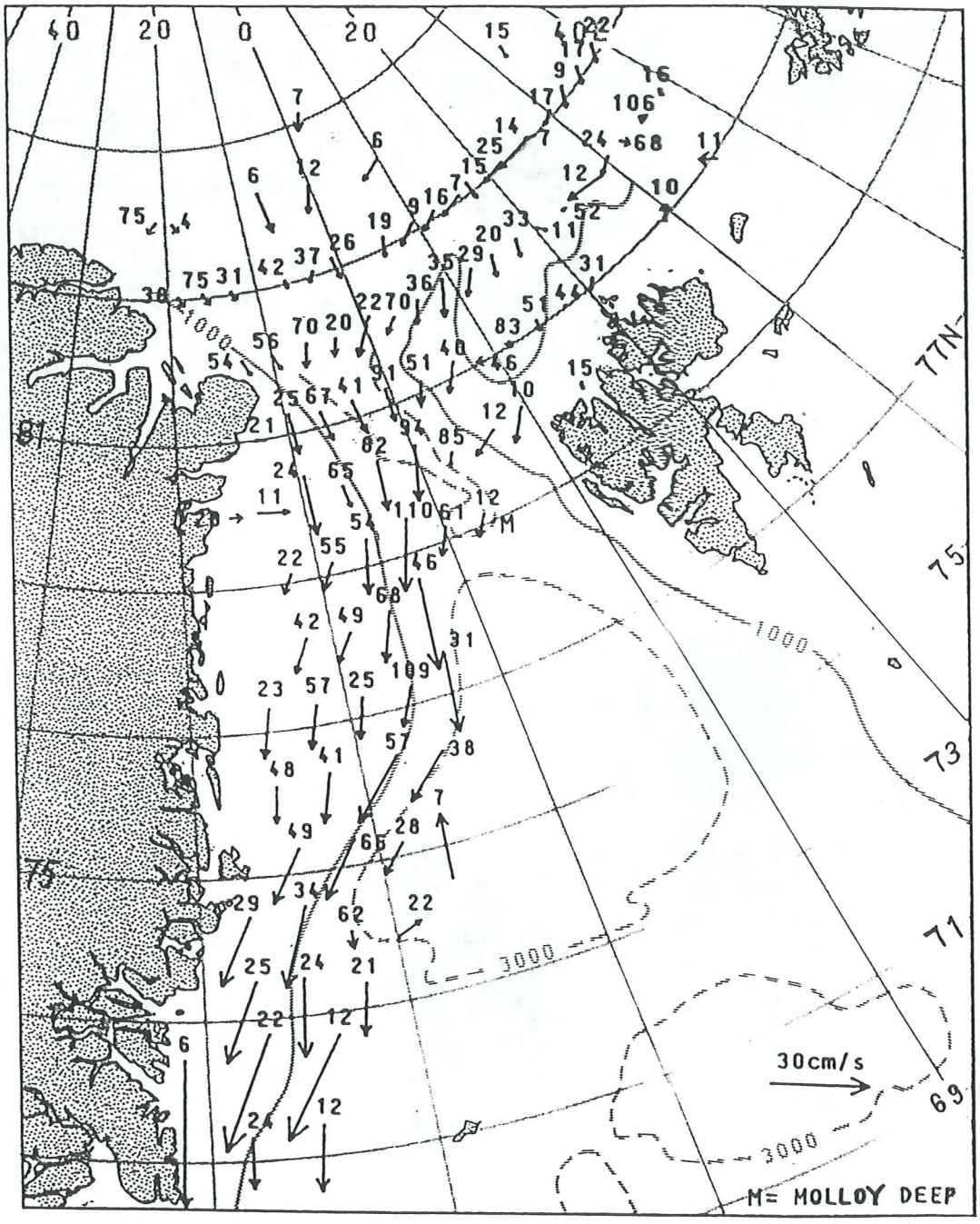

Fig. 10. The spatial distribution of ice drift vectors in the Greenland Sea. The numbers give the number of daily average drifts used for the drift speed computations. Adopted from (Vinje & Finnekåsa 1986a).

Methods for determination of ice thickness

Direct and indirect methods can be used to determine the vertical extension of the ice cover. The normally used direct method is to drill sample holes through the ice, usually on larger floes. With well distributed sample points this also gives information about the ice bottom-side topography. Drilling has been used for example by Thorndike (1980), Vinje & Finnekåsa (1986) and by Kovacs & Holladay (1989). Theoretically small floes can be lifted up and measured and larger, stranded floes can be measured in situ.
Ice thickness is also measured on icebreakers on arctic routes. It was for example done to some extent on the Swedish icebreakers Ymer and Oden on their Arctic expeditions in 1980 and 1991, respective. Oden also made icebreaking tests in the Greenland Sea in 1989 (Backman 1990), fig. 11.

A semi-direct method is tested by Iizuka et. al. (1988). They used a step frequency radar, similar to seismic equipment. Except echo-time also phase and amplitude information was utilized. Transmitters were placed on the surface of low salinity, level ice and the method gave satisfactory results on up to 70 cm of ice. They also give a good overview of radar sounding of ice.

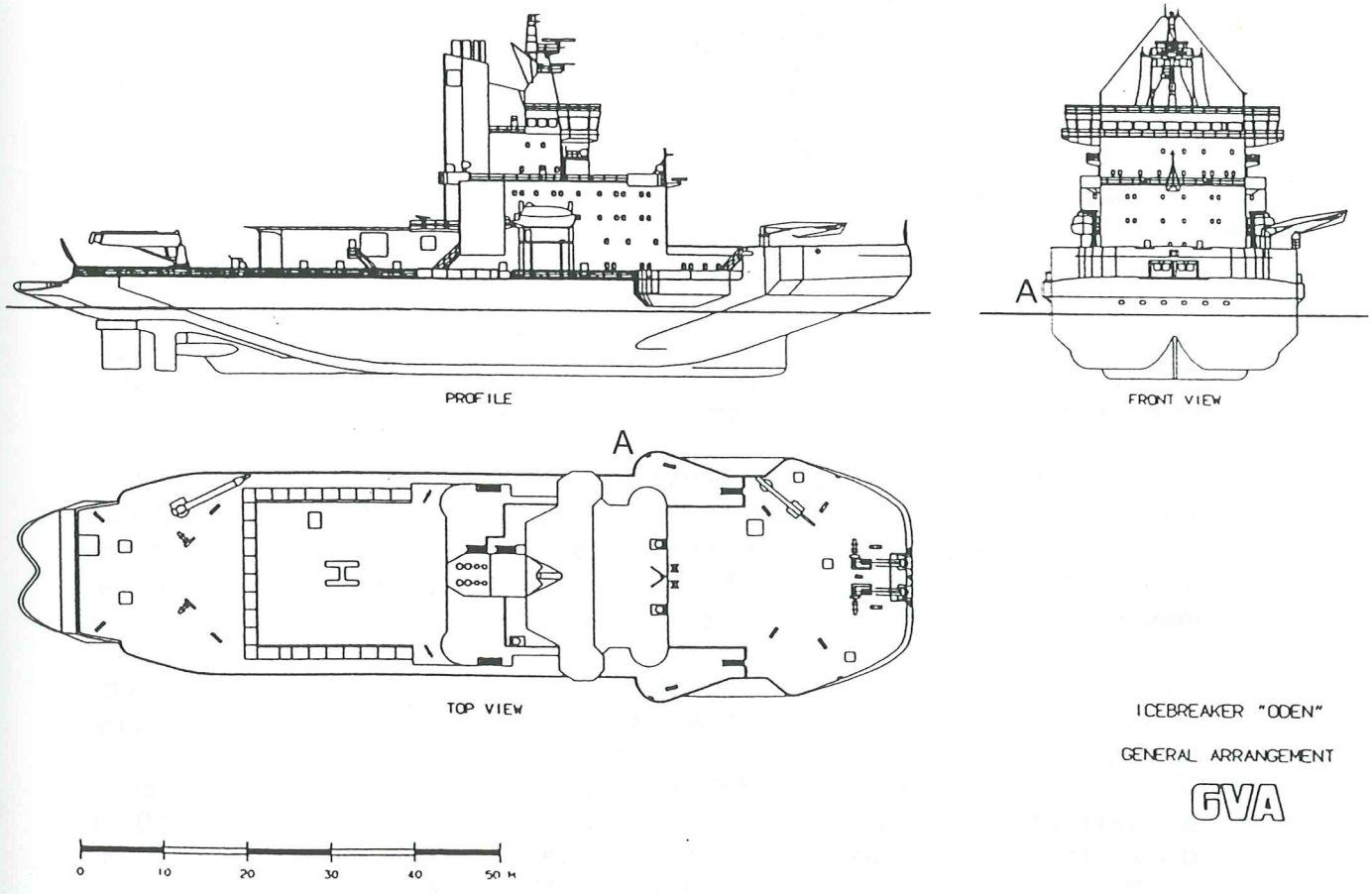

Fig. 11. The Swedish icebreaker Oden with the new hull shape for improved ice breaking capability and performance. Oden is constructed for Arctic conditions and the first vessel in a new generation of Swedish heavy duty icebreakers. Note the reamers on each side, A. They help widening the channel, using heeling, when narrow turns are needed. Adopted from (Johansson & Liljeström 1989).

Indirect methods often involve remote sensing. A more easily observed parameter is measured and some model is used to compute the ice thickness. During AIDJEX ice thickness was inferred from grey level on satellite images (Hall 1980) (Thorndike 1980). This was operational to 60 cm of ice. The freeboard of level ice, or ice sail height on ridged ice, can be determined. Based on this a probable ice thickness can be found. Values of 1:5, 1:7 and 1:9 have been given. The correlation can be seen in fig. 12. Wadhams (1980) has compared sail height and keel depth of pack ice along a track about 1000 km long NW from Fram Strait. Kozo & Diachok (1973) have made similar comparison across the EGC. Johnsen (1989) has compared top and bottom-side topography on single floes. Probably ERS-1 is well suited for freeboard and sail studies (Massom 1991)

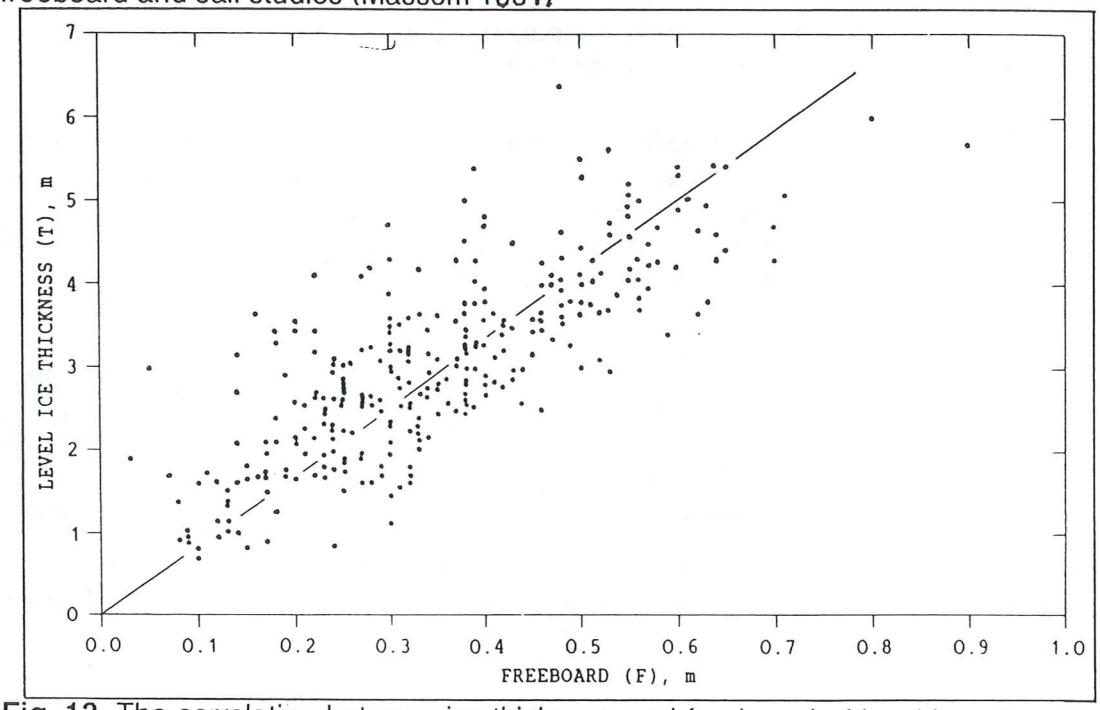

Fig. 12. The correlation between ice thickness and freeboard of level ice. Consider, however, the spread of the data. From (Vinje & Finnekåsa 1986a).

Kovacs & Holladay (1989) have experimented with electromagnetic induction to find ice thickness. A similar method as is used in geology. A helicopter towed "bird" emits electromagnetic energy, which give rise to an induced current. The inductively created signal is received by the bird and gives information about the ice/water interface. A laser altimeter in the bird gives the distance to the ice overside.

Soundbased, sonar, remote sensing of the ice underside has been done from submarines, fig.13. The access is however limited, as it is done mainly on military purpose. Some civilian profiles have been recorded though. Wadhams (1980) describe the classical profile NW of Fram Strait. Wadhams & Horne (1980) describe a profile where a narrower sonar beam has been used. Swithinbank (1972) documents a profile located between 79-90 degrees N, 1-8 degrees E. Williams et. al. (1975) also describes an Arctic sonar profile. Westhall & Li (1976) uses a narrow beam submarine sonar profile from the Denmark Strait to separate ice classes in the EGC. It is the first attempts to analyse ice underside data in the EGC. Kozo & Diachok (1973) took a cross-stream profile in th EGC, complemented with ice top laser profiles.

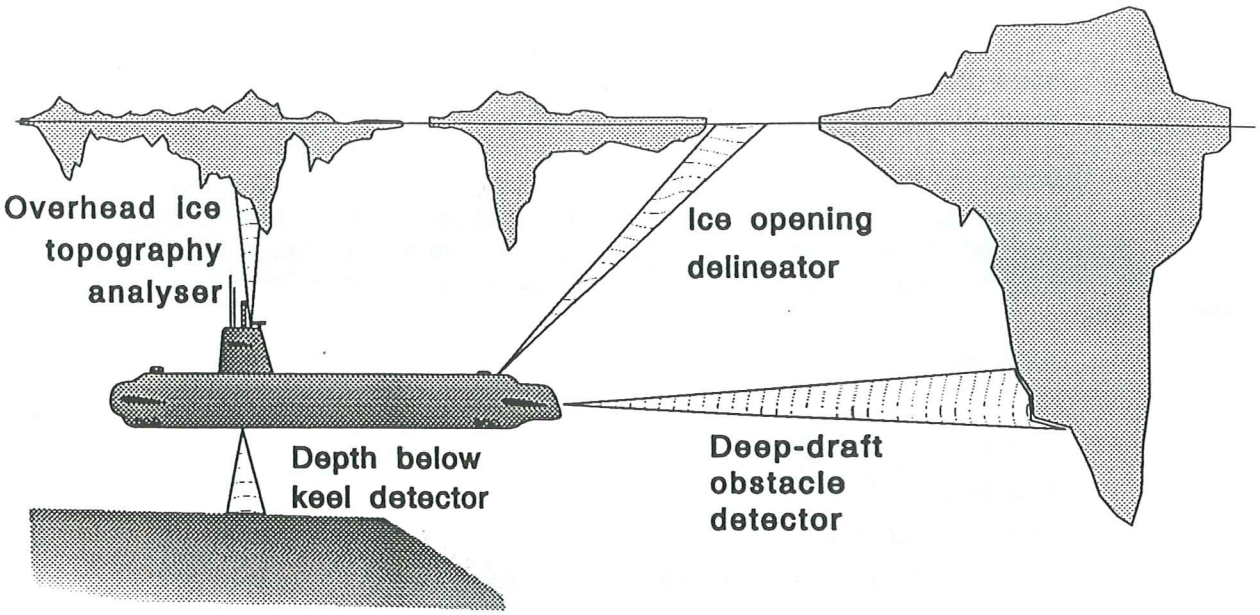

Fig. 13. Submarine sonar sounding and typical ice profiles. Based on figure in (Kozo & Diachok 1973)

SONAR - Sound Navigation And Ranging

Light-based remote sensing is not very successful in sea water. Light is soon attenuated by suspended matter in the water, particularly near coasts, harbours, river outlets etc. Instead sound based remote sensing is often used, for example sonar. Sound is not noticeably influenced by the clarity of the water. The soundspeed in water is about 1500 m/s, i. e. about five times the soundspeed in the air.

Sound was first used to find the distance from the boat hull to the sea bottom. J Y Costeau participated in the early development of sonar as a more general tool (Edgerton 1986). Sonar is now used to see what is in the water, at the bottom or under the bottom sediments. It's used to find submarines, bottom mines, fish, ship wrecks, cables, cars etc. In general it's also used to find the distance to some discontinuity, for example the bottom, the ice subsurface, a geological discontinuity or an archeological strata. A Doppler-sonar can be used to analyse vertical water velocity (GSP-group 1990). A schematic illustration is found in fig. 16.

Sound pulses are transmitted by the sonar transducer, reflected against some surface and received anew by the instrument, the transducer itself or a separate hydrophone. The sound pressure causes a voltage which leads to a registration.
The time between transmission and reception, multiplied by the soundspeed, gives the distance to the reflecting surface (and back).

$$\text{Distance} = \text{sound\_speed} * \text{time} * {}^{1}/_{2}$$

Not specular surfaces creates over-echoes, fig 14. In the case of sonars under the sea surface, depth-finders, dragged sonar "fishes" etc., secondary echoes will appear from reflection against the water surface. Double echoes with exactly the

same transit time are multiple echoes that have bounced against the surface at least once. It is not the case in deep water.

When the pulse impinges on a surface, part of the energy is reflected and part of it transmitted and maybe reflected at a deeper level in the matter. The reflected fraction depends on the density and soundspeed difference of the materials. The ratio of the acoustic pressure of the reflected wave to the incident wave is:

$$\text{reflected / incident} = r_2c_2 - r_1c_1 \,/\, r_2c_2 + r_1c_1$$

r_1 = density of medium 1
r_2 = density of medium 2
c_1 = soundspeed in medium 1
c_2 = soundspeed in medium 2

If $r_2c_2 < r_1c_1$ a phase shift occurs. Many sonars do not register phase information, i. e. that information is lost (Edgerton 1986).

High energy pulses of sound of short duration are needed in sonar equipment, to obtain adequate range resolution and, in case, penetration. Particularly moored sonars are thereto requested to consume as little energy as is possible.
Capacitors store electrical energy and can discharge it quickly. They can be charged with a weak source of energy, but still deliver high peak power when discharged. The power converted by the capacitor is:

$$\text{Power} = \text{Capacitance} * \text{Charge\_voltage}^2 * \text{Frequency} /_2$$

To work and observe in midwater, for example to find fish, the sonar need to be very powerful and the receiver sensitive.

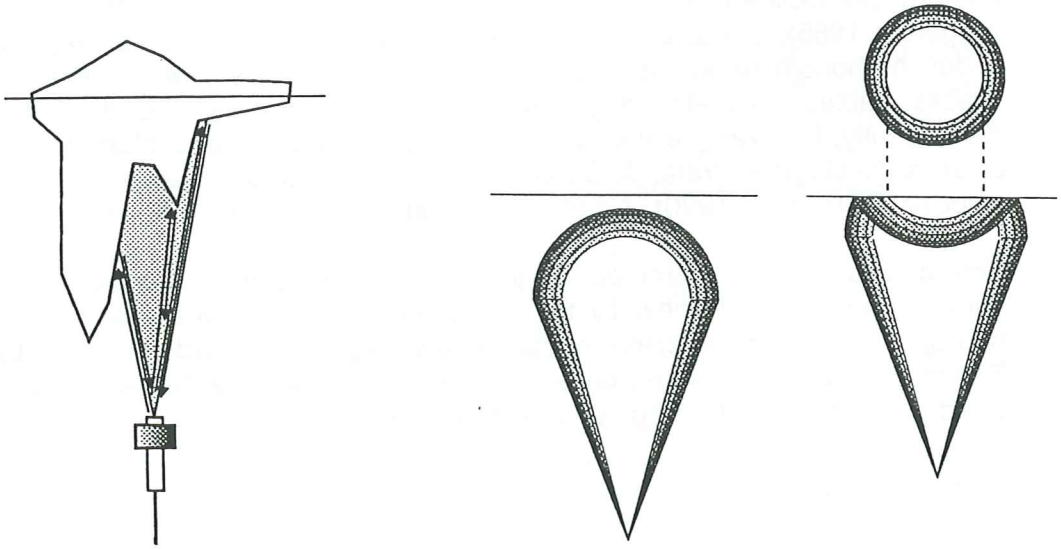

Fig. 14. "Over-echos" are caused by sub signals superimposed on the core signal.
Fig. 15. The footprint effect on a flat surface. B gives the simultaneous footprint. Consider the impact on not flat surfaces like the ice bottom-side. Adopted from (Massom 1991)

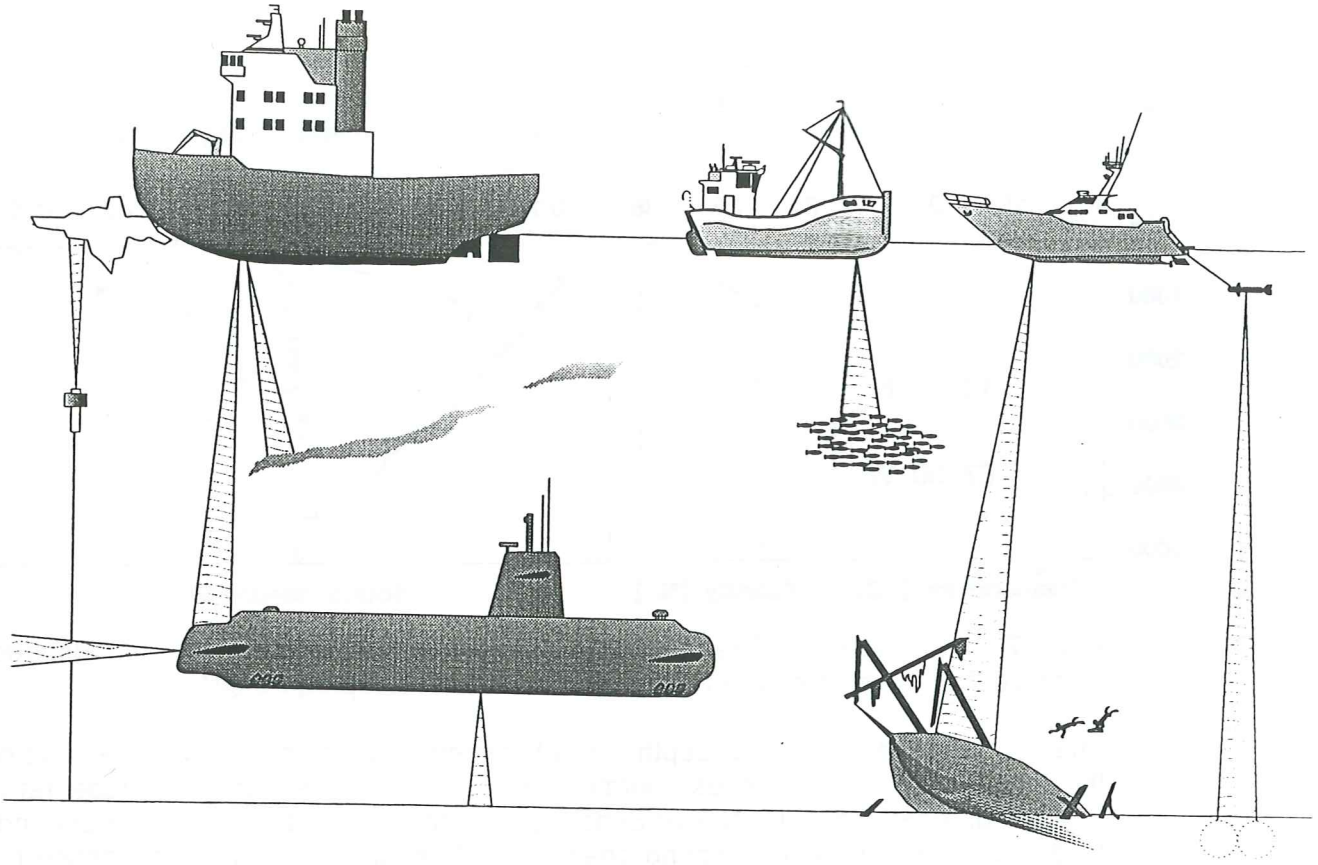

Fig. 16. Examples of sonar applications. Upward looking sonar for ice draft analysis. "Depth-finders", "Fish-finders", Obstacle detectors/navigation sonar, Sonar to find wrecks, submarines and sub-bottom features, Sonar fish for bottom topography surveying. The "cloud" below the icebreaker is a sound scattering layer. It is believed to be caused by microscopic organisms in mid-water (Edgerton 1986).

The beam-width is one of the most important parameters of a sonar. It determines the footprint of the beam and thereby influences spatial resolution, fig 15. A narrow beam gives high power concentrated within a small angle. The beam width depends on transducer diameter and frequency. A bigger transducer, using higher frequency results in a narrower beam. The beam-width can be made smaller or (more) asymmetric by using a number of connected transducer elements, operating in phase, or by using foam-rubber reflectors (Edgerton1986)

An important part of the sonar is the recorder. It gives coherent comparison of the information from the transducer. If the signal is registered detailed studies can be performed later. The recorder can be a rotating neon lamp, a cathode ray tube (CRT) or oscilloscope, a wet- or dry paper type registration unit or nowadays commonly also on digital computer memory.

Soundspeed in sea water

Soundspeed in water depends on pressure, temperature, chemical composition and other factors, fig 17. Effects due to this can be neglected, except when high precision is needed or refraction is considered (Edgerton 1986). Underwater sound is attenuated inversely proportional to the distance, in deep water, called spreading loss. Added to that is an attenuation factor that increases with the frequency. It is caused by viscous effects in fresh water (Mellen 1986). Some conducting salts

increase the sound absorption, particularly $MgSO_4$. Sound energy is transferred to heat. The chemical equilibrium in sea water influences the compressibility (Mellen 1986). The absorption is 25 times higher in sea water compared to fresh water.

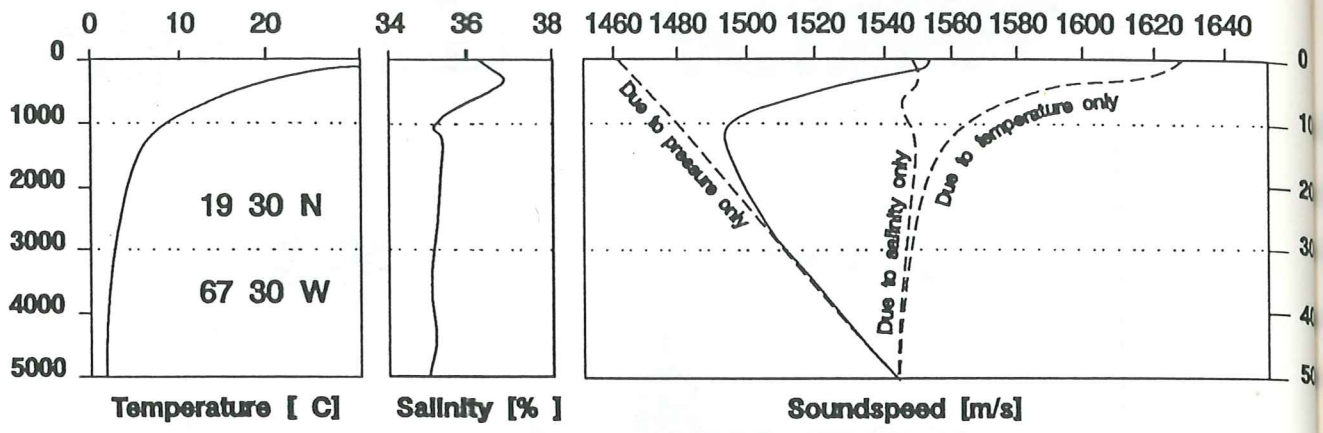

Fig. 17. The influence of temperature, pressure and salinity on the soundspeed. Observe that the profiles are not from Arctic waters. Adopted from (Nutile1976).

The soundspeed profile with depth varies between different locations, depending on the influencing water masses. Hurdle (1986) gives a selection of representative profiles for locations in the Nordic Seas, fig 19. The knee on the curves corresponds to the axis of a refractive sound channel, or "tunnel", where the soundspeed is lowest, referred to as a SOFAR (SOund Fixing And Ranging) channel. It gets close to the surface towards the poles and can reach the surface there, in ice covered waters.The effect of the channel is that the soundspeed propagation changes from spherical spread to cylindrical spread. It can be used for sound transmission over long distances, for example between Australia and Bermuda (Munk 1991).

In the deep ocean the temperature have major influence down to about one km, then pressure takes over. Salinity has relatively weak influence (Hurdle 1986), fig. 17. 1 C change of temperature changes the soundspeed about 4 m/s, 1 per mille change of salinity changes the soundspeed about 0.125 m/s and 100 m in depth changes the soundspeed about 1.7 m/s, according to Hurdle (1986). The formula by Kinsler et. al. (1982), used in this project gives values about 5, 1.402 and 1.7 m/s, respectively, computed with standard parameters for the Greenland Sea..

The largest variation in soundspeed occurs in the uppermost layers, due to local weather and seasonal changes. In the Greenland Sea, geographically the soundspeed is lowest in the northern part, due to low salinity and temperature. Ocean fronts result in varying soundspeed, for example at the East Greenland Front along the Greenland continental shelf, particularly in the summer.

Computation of soundspeed in liquids involve second-degree partial differential equations that are difficult to solve. The relationship between the different physical properties is complex and not well understood. In practice therefore soundspeed is either computed from the travel time over a known distance, or by using some empirically derived formula. DelGrosso & Mader (1972) gives a formula based on interferometer measurements, tab. 3. The estimated error is 0.05 m/s.

$$
\begin{aligned}
c = c_0 &+ a_1 \times T + a_2 \times T^2 + a_3 \times T^3 + a_4 \times T^4 \\
&+ a_5 \times (S - 35) + a_6 \times P^2 + a_7 \times P^3 \\
&+ a_8 \times T \times (S - 35) + a_9 \times T \times (S - 35)^3 \\
&+ a_{10} \times T^2 \times (S - 35) + a_{11} \times T \times P \\
&+ a_{12} \times T \times P^2 + a_{13} \times T \times P^3 + a_{14} \times T^2 \times P^2 \\
&+ a_{15} \times T^3 \times P + a_{16} \times (S - 35) \times P \\
&+ a_{17} \times (s - 35) \times P^2 + a_{18} \times (S - 35) \times P^3 \\
&+ a_{19} \times (S - 35)^2 \times P + a_{20} \times (S - 35)^2 \times P^2 \\
&+ a_{21} \times (S - 35)^3 + a_{22} \times (S - 35) \times T \times P \\
&+ a_{23} \times (S - 35) \times T^2 \times P
\end{aligned}
$$

$c_0 = +0.140\ 194\ 964\ 197 \times 10^{4}$

$a_1 = +0.500\ 642\ 920\ 686 \times 10^{1}$

$a_2 = -0.583\ 540\ 720\ 391 \times 10^{-1}$

$a_3 = +0.349\ 631\ 461\ 597 \times 10^{-3}$

$a_4 = -0.164\ 875\ 703\ 289 \times 10^{-5}$

$a_5 = +0.134\ 606\ 695\ 473 \times 10^{1}$

$a_6 = -0.593\ 403\ 057\ 954 \times 10^{-4}$

$a_7 = -0.209\ 170\ 685\ 764 \times 10^{-7}$

$a_8 = -0.112\ 689\ 485\ 296 \times 10^{-1}$

$a_9 = -0.583\ 732\ 276\ 240 \times 10^{-6}$

$a_{10} = +0.103\ 658\ 662\ 691 \times 10^{-3}$

$a_{11} = +0.595\ 900\ 933\ 419 \times 10^{-3}$

$a_{12} = -0.131\ 201\ 344\ 149 \times 10^{-5}$

$a_{13} = +0.402\ 773\ 046\ 625 \times 10^{-9}$

$a_{14} = +0.144\ 431\ 845\ 812 \times 10^{-7}$

$a_{15} = -0.101\ 232\ 803\ 918 \times 10^{-5}$

$a_{16} = +0.157\ 450\ 572\ 397 \times 10^{-1}$

$a_{17} = +0.533\ 284\ 097\ 890 \times 10^{-5}$

$a_{18} = +0.353\ 545\ 616\ 177 \times 10^{-9}$

$a_{19} = -0.522\ 655\ 412\ 446 \times 10^{-3}$

$a_{20} = -0.858\ 535\ 445\ 194 \times 10^{-7}$

$a_{21} = +0.572\ 274\ 443\ 678 \times 10^{-5}$

$a_{22} = -0.117\ 388\ 164\ 634 \times 10^{-4}$

$a_{23} = +0.597\ 262\ 459\ 578 \times 10^{-6}$

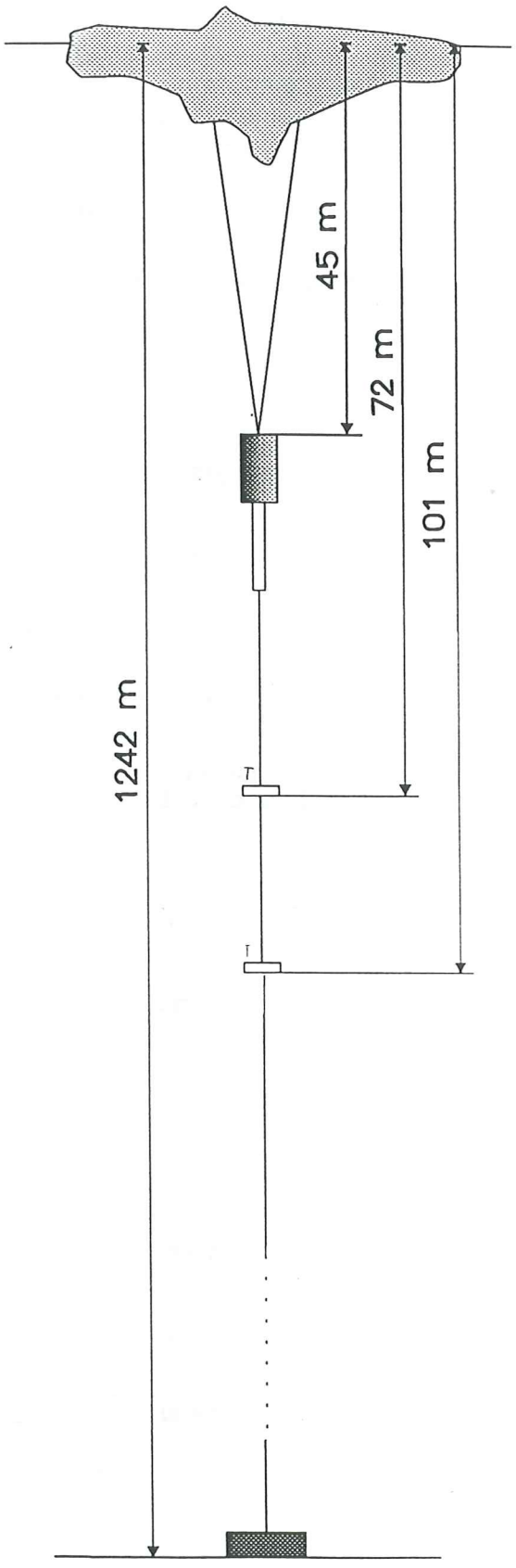

Tab. 3. The formula given by DelGrosso & Mader (1972), based on interferometer measurements.

Fig. 18. The configuration of the ULS moored in the Greenland Sea 1987-1988.

Mackenzie (1981) gives a simplified version, using a pressure to depth transformation, still with a fair accuracy. Kinsler et. al. (1982) have reduced the computation load, and the accuracy, somewhat further. The accuracy of their formula is considered sufficient for the ULS used in this project, moored in the Greenland Sea in 1987-88.

The equation given in Mackenzie (1981):

$$\begin{aligned}\text{Sound\_speed} = \quad & 1448.96 + 4.591 \times T - 0.05304 \times T^2 \\ & + 0.0002374 \times T^3 + 1.340 \times (\text{Salinity} - 35) \\ & + 0.01630 \times \text{Depth} + (1.675 \times 10^{-7}) \times \text{Depth}^2 \\ & - 0.01025 \times T - (7.139 \times 10^{-13}) \times T \times \text{Depth}^3\end{aligned}$$

The equation given in Kinsler et.al. (1986):

$$\begin{aligned}\text{Soundspeed} = \quad & \text{Surface\_soundspeed} + 4.6 \times T \\ & - 0.055 \times T^2 + 0.003 \times T^3 \\ & + (1.39 - 0.012 \times T) \times (\text{Salinity} - 35) + 0.017 \times \text{Depth}\end{aligned}$$

T = temperature in both equations.

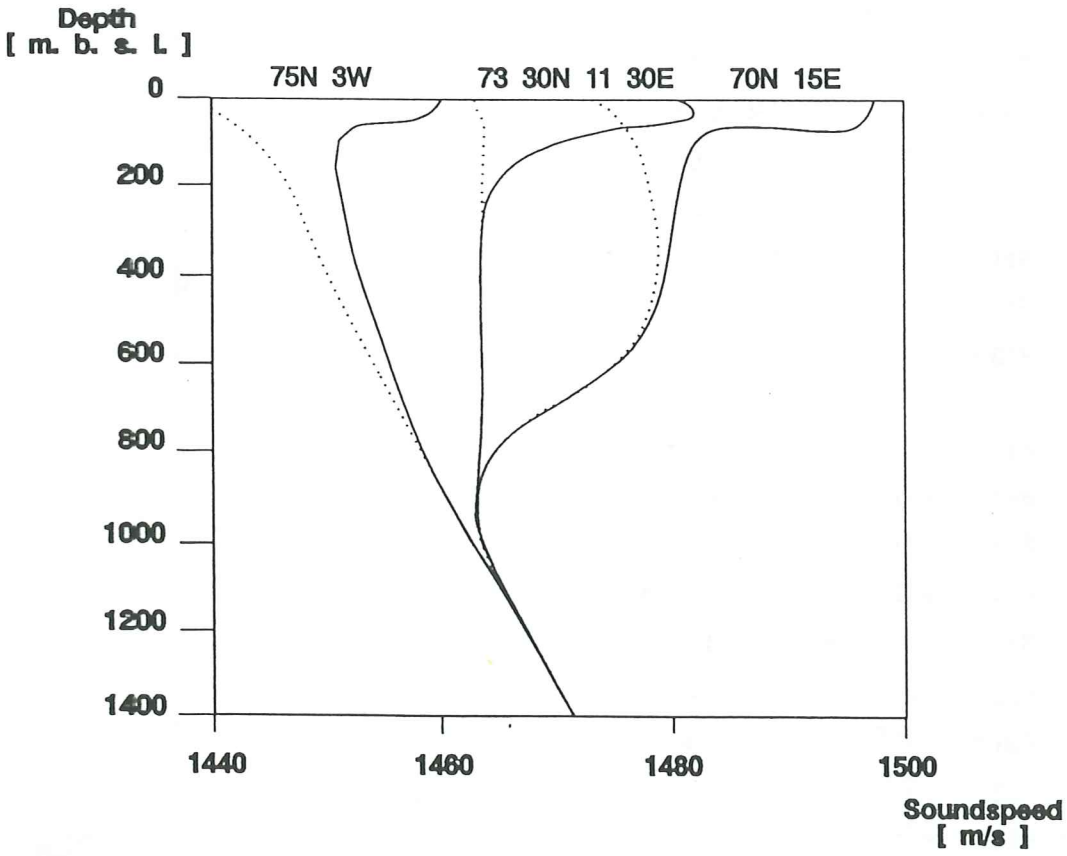

Fig. 19. Sound profiles from three locations between Norway and Greenland. Note the influence of the North Atlantic Water of the North Atlantic Current. Solid line - summer. Dotted line - winter. Adopted from (Hurdle 1986).

The ULS-Upward Looking Sonar-moored in the Greenland Sea 1987-88

On a suggestion from NPRI upward looking sonars have come into use for ice draft analysis. They are attached to the top of moorings in deep water. The Christian Michelsen Institute in Bergen has developed an operational buoy. The first really operational one was deployed successfully in the Greenland Sea in 1987-88. It is data from this buoy that has been used for the tests performed in this project. The interest for the buoy type, and its successors has rissen remarkably since 1988. In 1991 ULS bouys have been deployed along latitudes in the Greenland Sea to better monitor the spatial variation of the ice drift in EGC, fig. 20. Technical specifications for the buoy deployed 1987-88, CMI ES-300_II, are given in tab. 4., together with similar data for the successor, CMI ES-300_V, intended for Antarctic conditions.

	CMI ES-300_II	CMI ES-300_V
Operational depth	20-70 m	10-190 m
Sonar beam width	5.0 deg.	2.0 deg.
Operational acoustic frequency	300 kHz	300 kHz
Resolution	0.1 m	0.01 m
Pressure transducer range	20-70 m	10-190 m (?)
Resolution	0.02 m	3-5 hPa
Tilt resolution (xy)	1 deg	1 deg.
Data recording interval	4 min (used)	1/4,1, 4 or 8 min.
Data recorder	Sea Data Model 610	Not known
Storing capacity	550 days	25, 101, 387 or 738 days, depending on resolution
Storage	300 ft cassette	1 (2 or 3) Mbyte
Total length of instrument	1.70 m	1.83 m (?)
Diameter of float	0.55 m	0.60 m
Diameter of cylinder	0.16 m	0.22 m
Weight in air, without float	58 kg	121 kg (with or without float -
Total weight in air with float	79 kg	not known which)
Net buoyancy in sea water	55 kg	54 kg
Nominal operational depth	45 m	150 m
Allowed depth without damage	70 m	400 m

Tab. 4. Technical specifications for the ULS, CMI ES-300_II, deployed 1987-1988. As a comparison data for the successor CMI ES-300_V is given. Question mark denote uncertainty. Adopted from (Vinje & Berge 1989) and (Johannesen 1990).

The buoy used in 1987-88 was deployed at 75 03.4 degrees N, 12 09.2 degrees W. It was attached on top of a current meter mooring of the Alfred Wegener Institute for Polar and Marine Research, Bremerhaven, Germany. The mooring anchor was at a depth of 1242 m and the nominal depth of the ULS was 45 m below the seasurface, fig. 18. It was deployed at 0930 UT on 22 of June 1987 and retrieved 1800 UT on 20 of June 1988. The recording interval was set to four minutes which gave a time series of about 130 000 samples. The whole series of draft values is plotted in 14 day diagrams in (Vinje & Berge 1989). Draft is computed based on a constant temperature. Ice draft and ULS buoy depth diagrams for selected periods are published in (Olsson 1992), with 24 h resolution Draft is computed based on temperature values below the ULS buoy, fig. 22.

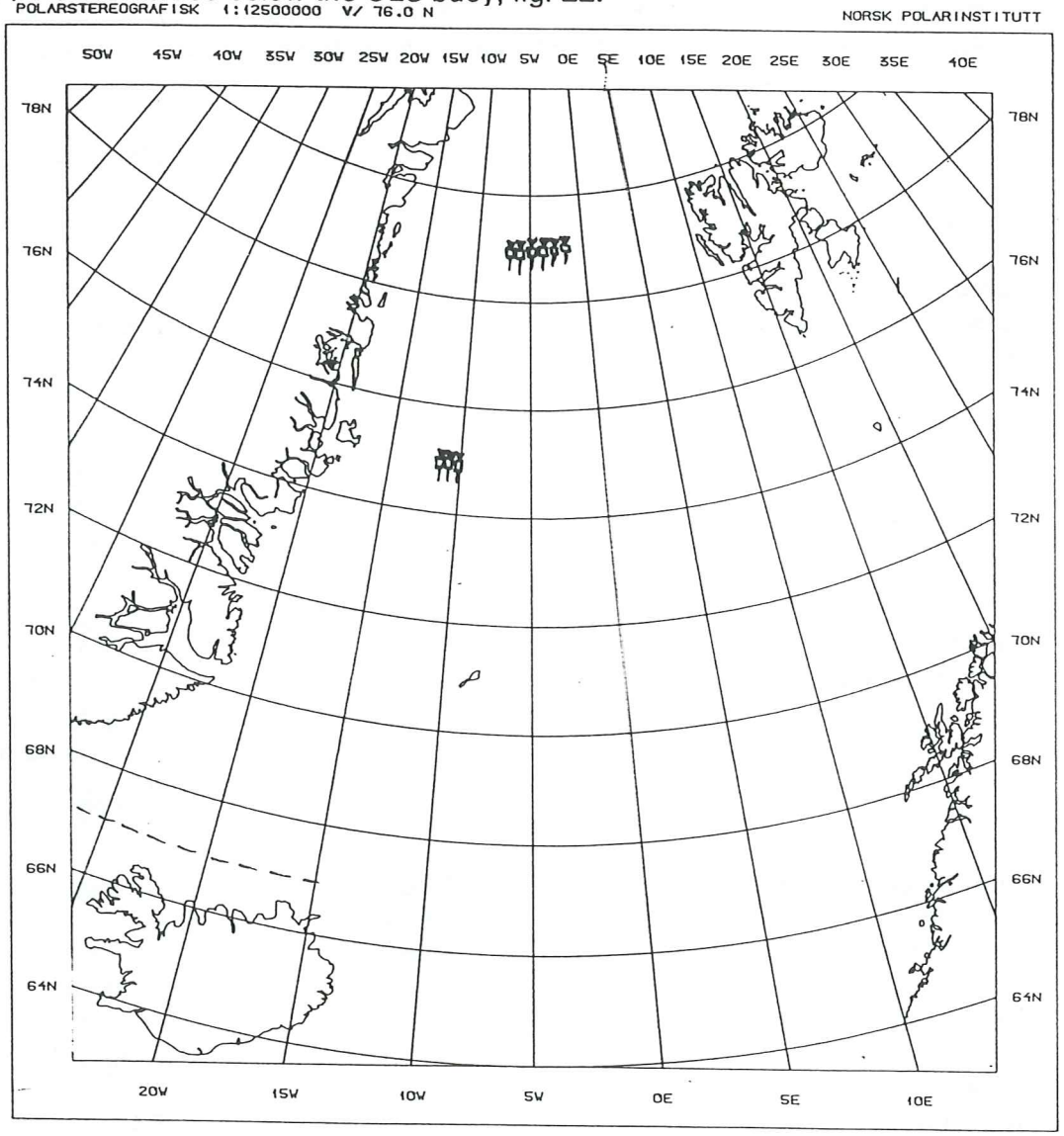

Norwegian, German and USA ULS deployments 1991

Lat 79N	2 30W 2300 m	Lat 75N	12 30W depth unknown
- " -	3 20W 2000 m	- " -	11 30W -- " --
- " -	4 00W 1500 m	- " -	10 30W -- " --
- " -	5 00W 1200 m		
- " -	6 00W 500 m	Lat 67N	Lon and depth unknown
- " -	7 00W 350 m		

Fig. 20 The deployments of ULS in the Greenland Sea in 1991.

Developed program for ice draft computation

The program for ice draft computation was developed first. A basic version was implemented to start with. It was later refined and optimized. The program is written in ANSI C under ULTRIX. Dynamic allocation is used. Storage capacity, however, seems to limit the computation period to about ten days. Several different data files are used as data sources. All times are converted to the internal representation of the computer, to improve performance. This means in the implemented version at NPRI that times are converted to integer time passed since 1 January 1980. The program is functional until 2080, without adjustment. It automatically finds the appropriate file and the desired data in it, if the file exists on the directory. Statistics are computed for the draft and the ULS buoy depth and the values can be tabulated on a file.

The temperature is an important variable in the computation of the soundspeed as is evident from the formula. Quite a variation can be seen in the temperature series from 72 and 101 m. Seasonal temperature variations are however, greatest at the surface, in the upper 10-15 m, according to Helland-Hansen & Nansen (1909)
The temperature handling has been improved in three stages. A simpler program existed before, written in Fortran. It was used for the original data extraction in 1988 (Vinje & Berge 1989). It made use of a constant temperature of -1.0 C.
The first stage of this project also used constant temperature, because temperature data hadn't arrived yet. Unfortunately the temperature sensor at the buoy malfunctioned.

Later temperature from the nearest sensor below, at 72 m, about 30 m under the buoy, was used to get an approximation of the temperature in the water column. This gave at least some correction for the temperature variation. A second attempt was to use linear regression, using both values. This gave much to high temperatures, which could be expected considering the shape of the temperature curve. Using linear regression between the 72-m temperature and the seasonal ice subsurface temperature gave a better approximation of the real temperature in the water column. The temperature-change with depth is, however, far from linear, as can be seen in fig 21.

The hyperbolic sine function was expected to give a good fit but to use demanding computations (Bjørn Erlingsson, NPRI, pers. comm.). The fitting of a logarithmic function was considered the optimum approximation (Erlingsson 1991) (Torgny Vinje, NPRI, pers. comm.). The logarithmic profile was locked in the upper end using the seasonal ice subsurface temperature and a zero derivative at the subsurface.

Finally a numerical method, Runge-Kutta, was utilized. The numerical method also considers possible refraction.

Salinity is also very important, but no measurements were made at the location of the ULS.

Ice draft computations

The ice draft is computed as the difference between the depth of the sonar and the distance to the ice. Reflections from an ice-free water surface at calm weather was used for calibration of the ULS. An early calibration sequence showed a systematic error of about one dm. Inquiry to the manufacturer revealed that this represented

the distance between the depth measuring transducer and the sonar transducer (Torgny Vinje, NPRI, pers. comm.). The depth transducer is located below the ultrasonic transducer in the housing buoy of the ULS used in 1987-1988. Addition of a correction factor for this made the draft measurements much more accurate. The used correction factor is -0.13 m.

Draft = ULS_depth - Distance_to_ice_subsurface + Correction_factor [m]

The depth of the sonar (ULS_depth) is computed from the measured pressure at the buoy, reduced for the current air pressure at the time of the measurement. This gives the pressure exerted by the water. Dividing the pressure value by the pressing force of the water, density times local gravitational acceleration, gives the depth.

ULS_depth = (Measured_pressure - Air_pressure) / Water_density ¤ Local_gravity [m]

Air pressure was digitized from synoptic weather maps. The air pressure was recorded for 00Z and 12Z. The pressure 00Z is used for measurements between 1800 h and 0600 h and the pressure 12Z is used for measurements between 0600 h and 1800 h. If any value is missing a default value of 1012 mbar, or hPa, is used.

The density depends very much on the salinity. A salinity time series has unfortunately not been available during the project period. A constant salinity of 33 per mille have been used for the computations, based on CTD, Conductivity, Temperature and Depth, measurements in the area. The local gravitational acceleration for the considered position is taken to be 9.829 m/s^2.

The measured pressure is computed using calibration constants ("gain and offset") supplied by the manufacturer. A Digiquartz 8060 D. C. calibration unit has been used for the calibration. The transducer is checked together with it in a pressure tank. The accuracy of the Digiquartz 8060 D. C. is said to be about one magnitude better than that of the transducer (Svein Værholm,CMI, pers. comm.). The pressure transducer gives a recording of a numerical unit for each measurement.

Measured_pressure = Numerical_unit ¤ Gain_factor + Offset_factor [Pa]

Measurements with numerical units over 4095, corresponding to about 70 m below the surface was excluded. The transducer was not constructed for deeper levels, but was on occasions dragged deeper. The gain and offset factors for the used transducer was 195.494 and 4369.6.

The distance to the ice subsurface is computed as one way transit time times the current soundspeed times the cosine of the tilt of the ULSbouy.

Distance_to_ice_subsurface = One_way_transit_time ¤ Sound_speed ¤ cos(Tilt) [m]

As the buoy turned out to be very stable the tilt values are usually small giving a cosine close to one. Measurements with a tilt exceeding 20 degrees have been excluded. They are extremely few. The tilt of the buoy is considered when using the Runge-Kutta method, described below.

The two most similar response times, out of four, each fourth minute was stored as numerical units. The average one way transit time was computed using calibration constants ("gain and offset") supplied by the manufacturer. Half the mean of the two numerical units, representing response time, was used.

Numerical_unit_average = ((Numerical_unit_1 + Numerical_unit_2) / 2) / 2

One_way_transit_time = Numerical_unit_average ¤ Gain_factor + Offset_factor [s]

Observations are excluded if any of the two response times exceeds 0.05 s (1952 units) or if the difference between them exceeds 0.001 s (40 units). This time difference corresponds to a draft difference of about 1.4 m (Vinje & Berge 1989). Such measurements, and those with to long response time, are considered to be involving secondary sonar echos, from some off-nadir location. The gain and offset used in the computations are 0.0000512 and 0.00004, respectively.

The sound speed is dependent on depth, water salinity and temperature. The formula used is the simplified version given by Kinsler et al. (1982), as mentioned above.

Soundspeed = Surface_soundspeed + 4.6 ¤ T - 0.055 ¤ T^2 + 0.003 ¤ T^3 + (1.39 - 0.012 ¤ T) ¤ (Salinity - 35) + 0.017 ¤ Depth

T = The daily mean temperature at Depth

The sea surface soundspeed used is 1449.0 m/s, which is valid for surface sea water at a salinity of 35 per mille and a temperature of 0 C. In fresh water the corresponding soundspeed is 1403 m/s (Kinsler et. al. 1986).

As mentioned above salinity data has not been available. A constant value of 33 per mille is used here. Standard salinity values can be taken from tables, according to rules set up by UNESCO (Nikolai Doronin, IAA, guest researcher at NPRI, pers. comm.).

Temperature data were received during the project. The available temperature series are from 72 and 101 m below sea surface, respectively, at the same mooring. The temperature comprise daily means. Using a constant depth of 25 m below sealevel and a constant temperature of -1 C gave a constant soundspeed of 1442 m/s^2, which was used earlier. Better temperature assessments have been included to obtain more accurate values and to better cover the variations with time. This is described separately below.

One per mille difference in the salinity, at constant depth and temperature, gives a difference in the soundspeed of about 1.4 m/s. One degree difference in the temperature, at constant salinity and depth, gives a difference in the soundspeed of about 5 m/s. Ten meters difference in the depth, at constant temperature and salinity, gives a difference in the soundspeed of 17 cm/s, or less, with the used equation, at those depths that are of interest here.

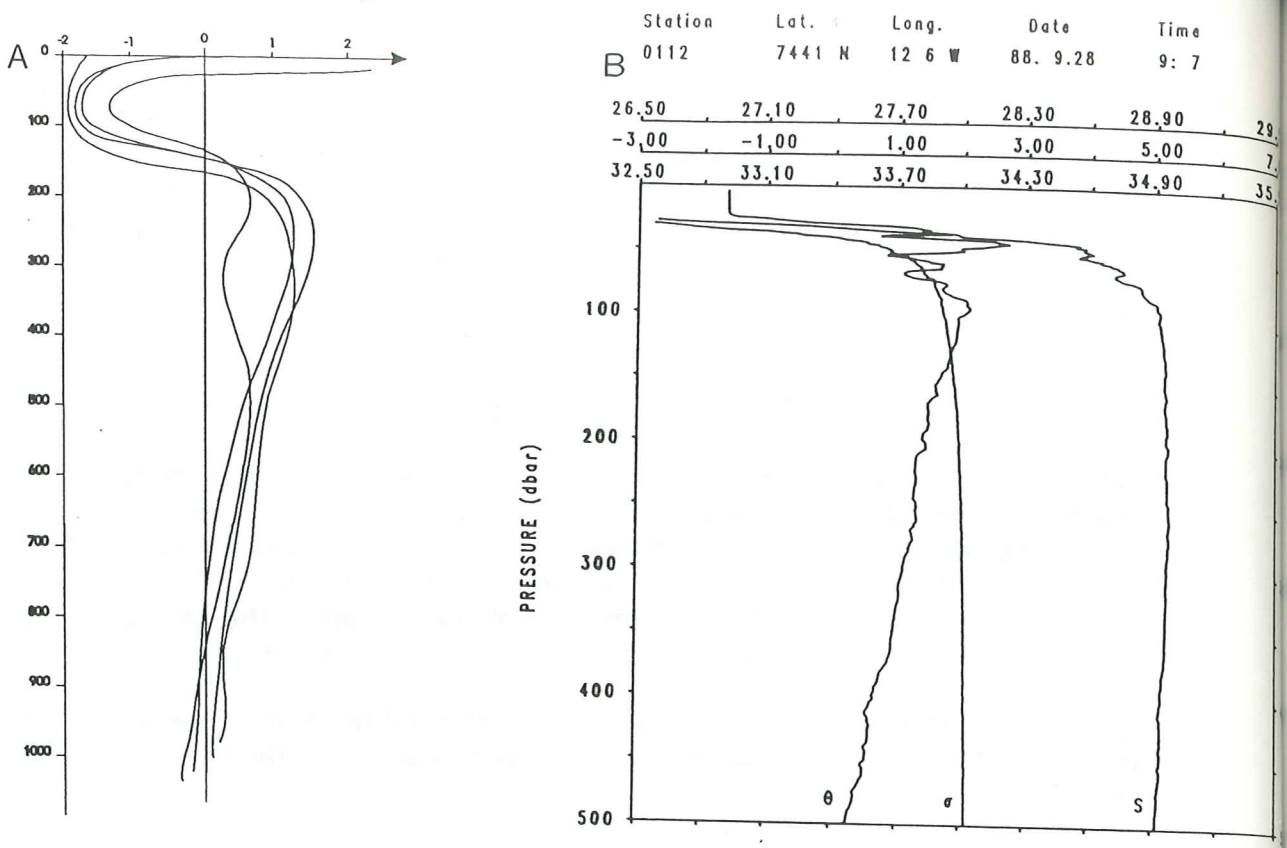

Fig. 21. Temperature profiles in the Greenland Sea. A shows some profiles from the EGC. Adopted from (Helland-Hansen & Nansen 1909). Similar curves are found in (Aagaard & Coachman 1968). B : Profile from one of the CTD measurements closest to the ULS mooring location, during the period June 1987 to June 1988.

Improvements of the temperature used for soundspeed computation

The logarithmic temperature profile

The logarithmic temperature equation is determined using two iterative segments, one to find a good temperature constant and kappa-value for the formula

$$Temperature(Depth) = Temperature_{SS} \times e^{Kappa \times (Depth - Draft)} + Temperature_J \times (1 - e^{Kappa \times (Depth - Draft)})$$

and the second to determine the most representative temperature level in the water column, here assumed to be located half way between the buoy and the ice subsurface.

The first iteration segment consists of the two formulas

$$Kappa_J = (1 / (DD - SD)) \times \ln((T_{DD} - T_{J-1}) / (T_{SD} - T_{J-1}))$$

$$T_J = (T_{DD} - T_{SS} \times e^{Kappa_J \times (DD - Draft)}) / (1 - e^{Kappa_J \times (DD - Draft)})$$

where T = Temperature
DD = Deep Depth (in meters or as index)
SD = Shallow Depth (in meters or as index)
SS = SubSurface (index)
J, J -1 = index of the iteration

The draft is neglected in the computations as this parameter normally is small compared to the depth of the ULS. A mean draft of 2.5 meters has also been tested to improve the approximation. If we have T_J for J = 0 such that dT / dDepth = 0 at Depth = Draft we get T_J, (J = 0) = T_{SS}. T_{SS} is season dependent. At present only two values are used, one for the period September to March and one for the rest of the year. The used values -1.75 C and -1.35 C respectively, for the ice bottom boundary layer, are taken from (Sverdrup et al. 1970). The iteration continues until the temperature difference is below a control value or the number of iterations exceeds a certain limit.

The second iteration segment uses four steps:

Middel_depth = Depth_in / 2

Temperature(Middle_depth) = $Temperature_{SS}$ ¤ $e^{Kappa(Middle\_depth)}$ + $Temperature_J$ ¤ (1 - $e^{Kappa(Middle\_depth)}$)

Soundspeed = Surface_soundspeed + 4.6 ¤T - 0.055 ¤T^2 + 0.003 ¤ T^3 + (1.39 - 0.012*T) ¤ (Salinity - 35) + 0.017 ¤ Middel_depth
(T = Temperature)

Distance_to_ice_subsurface = One_way_transit_time ¤ Sound_speed ¤ cos(Tilt)

The Distance_to_ice_subsurface is used as the Depth_in the next iteration. The first run the depth of the ULS, minus 2.5 meters, is used as Depth_in. The iteration continues until the difference in distance to ice subsurface is below a control value or the number of iterations exceeds a certain limit.

The Runge-Kutta approach

To consider the varying soundspeed with depth and temperature to a larger extent a fourth order Runge-Kutta method has been used. As the method differs quite a lot from the former, a more detailed description is given.

Runge-Kutta methods comprise numerical methods for the solution of initial value problems. They are designed to imitate methods with Taylor series expansion, but without requiring analytic expressions for the higher order derivatives of y. They only involve evaluation of the original function f. The interval is partitioned into a finite number of sub-intervals. The combination of values f(x,y) from these intervals, close to the solution curve, gives good accuracy. The convergence to the exact solution is faster for higher order methods, when the spacing is decreased.

The most well-known Runge-Kutta method is the fourth order Runge-Kutta, also called the classical Runge-Kutta. It employs the four following strategic equations:

$$k_1 = h \text{ ¤ } f(x,y)$$
$$k_2 = h \text{ ¤ } f(x_n + h/2, y_n + k_1/2)$$
$$k_3 = h \text{ ¤ } f(x_n + h/2, y_n + k_2/2)$$
$$k_4 = h \text{ ¤ } f(x_n + h, y_n + k_3)$$

$$y_{n+1} = y_n + 1/6 \text{ ¤ } (k_1 + 2 \text{¤} k_2 + 2 \text{¤} k_3 + k_4)$$

The error is $O(h^4)$.
A very simple example to illustrate the method is the solution of the differential equation:

$$y' = x + y$$
$$y(0) = 1$$

taken from Pohl et. al. (1984).

h = 0.1

x	y	f=x+y	k=h¤f
0	1	1	0.1
0.05	1.05	1.1	0.11
0.05	1.055	1.105	0.1105
0.1	1.1105	1.2105	0.12105

$1/6$ ¤ (0.1 + 2¤0.11 + 2¤0.1105 + 0.12105) = 0.110342

0.1	1.110342	1.210342	0.121034
0.15	1.170859	1.320859	0.132086
0.15	1.176385	1.326385	0.132638
0.2	1.242980	1.442980	0.144298

$1/6$ ¤ (0.121034 + 2¤0.132086 + 2¤0.132638 + 0.144298) = 0.132463

y(0.2,0.1) = 1.110342 + 0.132463 = 1.242805

The correction term equals 0, i. e. the error is negligible and all six decimals are significant.

Implementation in the program

The method is implemented in the program with support from John Thingstad, the University of Oslo, to get it more computer effective.

Starting from the depth of the ULS buoy the distance to the ice subsurface is computed by integration of a number of sub-distances. Each sub-distance is the vertical component of the sound path passed during one timestep. It is computed using the temperature representative for that depth.

The temperature as a function of depth is still logarithmic and found by solving:

$y_1 = a \cdot e^{b \cdot x_1} + c$

$y_2 = a \cdot e^{b \cdot x_2} + c$ for a, b and c,

$y_3 = a \cdot e^{b \cdot x_3} + c$ x = depth y = temperature

i. e.:

$b = (x_3 - x_1)/(x_1 \cdot (x_2 - x_3)) \cdot \ln((y_3 - y_1)/(y_2 - y_1))$

$a = (y_2 - y_1)/(e^{b \cdot x_2} - e^{b \cdot x_1})$

$c = y_1 - a \cdot e^{b \cdot x_1}$

This is possible using the three temperature point measurements, at deep depth, shallow depth and at the ice subsurface. Preferably one of them should be measured at the buoy. On the new series, from the season 1990-1991, temperature was successfully recorded on the bouys.
The current depth is inserted in the formula to get the temperature at that depth.

The soundspeed corresponding to a sub-distance is computed using fourth order Runge-Kutta and the formula from (Kinsler et. al.1982).

k_1 = soundspeed(temp(depth), salinity, depth)

k_2 = soundspeed(temp(depth + step/$_2 \cdot k_1$), salinity, depth + step/$_2 \cdot k_1$)

k_3 = soundspeed(temp(depth + step/$_2 \cdot k_2$), salinity, depth + step/$_2 \cdot k_2$)

k_4 = soundspeed(temp(depth + step $\cdot k_3$), salinity, depth + step $\cdot k_3$)

Salinity is held constant at present.
The step used is transit time /$_{10}$.

current_soundspeed = $(k_1 + 2 \cdot k_2 + 2 \cdot k_3 + k_4)/6$

current_distance = step $\cdot$ current_soundspeed

The distance is translated to vertical distance and compensated for refraction with the use of angle and speed from the previous step in accordance with Snell's law (Bergdahl 1977).

vertical_subdistance = current_distance $\cdot$
cos(current_soundspeed / previous_soundspeed) $\cdot$ previous_angle

Finally draft = depth - sum_of_ sub-distances.

Computed statistics for the draft and ULS depth of a selected time interval

Statistics are computed both for the draft values and the ULS depth values. A modified version of a routine from Numerical Recipes in C (Press et. al.1990) is used. The parameters computed are mean value, maximum and minimum value, distance to mean, variance, standard deviation, skewness and kurtosis. Skewness

and kurtosis are computed after a check that the variance does not equal zero, which prevents the computation. The number of rejected samples is counted and not included in the computations. Unrealistic values are also excluded, for example too much negative draft or depth values too close to the surface. For the computation of draft statistics the user is asked for the limit value for exclusion of drafts. Any limit can be chosen, depending on the purpose. In the test series -0.2 m is used. When using this limit, there is some margin for inclusion of values caused by wave effects, but gross fliers are excluded. Minimum and maximum value extraction, however, uses the whole draft array, excluding only those values rejected in the draft computation process. For the ULS depth statistics a constant value of 20 is used at present.

The algorithm for the draft unit:

1. Ask the user for the desired time interval (start time and end time). Year, month and day are compulsory. Hour and minute are optional. Read as character strings.

2. Convert the given time values from character to integer format. Separate different time parameters, hour, year etc. Compute Julian daynumber and minute-number in day. Compute time passed since 1 January 1980.

3: Compute the probable number of samples within the time interval. Compute the offset value for the data file (in bytes) to the first sample of the interval.

4. Combine path, file prefix, year, month and file type to one unit for the first ULS data file (month) of the interval. Try to open the corresponding file for reading. If not succeeded or if the file doesn't exist on the directory, give error message and exit.

5. Sort the file in case it is slightly unsorted. The ULS data files are sequential, but some times a few records are in wrong sequence.

6. Move to the position defined by the computed offset and search the vicinity for the first record of the time period.

7. Read the ULS values from the file and check if they are within reasonable limits. If not, set mark and continue sequentially to the next record. In reading the rest of the data line check if the data are followed by any of the specified marking characters. If so, store a value in a "marking" array and add one to the (appropriate) counter.

8. If the values are considered correct find the air pressure value for the twelve hour interval that encompasses the current time.

9. Find the depth of the ULS by using the water pressure, adjusted for the contemporary air pressure, salinity and local gravitational force.

10. Find the correct temperature values and solve the temperature equation.

11. Compute the distance to the ice bottom-side using the transit time and computed soundspeed, based on temperature.

12. Compute the draft as the difference between the depth of the ULS and the distance to the ice subsurface.

13. Store time, draft and ULS depth in separate arrays and on temporary file for statistical computations later.

14. Repeat 7-13 for as many records as the computed number of samples, minus a few. If end of file is encountered change to the following ULS data file (if it exists) and continue.

15. Check the few remaining records to find the finishing record of the interval, repeating 7-14 for the computation.

16. When the whole interval is past, or no more ULS data file is found, compute statistical parameters for draft and ULS depth data.

17. If the user requests it, print the statistical values on a file also including position, interval, temperature(s) and sound speed.

18. If the user requests it, tabulate the data arrays on a file in ASCII format. Values except draft is optional. Header is optional.

19. Store average draft for the period, compute and store average draft per day. This is used in the combination with average drift to compute volume (vertical area).

Test and results

The draft unit was tested on all time periods that were cloud-free for minimum three days over the Greenland Sea, given in tab. 8. Example of a 24 h diagram is given in fig. 22. Statistics examples are given in tab. 5 and 7. Example from a tabulated data file is given in tab. 6.

Mean:	Std. Dev.:	Std. Error:	Variance:	Coef. Var.:	Count:
-3,374	3,168	,074	10,037	-93,905	1835
Minimum:	**Maximum:**	**Range:**	**Sum:**	**Sum of Sqr.:**	**# Missing:**
-24,313	-,144	24,169	-6190,904	39294,91	0
Mean:	**Std. Dev.:**	**Std. Error:**	**Variance:**	**Coef. Var.:**	**Count:**
-46,979	2,36	,055	5,571	-5,024	1835
Minimum:	**Maximum:**	**Range:**	**Sum:**	**Sum of Sqr.:**	**# Missing:**
-56,544	-44,261	12,283	-86206,524	4060115,846	0

Data for the period 880420. Unreasonable values and values above 0.2 m not included.

Tab. 5. Example statistics computed for the ice draft and ULS depth.

Julian day	Minute number	Draft	Depth of ULS
2	24	1.391	44.094
2	28	4.320	44.094
2	32	3.508	44.074
2	36	4.576	44.055
2	40	4.835	44.094

Tab. 6. Example from a tabulated data file.

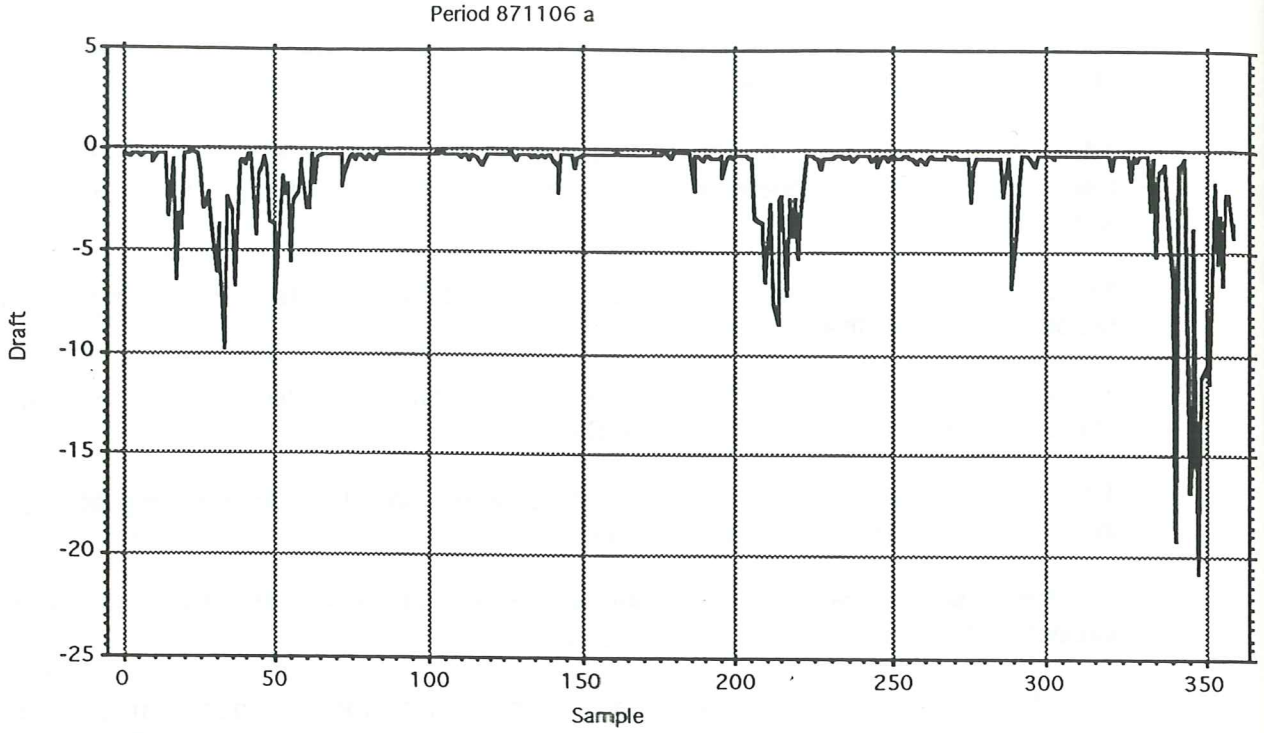

Period 6/11 87 - 7/11 87 a, draft.

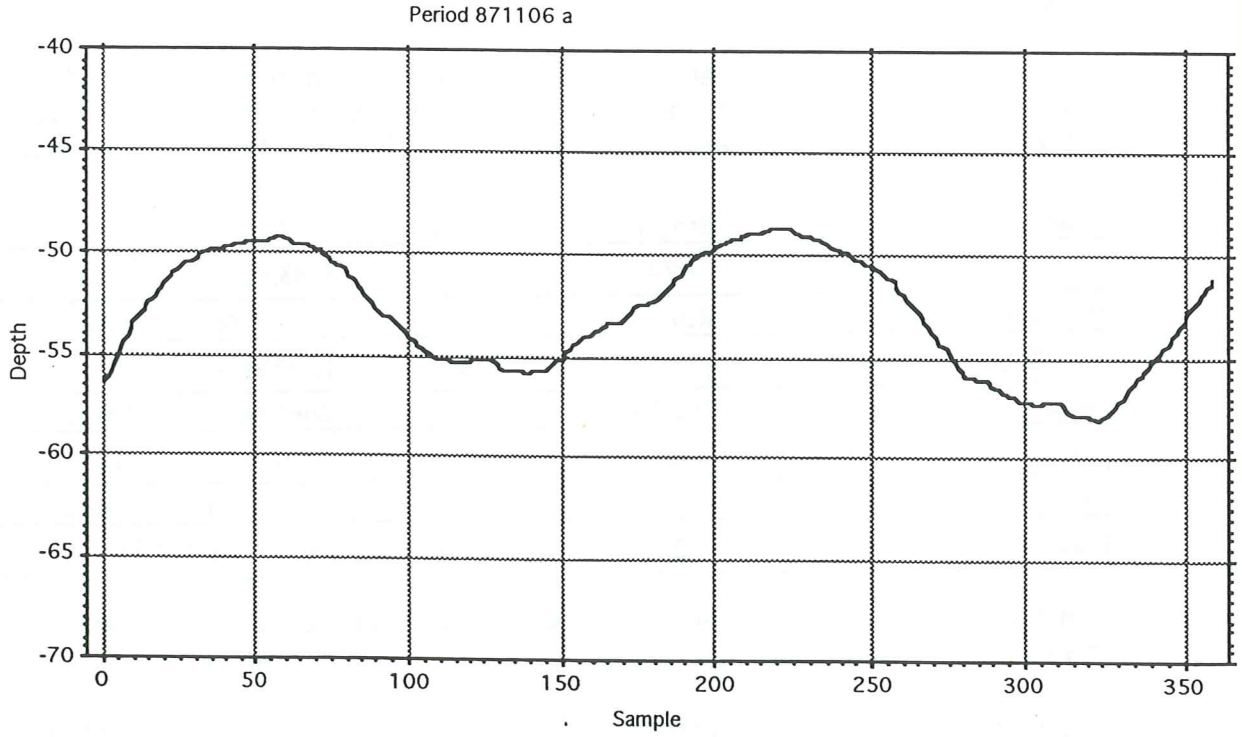

Period 6/11 87 - 7/11 87 a, uls depth.

Fig. 22. Example of a 24 h draft and ULS depth diagram plotted from data computed with the developed program. Temperature from 72 m b. s. l. used for soundspeed computation. From (Olsson 1992).

Descriptive parameters for ULS measurement.
Printed Fri Jul 19 03:52:45 1991

The period is from 20 Jan 1988 at 10:08 to 21 Jan 1988 at 12:16.

Latitude: 75 3.2 Longitude: -12 -11.2 Waterdepth: 1242 m

Temp. at 101 m	Temp. at 72 m	Computed temp.	Soundspeed
-0.151	-1.236	-1.236	1440.224
-0.321	-1.466	-1.466	1439.962

==========

The data are DRAFT data.

MEAN of this period is: 2.330 based on 388 values

54 samples were marked as approximate
3 samples were regarded out of reasonable limits and therefore not included

The MAXIMUM value is: 12.593 and the MINIMUM value is: 0.171

Values less than -0.20 were not included in the statistical computations.

The MEAN DEVIATION is: 1.649 and the STANDARD DEVIATION is: 2.098

The VARIANCE is: 4.403

The SKEWNESS is: 1.302 and the KURTOSIS is: 2.017

==========

The data are ULS DEPTH data.

MEAN of this period is: 44.523 based on 391 values

The number of approximate values as above.

The MAXIMUM value is: 47.699 and the MINIMUM value is: 42.659

The MEAN DEVIATION is: 1.138 and the STANDARD DEVIATION is: 1.430

The VARIANCE is: 2.046

The SKEWNESS is: 0.840 and the KURTOSIS is: -0.473

Tab. 7. Example of description table for the draft computation. Current information may be included. From (Olsson 1992).

Ice motion assessment methods

Ice drift can be achieved by several methods, most of them indirect. Someone or something can be put on a floe and log the drift during the voyage. The drift can be modelled, based on various influencing factors. Wind and current are dominating factors. Remote sensing from various platforms can be utilized, and is earning a growing interest, not least using ERS-1 data. Satellites represent "stable" platforms for ice displacement studies (Hall & Martinec 1985).

Already in the late 19:th century Nansen let the vessel Fram travel with the drift ice in the Transpolar current and made several important observations (Nansen 1897). Fig 23. Later research camps have been established on larger ice floes, measuring various ice parameters, usually including drift. One of the most extensive of these projects was AIDJEX (Arctic Ice Drift Joint EXperiment) in 1970-1978. One major dedication was towards ice drift modelling and evaluation of the different factors contributing to the resultant ice drift. For example Moritz (1988) made ice drift modelling for the East Greenland Current area.

A rather successful method of logging ice drift is to airdrop so called ICEXAIR capsules, connected to the ARGOS tracking system, on the ice, for example in the Transpolar current, fig 24. This has been done by the Norwegian Air Force since 1978 (Vinje & Finnekåsa 1986b). The capsules are transmitting a carrier wave, sea and air temperature, air pressure, battery status and an indicator for drift in water. The Doppler shift of the carrier is used to determine the position of the buoy. It is computed at the ground receiving station. The accuracy is +/- 200 m (Johnsen & Vinje 1987). With time the tracking results in trajectories for each capsule. Together they can give a good impression of the general ice drift pattern, Fig 25. Locally they also show short time details. Similar transmitters are also used to track for example polarbears and icebergs.

A method mainly used for tracking icebergs is to continuously survey the position of invariant features on them from a known position, usually on land. This, however, requests that they can pass not too far away without running aground.

Even though "ice-rides" secure high precision, particularly if GPS satellite positioning is used, it is laborious and expensive. It's therefore not really practical to do it over more extensive areas. To get good coverage both in time and space, remote sensing offers a suitable alternative. Depending on scale, helicopters, aeroplanes or satellites can be the most appropriate platform. Tryde (1986) gives examples and a little comparison. Korsnes (1991) has also used different platforms. Airborne platforms can get to a specific point at a chosen occation and often operate also under cloud cover. Orbiting satellites have the advantage of frequent reoccurrence over the same area and, for polar orbiting platforms, coverage further north. The convergence of the orbits towards the pole increases the degree of overlap between consecutive orbits in polar areas, compared to further south. This gives better possibilities for monitoring, for example ice. It also offers more chances to find cloudfree images over a region of interest.

Three satellites, of two different concepts, have been of major concern in this project: NOAA-9 and NOAA-10 and ERS-1. The NOAA satellites use passive instruments covering the spectrum between red and thermal infrared. ERS-1 uses mainly active instruments in the microwave part of the electromagnetic spectrum, for example imaging synthetic aperture radar (SAR). The SAR transmits radar pulses.

The return signal is sampled along the trajectory. The Doppler shift of the echos are used to synthesize a larger aperture than the real aperture. The resolution is independent of range. Azimuthal resolution is half the size of the real aperture. More details on SAR and computations giving resolution can be found in (Stewart 1985). The satellites are briefly described below.

Fig. 24. Example of ICEXAIR bouys at Longyearbyen. Courtesy T. Vinje.

NOAA -National Oceanic and Atmospheric Administration - satellites

The NOAA meteorological satellite system is sun synchronous. The satellites have near-polar orbits at 98.9 degrees. Two satellites are positioned with a nominal orbit plane separation of 90 degrees. One is operating in morning descending orbit and the other in afternoon ascending. Orbital height is about 840 km. In a geometric study over Scania, Sweden, Brasjö (1990) found a somewhat higher altitude to give better results. The first satellite in the second generation of the system, TIROS-N, was launched in 1978. A comprehensive listing of system parameters is found in table tab. 8. (Langaas 1992).

The major instruments on the NOAA satellites are:

AVHRR	Advanced Very High Resolution Radiometer
TOVS	TIROS Operational Vertical Sounder
DCLS	Data Collection and Location System
SEM	Space Environment Monitor

On the AVHRR previously broad VIS/NIR-bands are separated into five channels. Their spectral band width is listed in tab.8. The spatial resolution varies between 1.1x1.1 km and 2.4x6.9 km.fig. 26. The swath width is approximately 3000 km, scan angle 55.4 degrees. The wide swath causes an increasing amount of atmospheric contamination and geometric distortion towards the swath edge. The effects of intervening atmosphere on surface radiance measurements may be significant. Odd-numbered satellites therefore have "split-window" channels in TIR (Massom 1991).

Temporal coverage towards the poles is good. Poleward of 60 degrees N or S the distance between two consecutive tracks is less than the swath width (Massom

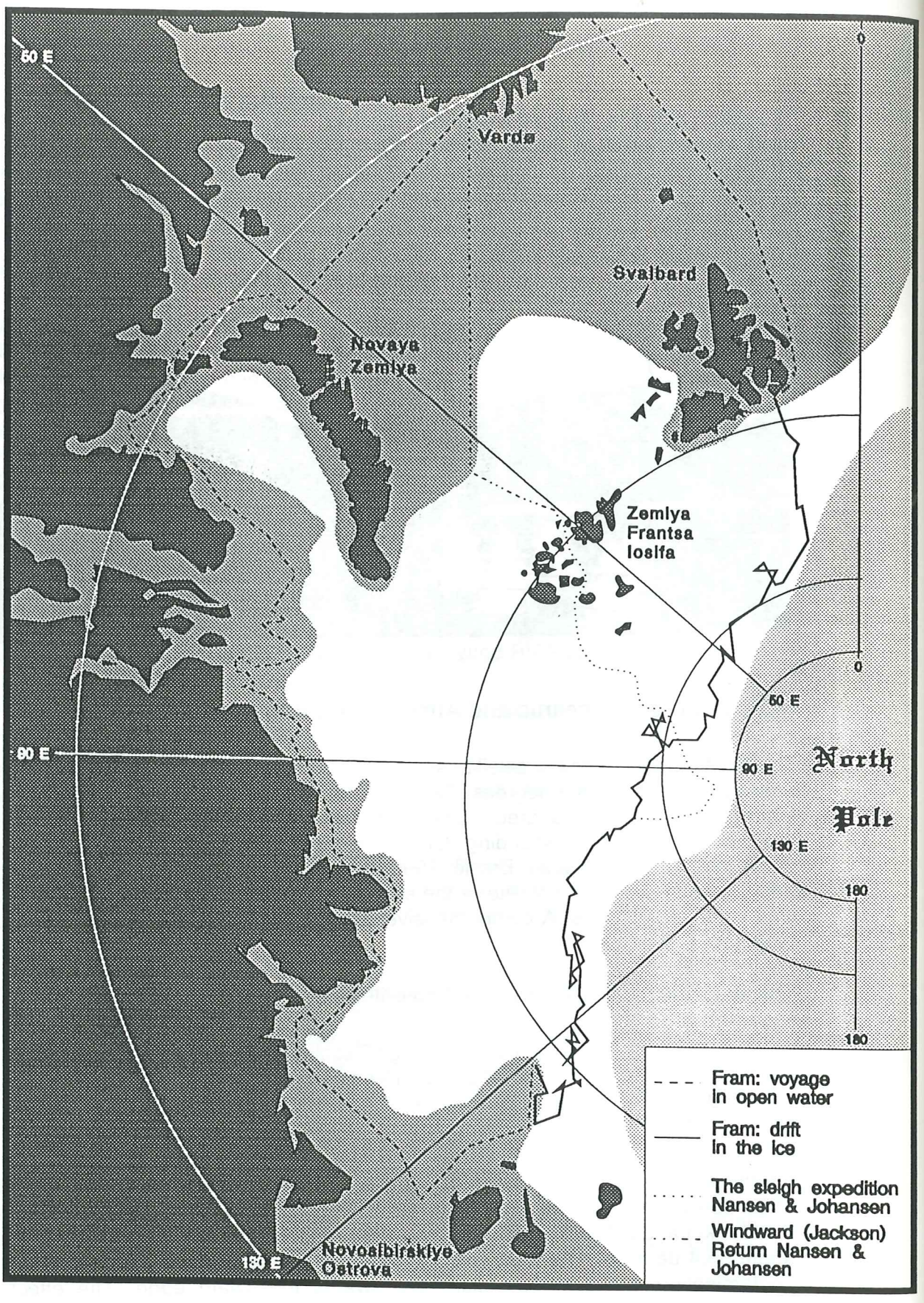

Fig. 23. Generalized version of the map showing the route of the first Fram expedition 1893-1896. Except nuclear submarines and arctic icebreakers, Fram is the vessel that has been furthest north in the pack ice. 1992 is her 100:th anniversary. Adopted from (Nansen 1897).

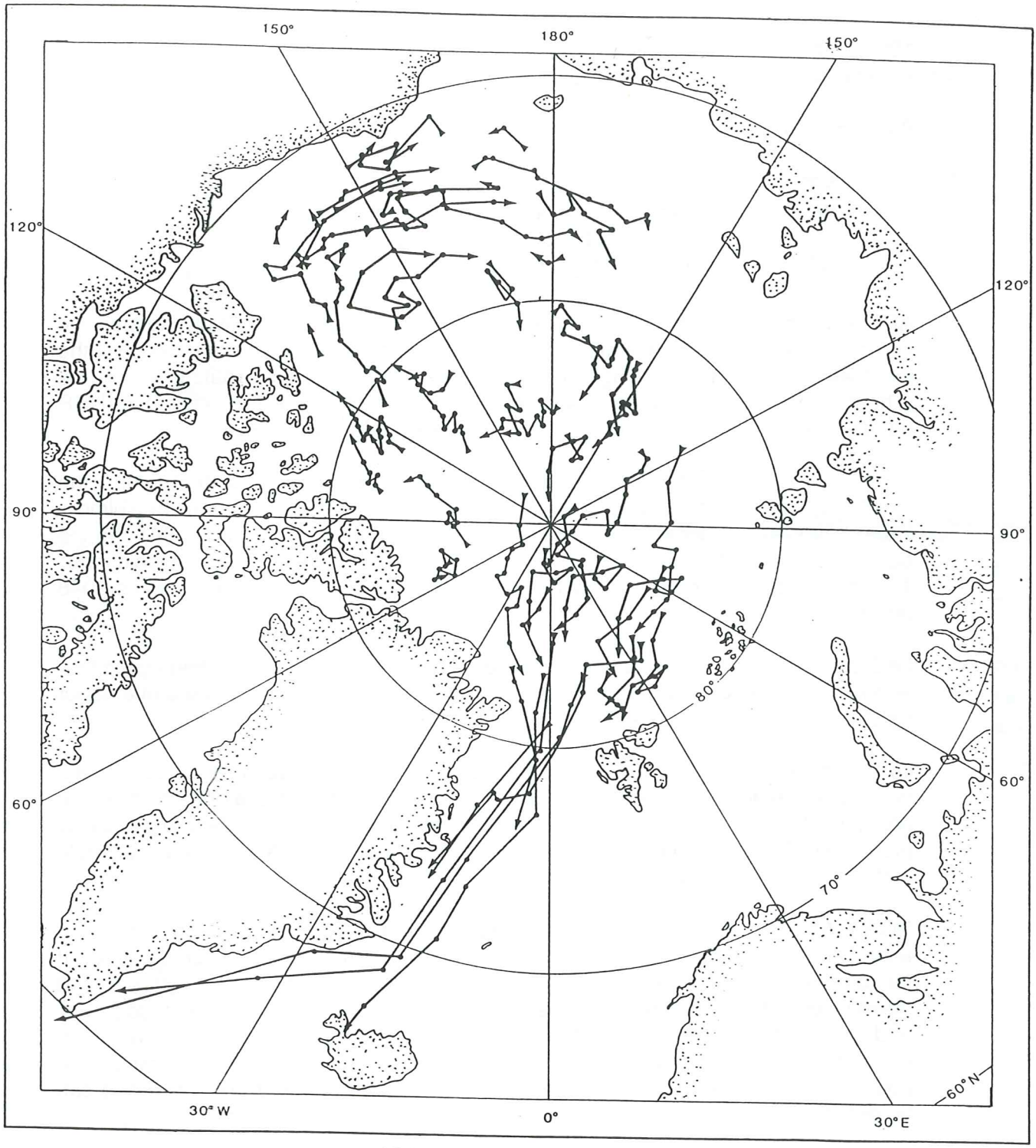

ARCTIC OCEAN BUOY PROGRAMME

DRIFT OF BUOYS DURING THE FIRST YEARS

Fig. 25. Arctic ice drift as illustrated by drift vectors from drifting ICEXAIR bouys. Courtesy T. Vinje.

1990). It covers regions further poleward than the Landsat satellite system. The view is, however, limited by clouds and polar-night darkness.

AVHRR data is generated in four formats:

APT	Automatic Picture Transmission
HRPT	High Resolution Picture Transmission
LAC	Local Area Coverage
GAC	Global Area Coverage

APT is a continuously transmitted signal. It can be received by relatively inexpensive equipment and an omni-directional antennae. It was for example done onboard the icebreaker HMS Ymer during the Arctic cruise 1980 for ship routing in the ice (Thompson 1986). APT data is a processed subset of two of the original AVHRR bands. The data is analog with a resolution of 4 km (Massom 1991).

HRPT is successor of APT. It is direct readout to a receiving station, when the satellite is above the horizon. For example the west Arctic is covered by Gilmore Creek (Alaska), southeast Canadian Arctic by Wallops Island (Virginia,USA) and the North Atlantic/Nordic Seas by Tromsø (Norway) satellite station. Spatial resolution is 1.1 km and spectral resolution is 1024 levels(10 bit). Each scan line contains 2048 pixels.

LAC data is full resolution data recorded onboard the satellite. Recording capacity is about 10 min per orbit, about 4000 km on the ground. Resolution is the same as for HRPT.

GAC is data recorded for an entire orbit, 102 min. Spectral resolution is 1024 levels, but spatial resolution is 4x4 km. Four out of every five samples along the scanline are used to compute one average value. Just data from every third scan line is processed (Massom 1991). The pixels are not square. With GAC virtually the whole surface of the Earth can be viewed daily.

NOAA AVHRR images have been used for broad scale general pack ice drift analysis, for example (Zhang 1988) (Zhang 1989) (Dech 1990) (GSP-group 1990). It has been used to separate different ice types. Floe, lead and fracture patterns and polynya evolution have been studied. Variations in ice sheet surface topography and emissivity can be detected. Arctic sea ice snow cover evolution has been monitored. Subarctic snowcover and water equivalent have been assessed. The polar (oceanic) front can be detected from sea surface temperature. Upwelling can be detected. Normally that corresponds to zones of high biological productivity.

Other instruments onboard

TOVS is used to compute vertical atmospheric temperature and humidity profiles. It consists of three subsystems:

HIRS/2	High Resolution Infra Red Sounder II
SSU	Stratospheric Sounding Unit
MSU	Microwave Sounding Unit

DCLS is by CNES referred to as ARGOS. It is a system for locating the position of transmitters connected to fixed or moving objects, for example ice bergs or polar bears. It can also monitor environmental data from the transmitters.

SEM measures solar proton, alpha particle and electron flux density. It also scans energy spectrum and particulate energy disposition at satellite altitude. It consists of three subsystems:

TED	Total Energy Detector
MEPED	Medium Energy Proton and Electron Detector
HEPAD	High Energy Proton and Alpha Detector

The last HEPAD on the NOAA system was flown on NOAA-7. It is now flown on GOES satellites (NOAA 1988).

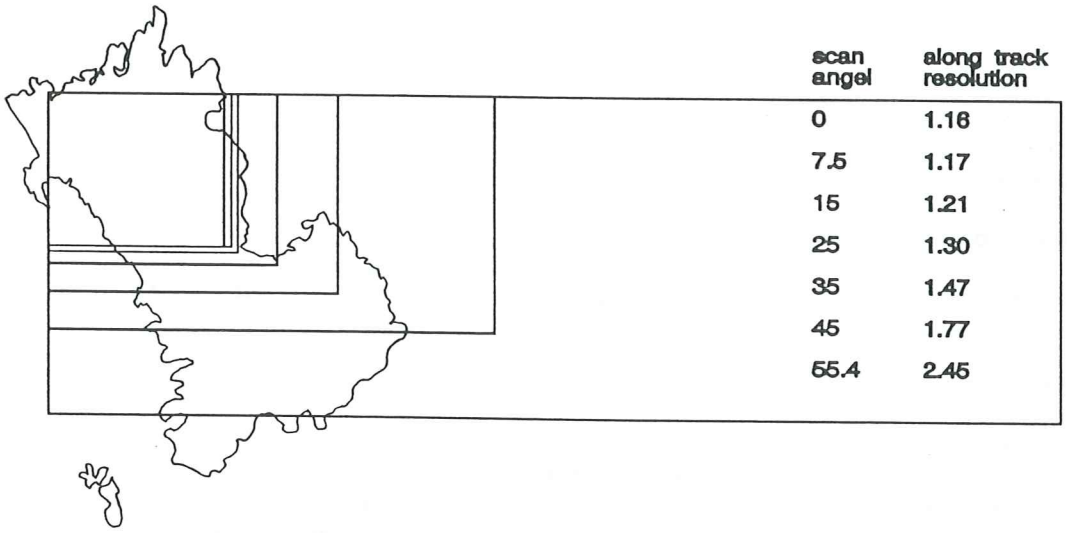

scan angel	along track resolution	across track resolution	nadir distance
0	1.16	1.16	0
7.5	1.17	1.18	110
15	1.21	1.26	223
25	1.30	1.48	308
35	1.47	1.92	583
45	1.77	2.94	833
55.4	2.45	6.70	1350

Fig. 26. The resolution of NOAA AVHRR data compared to the perimeter of the island Hallands Väderö, west of Sweden, at a scale of 1:50 000. Based on resolution information in a figure in (Saull 1985).

Status	
TIROS-N	launched October 1978
NOAA-6	launched June 1979, deactivated March 1983, reactivated June 1984, deactivated March 1987
NOAA-7	launched June 1981, deactivated July 1987
NOAA-8	launched March 1983, deactivated June 1984
NOAA-9	launched December 1984, deactivated October 1989
NOAA-10	launched September 1986, operational status
NOAA-11	launched October 1988, operational status

Operator: National Oceanic and Atmospheric Administration (NOAA), USA

Commercial status: Public domain data

Receiving stations[1]:		
	Africa:	6
	Antarctica:	5
	Asia:	18
	Australasia:	9
	Europe:	22
	North America:	7
	South America:	3

Orbital Characteristics

Coverage cycle:	9 days
Orbital period:	102 min
Orbit inclination:	98.9
Orbital height:	833 km

Nominal equatorial passing times (at launch):

	Descending node	Ascending node
NOAA-6, -8 and -10	07:30-08:30	19:30-20:30
NOAA-7, -9 and -11	13:30-14:30	01:30-02:30

Sensor Characteristics

Scan angle range:	+/- 55.4	
IFOV:	1.39 - 1.51 mrad	
Ground resolution cell:	At nadir	1.1x1.1 km
	AT extreme scan angle:	2.4 km (along track)
		6.9 km (across track)
Ground coverage:	3000 km (across track)	
Quantization:	10 bits (1024 gray levels)	
Line rate:	360 lines/min	

Spectral range [micrometer] of the Spectral channels

1[2]	2[3]	3[4]	4	5[5]
0.58-0.68	0.72-0.95	3.55-3.93	10.3-11.3	11.5-12.5

Calibration:		
	infrared channels	stable black body and space
	visible channels	no in-flight calibration other than space

Tab. 8. Characteristics for the later NOAA satellites and the AVHRR.

[1]Those contained in the ESA Earthnet Programming Office Database of AVHRR HRPT ground stations, June 1991.

[2]Channel 1 on TIROS-N: 0.55-0.90

[3]Channel 2 is usually given as 0.72-1.1. According to spectral response curve in Kidwell(1986), and confirming letter from Kidwell (1987) o.72-0.95 is a more correct range.(ref. Langaas, 1992)

[4]Channel 3 will from the next generation be divided into two channels denoted 3a and 3b. 3a will cover the range 1.55-1.65 and be used in daylight hours. 3b will be spectrally similar to the current channel 3 and be used at night time only.

[5]Channel 5 of the AVHRR was/is not included on NOAA-6, -8 and -10.

ERS-1 European Remote sensing Satellite -1

ERS-1 is the first satellite in a new generation of remote sensing satellites for environmental monitoring. It was launched in July 1991 and has thisfar been successful. The near-polar orbit is at a height of 780 km (Massom 1991) 785 km, (Arheimer & Glave 1991), above the earths surface, at an inclination of 98.52 degrees (reference orbit). Expected lifetime of the satellite is three years. The schedule is as follows (Massom 1991):

Phase 0:	Orbit acquisition, initial switch on and testing of the satellite, about 2 weeks
Phase I:	Commissioning phase, 3 day repeat cycle, 3 months
Phase II :	First multi-disciplinary phase, 35 day repeat cycle
Phase III:	First ice phase, 3 day repeat cycle, longitudinal phase optimised for Arctic sea ice experiments, 3 months
Phase IV:	Long multi-disciplinary phase, same characteristics as phase 2, 9 months
Phase V:	Second ice phase, same characteristics as phase 3, 3 months
Phase VI:	Long geodetic phase, 176 day repeat cycle, until end of mission

The platform is based on a concept developed in the SPOT program. It is equipped with five major instruments working in infrared and microwave wavelengths:

ATSR-M	Along Track Scanning Radiometer and Microwave sounder
ALT	radar ALTimeter
AMI-SAR	Active Microwave Instrument - Synthetic Aperture Radar
AMI-SCATT	Active Microwave Instrument - wind SCATTerometer
PRARE	Precise Range And Range-rate Experiment

ATSR-M consists of a four band infrared radiometer (1.6, 3.7, 11, 12 microns), together with a nadir-looking, two channel passive microwave sounder. The swathwidth is 500 km and ground resolution is 1 km for the infrared radiometer and the microwave sounder has a ground resolution of 22 km.

Sea surface temperatures over 50x50 km in up to 80 % cloud cover can be measured at an absolute accuracy of 0.5 K and the radiometric resolution is 0.1 K (Massom 1991). This is better than for other similar satellite infrared sensing systems. It is achieved using conical scanning technique and improved blackbody calibration sources (Arheimer & Glave 1991).
The infrared radiometer is used to measure sea surface and cloud top temperatures. The microwave sounder gives information about the total water vapour content of the atmosphere. It also gives information for correcting the ALT direction. The fore scanning track is 52 (Arheimer & Glave 1991) 55 (Massom 1991) degrees ahead of the sub-satellite-point and the aft is at 0 degrees (nadir). Data from both swaths are combined to get atmospheric correction for the computation of surface temperature, together with information from the microwave sounder (Arheimer & Glave 1991).

ASTR-M has a good potential for ice and oceanographic studies and has near complete polar coverage. It can be used to map icetype, polynyas and ocean/ice boundaries. Band 1 can be used to discriminate between snow and clouds (Massom 1991).

ALT is a puls-radar directed at nadir. It has a pulse-limited footprint with a diameter of 16-20 km, depending on the surface. The precision of the altitude measurements is within 10 cm. Using the ATSR-M microwave sounder for range correction within 4 cm can be reached, if the sea state is known (Massom 1991). Return echos are processed onboard 20 times a second, to give time delay, wave form slope and power level, and averaged to yield 1 s mean values. It operates in two different modes: ice mode (1.5 m of range) and ocean mode (0.4 m of range). Ice parameters need more processing (Arheimer & Glave1991). Significant wave height is computed based on the response time of the signal and wind speed based on the energy level of the echo.

Possible applications are:

- detection of ice edge position
- ice surface roughness and topography -> drag coefficient
- ice concentration and compactness in the marginal ice zone
- detection and quantification of leads and polynyas
- wind- and wavefield information
- swell penetration in ice
- average sea ice thickness distribution (from freeboard measurements)
- separation of sea ice types
- ice sheet elevation
- glacier topography
- mapping of shelf margins
- ice sheet massbalance/ stability/ dynamics
- delineation of ice streams, drainage basins and outlet glaciers
- identification of equilibrium line
- delineation of dry and wet snow and bare ice zones on large ice masses
- detection of tabular icebergs, freeboard measurement -> thickness

The AMI-SAR has two modes: image mode and wave mode. The frequency is 5.3 GHz, 0.05 MHz (C-band) and the polarisation is VV (vertical transmitted and vertical received). The ground resolution is 30 m. In image mode the swathwidth is 80 - 100 km . In wave mode the sample width is 5 x 5 km, every 200/300 km. The incidence angle is 23 degrees to the right of the orbital track, about 250 km from the sub-satellite-track on the ground. The satellite can also be rolled to get an incidence angle of 35 degrees .

Image mode can not be stored onboard and is therefore just operational within line-of-sight of one of the receiving stations in Kiruna, Fucino, Gatineau, West Freugh or Fairbanks. It has a minimum switch-on-time of two minutes. The high energy demands of AMI-SAR in image mode limits its use to maximum 10 minutes per orbit. The coverage on earth is between 85 degrees N and 78 degrees S.

Remote sensing and image processing

Remote sensing of sea ice

To find ice drift displacement vectors it is important that the same feature can be recognized in both images. The large IFOV (Instantaneous Field Of View)towards the swath-limits of NOAA AVHRR images sometimes makes recognition impossible. Langaas (GRID-Arendal, pers. comm.) recommends use limited to the central +/- 35 degrees or so. Images from TSS often have the Greenland sea

towards the outer part of the image. If the pixel-size for the area of interest is reasonable in both images, the next step is to select the position of the feature in the respective image. In NOAA AVHRR images the features usually have differing contrast compared to the surroundings. In ERS-1 images the features normally have differing surface roughness compared to the surroundings.

Ice and water have rather different reflectance in the visible and near infrared part of the electromagnetic spectrum. The reflectivity of ice varies though, depending on impurities and possible surface cover (Hall & Martinec 1985). Ice/water images normally have bimodal graylevel histograms, fig. 27. Jayaweera (1976) made use of this early in the NOAA-satellite history. He separated ice and water by thresholding data from NOAA-2.

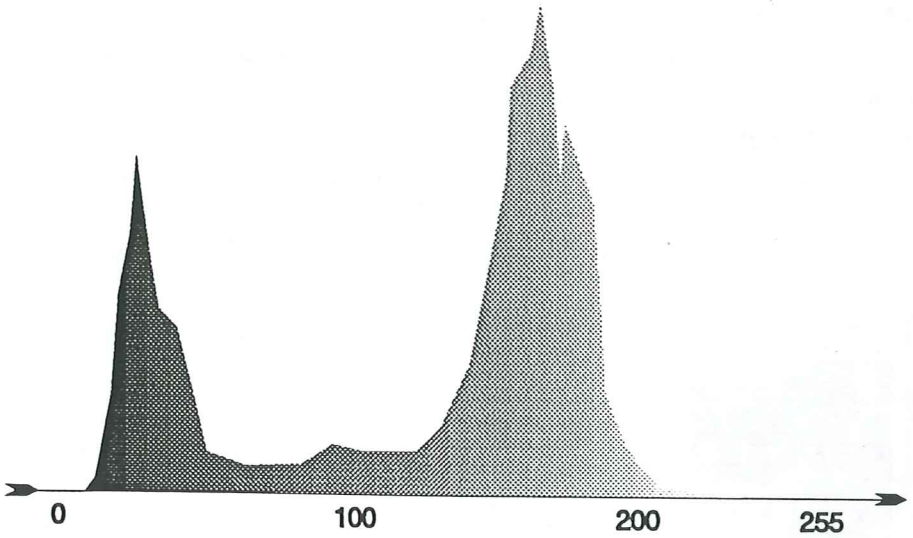

Fig. 27. The normal bimodal shape of the graylevel histogram of an ice image. Based on a figure in (Korsnes 1991).

However clouds, atmospheric attenuation and polar darkness makes remote sensing of the Arctic more difficult. New ice, melting and freezing and divergence of the ice field can make the appearance of the ice features change. Thereby recognition of them gets more difficult.

Cloud cover is a general problem to visual and infrared remote sensing in the Arctic. The marginal ice zone itself is a cloud generator. (GPS-group 1990). Several authors have dealt with the problem of separating ice and cloud features. Thompson (1986) uses colour composites of enhanced Landsat TM images to separate clouds, ice, water and land. It is primarily for visual inspection. High clouds are colder and differ markedly from ice and water in thermal infrared channels. Lower clouds can sometimes be separated in the visible and near infrared channels, but less easy in thermal channels. Hansen has set up a scheme for cloud separation using AVHRR data (Birger Ulf Hansen, UoC, pers. comm.). Alm (1991) separated both water and ice and different cloudtypes using channel 1 minus channel 2, together with channel 4. They are also the only useful channels of NOAA-9 (channel 5 is missing and channel 3 is distorted, at least 1987-1988). Channel 1 - 2 is similar to the second principal component. Alm (1991) separated ice and water under a cloud cover of moderate transmission (50 %). Dech (1990) also tracks ice floes under cloudy conditions. Nakayama et. al. (1987) separates low clouds, snow and sea in an area in northern Japan, using methods involving

fractal dimension, local fractal dimension and lower order statistics. The image used is channel 4 and classified blockwise.

Atmospheric attenuation makes the general graylevel vary between images. The wide swath of NOAA AVHRR, ca 3000 km, also causes more attenuation towards the swath edges (Sindre Langaas, GRID-Arendal, pers. comm.). The gray level in channel 1 and 2 can be normalized using non-turbid, clear water as a measure of zero ground reflectance (Stewart 1985) (Karin Hall-Könyves, UoL, pers. comm.) (Alm 1991). Larouche (Pierre Larouche, IMLFO, pers.comm.), however, questions its general applicability. Channel 1 and 2 are not useful during the polar darkness.

During polar darkness merely longer wavelengths, thermal and microwave, or active remote sensing can be utilized. Foster, however, reports the light sensitive DMSP can be utilized for ice studies during moonshine (James Foster, GSFC, pers. comm.). Primarily enhanced AVHRR channel 4 has been used for sea-ice studies during the winter season (Dey 1980). Gradient ratio, greylevel = $^{(x-y)}/_{(x+y)}$, reduces the effects of physical temperature variations in the ice radiating layer (Hall & Martinec 1985). Active microwave remote sensing is independent of external illumination source. Successful real-time test, using ERS-1 data were executed in the Barents Sea , at the beginning of March 1992. Fig. 28 gives the possible sun illumination for different northern latitudes.

Lat.	1/1	1/2	1/3	1/4	1/5	1/6	1/7	1/8	1/9	1/10	1/11	1/12
80 N			0600 0220	1605					2145	1015 0200	0000 0215	
79			0640 0200	1540 0250					2015	1030 0150	0000 0245	
78		0000 0115	0710 0150	1520 0220					1910	1035 0140	0000 0315	
77		0000 0200	0740 0140	1500 0200					1810	1040 0132	0000 0330	
76		0000 0230	0800 0130	1450 0145					1730	1045 0126	0105 0240	
75		0000 0225	0832 0124	1446 0137					1654 0215	1049 0120	0323 0207	
74		0000 0311	0847 0119	1435 0128	2325				1632 0153	1055 0115	0419 0148	0000 0036
73	0000 0005	0222 0213	0859 0114	1425 0122	2113				1613 0139	1059 0111	0501 0136	0000 0129
72	0000 0121	0331 0150	0911 0109	1417 0116	2013				1557 0129	1102 0107	0535 0127	0000 0159
71	0000 0152	0419 0136	0921 0106	1409 0111	1929			2303	1543 0121	1105 0104	0603 0120	0000 0221
70 N	0000 0215	0456 0126	0930 0102	1402 0107	1854			2117	1529 0115	1108 0100	0626 0114	0000 0238

24 hour daylight, i. e. the sun does not set

Twilight all night, never complete darkness

No daylight and no twilight, i. e. the sun does not rise. Moon- and starlight possible.

Fig. 28. Daylight and twilight duration at different latitudes. Twilight is the time between sunrise or sunset and when the sun is 6 degrees below the horizon. Only twilight is given when the sun is continuously below the horizon. Adopted from (Eide 1983)

Image enhancement

To improve the image analysis the images may be enhanced. The methods of colour composites and histogram modification, normally contrast enhancement, are image enhancement primarily for visual inspection. Filtering is a common procedure in image processing, to enhance certain features. It can also be used to smooth images, for generalizing etc. The image is convolved with a filter, i e each pixel is given a value, computed using some kind of weighing function of its neighbours. Edge enhancement is of interest to find ice floe edges and particular features. Edge enhancement filters are often directional. They add values on one side and subtract the values on the other side. Edges thereby get high values and homogeneous areas get low values, fig 29.

Texture based analysis can be used to separate areas of ice from areas of open water. Alm (1988) used nine rotated masks to delineate ice features. His method gives almost no border effects, which normally occur. Texture is also important in analysing SAR images. It has been studied by several researchers in different areas. For example (Barber & LeDrew 1991) used it to discriminate ice, land and water. Weydahl (1991) compared cross correlation values for forest and water.

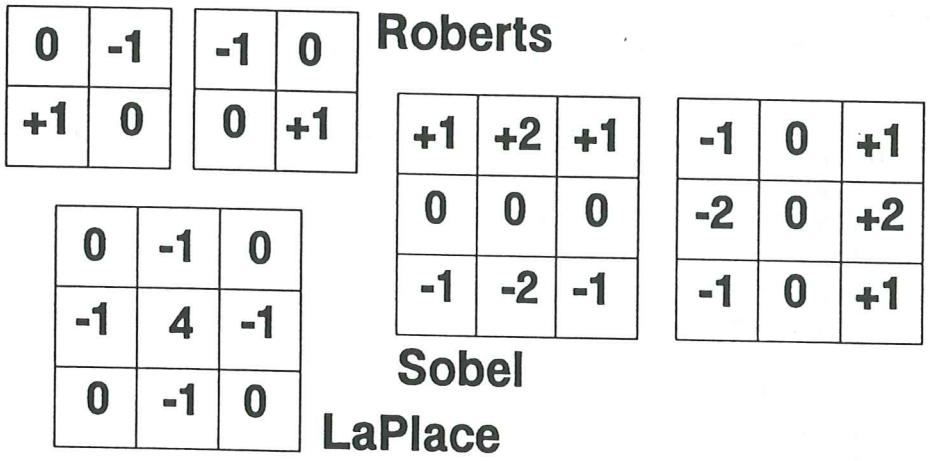

Fig. 29. Spatial filter examples. The figure shows general layout. Size may vary. Adopted from (Schowengerdt 1983) and (Pratt 1991).

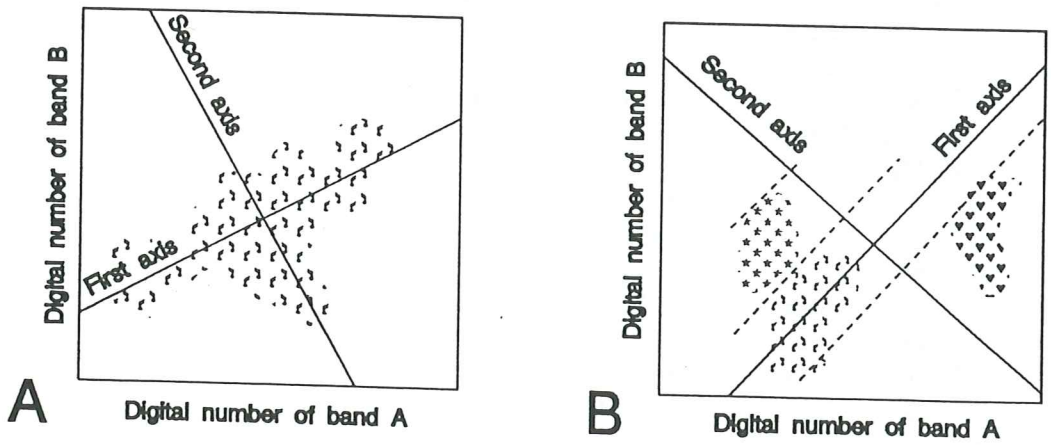

Fig. 30. Principal components, A, and canonical components, B, Principal components rotate the coordinate system axis to coincide with the maximum variation of the data set. Canonical components also optimize separability of clusters. Adopted from (Lillesand & Kiefer 1979)

Principal (and canonical) component transformation is a technique used to remove spectral redundancy (Schowengerdt 1983). A new n-dimensional data set is formed by linear combination of the original n features (channels). Principal component images are uncorrelated and ordered by decreasing gray level variance, i. e. the first component contains most variance and the n:th the least. Lillesand & Kiefer (1979) gives an example where the first principal component contains 97.6 % of the scene variance. The first principal component represents an effective single band composite of multispectral data. Principal component techniques are particularly appropriate in areas with little prior information concerning the region (Lillesand & Kiefer 1979). Fig. 30 illustrates principal components in two dimensions. The coordinate axes are rotated to coincide with the directions of maximum and minimum variance. The second principal component often occur as a "negative" to the first, as a result of their uncorrelated nature after the transformation. Canonical transformation also maximizes separability between classes.

Image enhancement tests

NOAA AVHRR images over the Greenland Sea, for all periods June 1987 - June 1988 that were cloudfree over the ULS region for at least three days, were received from Tromsø Satellite Station. They are listed in Tab. 9.

Date	Satellite	Starting time
6 Nov 1987	NOAA-10	10:36:05
7 Nov 1987	NOAA-9	12:21:39
16 Nov 1987	NOAA-10	10:19:54
20 Nov 1987	NOAA-9	13:23:00
23 Nov 1987	NOAA-10	09:26:52
4 Dec 1987	NOAA-10	10:28:00
6 Dec 1987	NOAA-9	13:51:22
15 Dec 1987	NOAA-9	12:12:31
16 Dec 1987	NOAA-10	09:26:50
27 Dec 1987	NOAA-10	08:47:40
30 Dec 1987	NOAA-9	12:51:30
12 Jan 1988	NOAA-10	09:40:00
14 Jan 1988	NOAA-9	10:09:31
20 Jan 1988	NOAA-10	10:06:20
21 Jan 1988	NOAA-9	12:14:30
26 Mar 1988	NOAA-9	13:55:00
27 Mar 1988	NOAA-9	05:25:00
27 Mar 1988	NOAA-10	09:08:59
20 Apr 1988	NOAA-10	10:27:40
25 Apr 1988	NOAA-9	13:31:00
12 May 1988	NOAA-10	10:49:10
13 May 1988	NOAA-9	13:36:20
9 Jun 1988	NOAA-10	10:39:31
10 Jun 1988	NOAA-9	05:10:45
10 Jun 1988	NOAA-10	10:17:29

Tab. 9. The NOAA AVHRR scenes selected for the project covering all almost cloudfree periods at least three days long over the Greenland Sea, June 1987 to June 1988. Each scene is exactly four minutes long, i. e. the finishing time is exactly four minutes after the starting time given in the table.

Some tests of image enhancement have been performed; colour composites, edge enhancement filtering and principal component transformation. To be able to make 3 band composites, or in general to use the Xshow/BIFF software, the received AVHRR data has to be transformed to 8 bit data. AVHRR images received from TSS have global grid, land contours and nation borders added to the original 10 bit (0-1023) data, as 1024, 2048 and 3072, respective. This must be removed before transformation to 8 bit data on the IIS/IVAS system 600. Transformation can be achieved by subtraction and multiplication of the gray values, described in Alm (1991). With the exception of some abnormal fliers, all pixel values can be enclosed by 256 values, irrespective of channel (Thompson 1986). This also agrees with the authors findings. Images from November (channel 4), April and May was transformed and utilized in the tests. Different combinations of the five channels were tested as colour composites. Linear contrast enhancement and histogram equalisation was used on the images to improve visual perception. LaPlace- Sobel- and Roberts filter were tested, with filter-sizes varying from 3x3 to 15x15 pixels, fig. 29.

Results

A distinct, elliptical cloud in the April images came out strongly and got very easily delineated on some of the colour composites. Sobel and Roberts filtering gave similar results, both better than the general LaPlace filtering. The visual impression was that Roberts filtering gave a slightly better result on the test images. The smaller window sizes gave the better results. The first principal component contains the most information and was originally intended to be the one used. However, the second, and maybe even the third, principal component could probably be useful in the ice context. The results indicate that the second principal component enhance the general contrast between iceareas and water-areas and the third enhance the ice/water transition. A composite using the first and third or second and third, could be useful. This need to be further examined though. No functional tests, to find ice displacement from the enhanced images was performed, as that program didn't work during the time available.

Ice motion tracking using invariant features

Ice drift from satellite images is generally found as the displacement of recognisable floes or features between two consecutive overpasses of the same location. The features can be traced manually, semi-automatically or automatically. Easily recognisable features is chosen in the first image and their position logged. The position of corresponding features is found in the second image. The difference in positions gives the displacements. This is performed manually by, for example, Kjell Kloster at NERSC in Bergen (pers. comm.) and by Ø. Finnekåsa at NPRI (pers. comm.) fig 31. Ice floes has also been followed by for example Tryde (1986) on Landsat images, by Zhang (1990) on AVHRR images and by Korsnes (1991) on SPOT and SAR images. Semi-automatic or automatic methods are developed by Fily & Rothrock (1987) and Zhang (1990), described below. Normally the time lapse between the images must not exceed three days. After two-three days many features can not be recognised. Ice floes are smoothed or broken and the divergence may become to large (Hall & Martinec 1985) (Zhang 1990). Floes > 10 km^2 are always likely to breake up. If a floe breaks up or not depends very much on its shape and the presence of ridges (Tryde 1986).

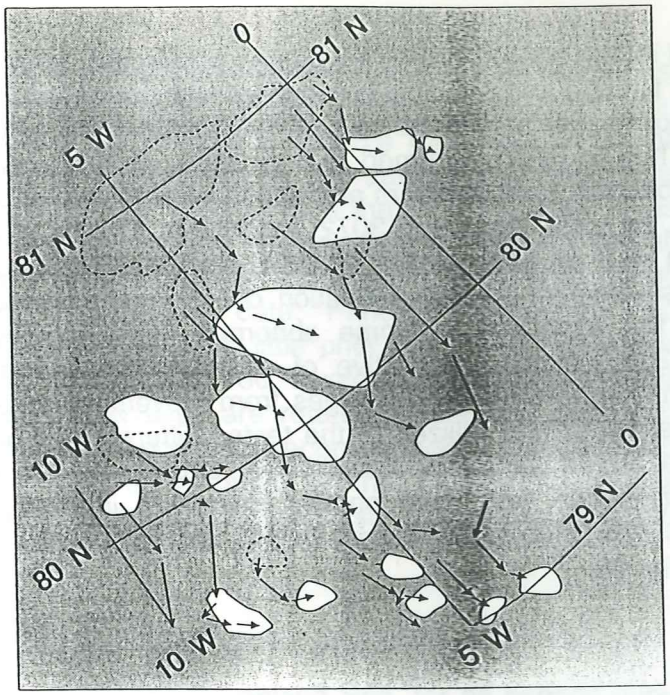

Fig. 31. Ice displacement analysis. Ice floes are followed on consecutive images. The vectors give an ice displacement field. Based on a figure supplied by K. Kloster.

Computer assisted method

Zhang (1990) has developed a computer assisted method for ice displacement analysis. Outstanding features are sought in one of the images. The corresponding feature is then sought in the other image. After six pairs of invariant features are found a transformation polynomial model is established. All subsequent pairs are used to correct the polynomial. For features selected after the first six pairs, the position in the other image is automatically transferred to the corresponding location, using the polynomial model. The sought feature ought to be in the neighbourhood. If there is clouds or uncertainty about the position, the feature pair should be excluded, not to introduce errors. The geometrical correction error in Zhang's data is less than two km and the registering accuracy of invariant features is assessed to one pixel. A test using more than 20 image pairs resulted in a displacement error of 1.7 km and a velocity error of 2 $cm/_s$, over 24 h.

Nested cross correlation

Fily & Rothrock (1987) have automated the process using nested cross correlation, on SAR data. Finding the maximum cross correlation is a common method , used for displacement analysis. Except for sea ice it has been used, for example for cloud displacement analysis (Massom1990). A template from one of the images is matched within a search area in the other image. The search area is located around some reasonable tie point. The point within the search area where the correlation coefficient is largest is chosen, fig 32.

$$R(i,j;k,l) = \sum_{p=-t}^{+t} \sum_{q=-t}^{+t} (a_{i+p,j+q} - \bar{a})*(b_{k+p,l+q} - \bar{b}) / n^2 s_a s_b$$

R(i,j;k,l) = correlation coefficient
n = dimension, size of correlation area, n x n
t = (n-1)/2
$\bar{a},\bar{b}$ = mean value of aij, bij, respective
sa,sb = standard deviation of aij, bij, respective

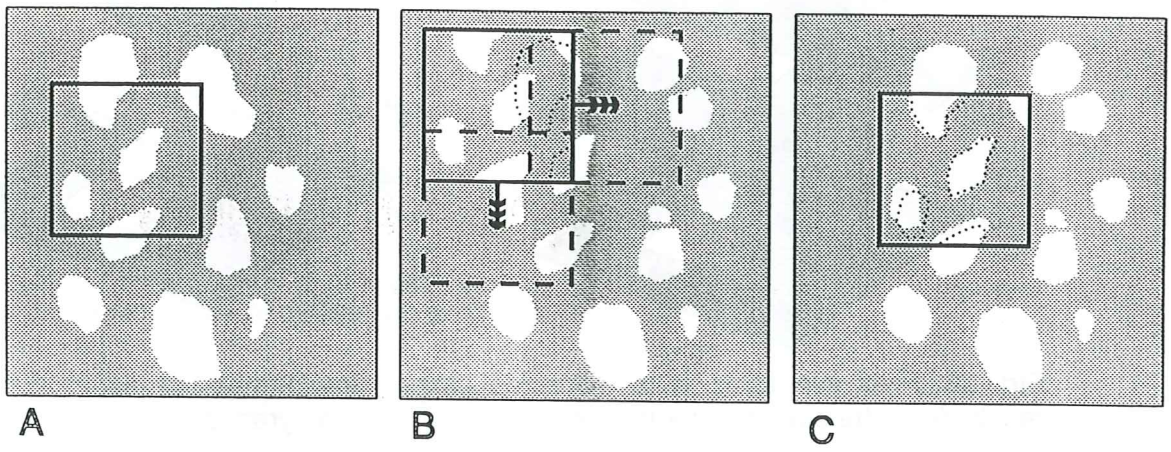

Fig. 32. Matching using maximum cross correlation. A template is delineated in the first image, A. The template is matched with the second image, within a search area, B. The maximum cross correlation within the search area is found, C.

Fily & Rothrock (1987) make use of an hierarchical resolution pyramid. to reduce computation time. The images are averaged to get a hierarchy of images with different resolution, fig. 33. Seed tie points are found at the coarsest resolution. Based on these a crude displacement field model is created, used to guide the searches at finer resolution. In SAR images some per cent of the brightest pixels can be used as seed tie points, at coarsest resolution. They can sometimes be quite unevenly distributed, depending on the structure of the ice field. The grid is filled by interpolation based on the seed tie points. Points with $R >= R_{min} = M_R - as_R$ is accepted. M_R and s_R is the mean and standard deviation of all Rs of the currently accepted tie points. a = a constant. Grid points with no displacement, displacement greater than the mean displacement, or with $R < R_{min}$ are left empty. The process continues to full resolution. Bad points from a coarser resolution can be weeded out. At each level the centre of the tie points from the next coarser resolution is used as centres for the template and the search area at each new resolution level. The search for maximum cross correlation is executed within k +/- r, l +/- r elements of the current resolution.

Zhang (1990) has adjusted the algorithm by Fily & Rothrock to NOAA AVHRR images and tested it on several image pairs (Zhang 1988) (Zhang 1989). A window size of 9 x 9 is used for all stages and an r = 3 for the first stage and r=2 for the remaining stages. As the resolution is much lower than for SAR, just three levels of averaging is needed (9,3,1).

Seed tie points can not be found as the brightest pixels in AVHRR images, as that normally is clouds. Seed tie points was therefore chosen with the computer assisted method. The results were checked by comparison with 218 manually measured

displacements. The mean error was 1.4 km at the coarsest resolution and 0.8 m at the finest. 65 % had an accuracy within one km. Most errors occur in the marginal ice zone.

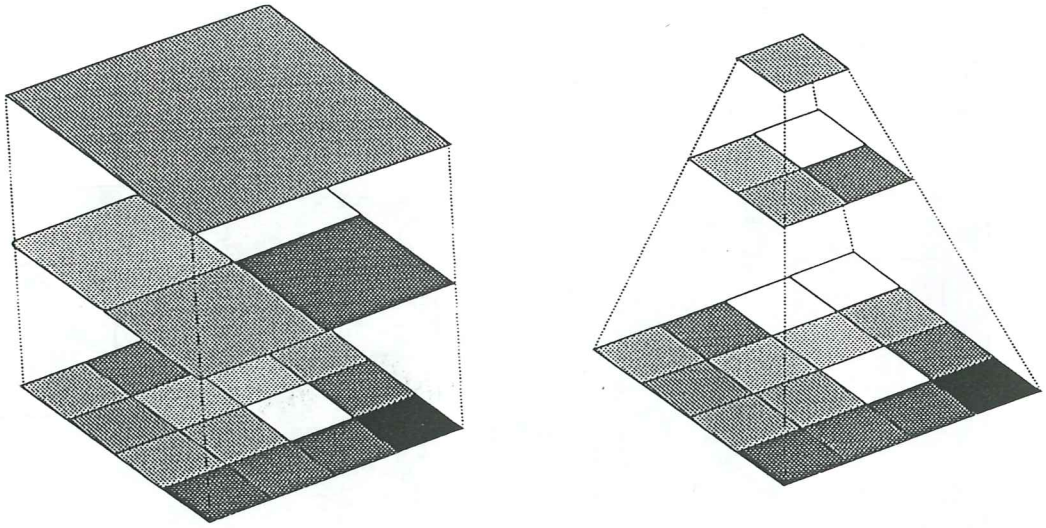

Fig. 33. Pixel averaging, A, and the reduction in the number of pixels, B, which results from the algorithm for the hierarchical resolution pyramid.

Hybrid method

Zhang (1990) has also developed an algorithm for a hybrid method, combining the computer assisted method with the nested cross correlation method. The computer assisted method is used to find the displacement polynomial. For each tie point after the sixth the search for maximum cross correlation is performed around the point predicted by the polynomial transformation. The size of the search area is determined by the accuracy of the polynomial model.

r = b ¤ e
b = a constant
e = standard deviation of the differences between the displacement found by the computer-assisted method and those predicted by the polynomial model:

$$e^2 = {}^1/_N \sum_{i=1}^{N} (d_i - d_{i'})^2$$

N = number of seed tie points
d_i = measured displacement of point i
$d_{i'}$ = predicted displacement of point i

This way the search area will be larger for a polynomial model of lower accuracy. Points are accepted as good if $R >= R_{min} = M_R - as_R$, as above.
If $R < R_{min}$ a new centre point is selected using the mean of the displacements of good surrounding points. Zhang found out that a = 2 and b =1.5 gave a fair performance.

The hybrid method is less cloud sensitive than the nested cross correlation method and less influenced by rotation in the ice field. The error in 95% of the tie points was

below two km, compared to seven km using the nested cross correlation method. The standard deviation was found to be twice as large in the southern Greenland Sea, compared to the northern part. Consequently more tie points are needed for the polynomial model in the southern region, to keep the size of the search area low and save computing time. 80 % of the CPU time is used to fill the grid using the nested cross correlation method, without prediction.

Better accuracy can be achieved if rotation is included in the correlation formula,i.e.:

$$R(i,j,\Theta;k,l) = \sum_{p=-t}^{+t}\sum_{q=-t}^{+t} (a_{i+p,j+q,\Theta} - \bar{a}) \times (b_{k+p,l+q} - \bar{b}) / n^2 s_a s_b$$

$R(i,j,\Theta;k,l)$ = correlation coefficient
n = dimension, size of correlation area, n x n
$t = (n-1)/2$
$\bar{a},\bar{b}$ = mean value of a_{ij}, b_{ij}, respective
s_a,s_b = standard deviation of a_{ij}, b_{ij}, respective
Θ = rotation

A unique orientation can be defined for separate floes to improve the possibility for identification and tracking (Korsnes 1991).

The hybrid method in C, adjusted for ERS-1

Schistad et. al. (1991) have implemented the hybrid algorithm in UNIX C, intended for ERS-1 SAR images. The first version merely uses seed points from the computer assisted method. The coordinates of six tie points are extracted to set up the polynomial:

$$x_{2i}(x_{1i},y_{1i}) = r_0 + r_1x_{1i} + r_2y_{1i} + r_3x_{1i2} + r_4x_{1i}y_{1i} + r_5y_{1i2}$$

$$y_{2i}(x_{1i},y_{1i}) = c_0 + c_1x_{1i} + c_2y_{1i} + c_3x_{1i2} + c_4x_{1i}y_{1i} + c_5y_{1i2}$$

x_{1i},y_{1i} = coordinates of pixel i in the first image
x_{2i},y_{2i} = coordinates of pixel i in the second image

$\{r_j\}$ and $\{c_j\}$ are computed by least squares solution. In matrix notation:

$$R = (M^tM)^{-1}M^tX2$$
and
$$C = (M^tM)^{-1}M^tY2$$

where M is the matrix of the monic polynomial term:

$$M=\begin{bmatrix} 1 & x_{11} & y_{11} & x_{11}^2 & x_{11}y_{11} & y_{11}^2 \\ 1 & x_{12} & y_{12} & x_{12}^2 & x_{12}y_{12} & y_{12}^2 \\ 1 & x_{13} & y_{13} & x_{13}^2 & x_{13}y_{13} & y_{13}^2 \\ \dots & \dots & \dots & \dots & \dots & \dots \\ \dots & \dots & \dots & \dots & \dots & \dots \\ \dots & \dots & \dots & \dots & \dots & \dots \\ 1 & x_{1n} & y_{1n} & x_{1n}^2 & x_{1n}y_{1n} & y_{1n}^2 \end{bmatrix}$$

After the polynomial model is established feature points are selected in the first image and the most probable location of it in the second image is computed, using the model. Maximum cross correlation analysis is then performed around the proposed tie point in the second image. If the correlation coefficient is below 0.5 the point pair is rejected. A later version is also automatically filling the grid. Coordinates of the ice displacement vectors are written to a table file in ASCII format corresponding to the ARC/INFO generate concept. It can easily be imported in ARC/INFO for map plotting.

A pyramid version, like Fily & Rothrock used, was tested on an area between Sørkapp and Bear Island, but was rejected. It needed more CPU time than the polynomial transformation method, as the correlation for many false tie points was computed. Zhang (1990) also questions the method in areas with a lower degree of ridging.

The program (Schistad et. al. 1991) is integrated in a program prototype also including routines for computation of the ice edge position and the ice concentration. Ice concentration is computed as the fraction of ice versus water within a defined area. The ice edge is defined as the isoline between ice concentration 0-10% and ice concentration over 10 %. The test images had a resolution of 120 x 120 m and the default resolution for ice concentration used was 1 x1 km.

Both the first and second version of the program was available at NPRI during the project period, but none of them did work. The second version needed a land mask, that was missing and not created during the project period. According to Anne Schistad (NCC, pers. comm.) the program, at least the first version, would work on AVHRR images as well. A resolution adjustment might, however, be needed.

Geometric correction

To be able to extract displacement vectors from a pair of consecutive satellite images, they have to be geometrically identical. (In practice: as much as possible.)

By geometrical correction is generally meant the adjustment of an image to some given template. Earlier this was accomplished by shifting transparencies with features from the image over the template (Hibler III et. al. 1976). The template could be a map projection or another image. There is mainly two methods for geometric correction (Lauknes 1990). One is to use a set of control points in the reference image (or map). The corresponding points are found in the image to be transformed. Transformation functions are found for example by using least square methods. This method is very labour intensive and time consuming. It is also difficult to find well distributed, good tiepoints for an area mostly consisting of ocean.

Hibler III et. al. (1976) describes a method of coordinate transformation between Landsat ice images with minimum land included. Coordinates of both images are transformed onto a common intermediately located tangent plane.

The second method is to try to model the recording situation, based on sensor/object geometry. The general mathematical form for geometric transformation is:

$O(u,v) = I(i,j) = I(f_1(u,v), f_2(u,v))$

f_1 and f_2 define displacement of the pixels in the image plane.

A geometrical transformation consists of two phases (Lauknes1990). Phase I The positioning problem - to find the functions f_1 and f_2. Phase II The resampling- or interpolation problem - to find pixel-values.

Lauknes (1990) and Ho & Asem (1986) (referenced in Brasjō 1990) have developed methods to transform NOAA AVHRR images to global coordinates, based on geometrical and orbital parameters. Brasjö (1990) has developed a method based on the algorithm by Ho & Asem, making use of interpolation techniques. It is about 80 % more computer effective with about the same accuracy as theirs.

Both methods make the simplification of a spherical earth and a circular satellite orbit. Thereby spherical trigonometry can be used. Ho & Asem first computes the static latitude and longitude (as on a non-rotating earth). Then a correction term is added to correct the longitude for the rotation of the Earth.

The algorithm is in general:

1. Find the time that has passed between the time of the equator passage (nodal time) and the time of the registration of the current scanning line.
2. Compute the angle between the point for the equator passage (nodal longitude and the sub-satellite-point.
3. Given the number of pixels from the sub-satellite point, find the scan angle to the pixel. Also find the angle defined by the pixel and the sub-satellite point at the centre of the earth.
4. Determine the angle between the nodal longitude and the current pixel location. Find the angle between the arc connecting the pixel and the nodal longitude and the equatorial plane.
5. Compute the static latitude and the static longitude.
6. Add the correction factor for the rotation of the earth.

$r = R_e + h_s$

r = distance between the satellite orbit and the centre of the earth
R_e = earth mean radius
h_s = satellite orbit height over the ground

$w_v = G/_r3$

w_V= angular velocity in circular orbit

G = gravitational constant of the earth = 3.9860 ¤ 10^{14} $m^3/_s2$

static_latitude = w_V ¤ delta_t

delta_t = time difference between nodal time and current line

S = p ¤ S_i

S = scanangle to the current pixel
p = number of pixels from sub-satellite point
S_i = scan increment angle - about 0.955 ¤ 10^3 rad

Q= arcsin(($^r/R_e$)/sinS)

Q= the angle between the current pixel and the sub-satellite point

A = arccos(cosQ ¤ cos W + sinQ ¤ sin static_latitude ¤ cos(az))
Z = arcsin((sinQ ¤ sin(az))/sinA) + i

A = the angle between nodal longitude and the current pixel
Z = the angle between the arc connecting nodal longitude and the current pixel and the equatorial plane
az = the satellite azimuth relative the orbital plane - negligible
i = inclination of the orbit

B = arcsin(sinA ¤ sinZ)

static_longitude = arccos(cosA / cosB)

E = W ¤ delta_t

E = correction factor for the rotation of the earth
W= the relative rotation velocity - the difference between the angular displacement of earth relative Aries and the rate of change of the nodal longitude due to the precession of the satellite orbit

current_longitude = static_longitude + E
current_latitude = static_latitude

Both Lauknes and Brasjö first computes longitude and latitude for the pixels and then transforms it to a map projection. Lauknes uses the polar stereographic projection and Brasjö uses Lamberts conical conformal projection. Lauknes uses a fifth degree polynomial for the pixel transformation and a second degree polynomial for the line transformation. He has also optimized the procedure by using look-up tables. Based on 140 control points he got an (RMS) error of 0.62 pixel for sample index and 0.51 pixel for line index. Brasjö makes use of various kinds of interpolation between computed tiepoints. Finally she uses linear regression and rotation based on a few tiepoints, at least one. This gives an error of seven pixels for line index and one pixel for sample index, based on 32 control points.

Lauknes program results in a NOAA quicklook image, 512x512 pixels, of the whole four minute scene (one channel). From Brasjös program one can get an arbitrary subsample. It's also possible to find the line and pixel for a given latitude and longitude. This can be used as a tool for registering images to each other and to find the most probable coordinates for something, for example the ULS location.

System 600 (IIS/IVAS) includes a routine called PAN_CORRECT. It compensates for the panoramic effect, caused by the curvature of the earth, and for the rotation. Image size, orbit height and maximum scan angle are important in-parameters. It also recomputes to a given pixel size, for example 1.0 km. After this correction a matching of two images to each other (or to a map projection) is much easier, using the standard routines of IIS/IVAS.

Weydahl (1991) uses a method of two frame windows and cross correlation for registering SAR images to each other.

Developed program for ice drift computation

The drift unit is simpler than the draft unit. As it reads just one file sequentially less format handling is needed. Vector files are supposed to contain vector end points in latitude and longitude. Three different file formats are accepted at present. A spatial, weighed average of the selected drift vectors is computed.

The drift computations make use of user defined frames, one to five in the present version, for the selection. If any end of a displacement vector falls within a frame it is given the weight associated with that frame. Weights are given by the user. Rectangular or circular frames are optional, fig 34.

If rectangular frames are chosen the program uses a UTM coordinate system, centred at a user-given meridian. The corner coordinates for each frame is computed as a plus/minus offset from the centrepoint.

Frame_corner = (Centre_x +/- User_given_x_offset , Centre_y +/-
User_given_y_offset)

Any vector end coordinates are transformed to UTM and matched with the corner coordinates. If the x coordinate falls between the border lines in the x direction, y is checked similarly, otherwise not. If it is to be included in the computations, it's x- and y-component is computed as the difference in UTM values.

$\text{Delta\_y} = y_2 - y_1$ $\quad\quad$ $\text{Delta\_x} = x_2 - x_1$ (in meters)

The component values are then multiplied with the frame weight and summed.
The resultant components are computed as the weighted average, i e :

$$\text{X\_resultant\_component} = \sum(\text{Weight} \times \text{Delta\_x}) / \sum(\text{Weight})$$

$$\text{Y\_resultant\_component} = \sum(\text{Weight} \times \text{Delta\_y}) / \sum(\text{Weight})$$

The length of the resultant is computed using the formula of Pythagorus:

$$\text{Resultant\_length} = \text{Sqrt}(\text{X\_resultant\_component}^2 + \text{Y\_resultant\_component}^2) \quad [\text{m}]$$

The azimuth is computed as :

Azimuth = Arctan(X_resultant_component / Y_resultant_component) + pi [rad]

If circular frames are chosen the program uses the global coordinates, latitude and longitude, directly. The computations are made in radians. The radius vector for each end point of a displacement vector is computed in km using the formula below, taken from the HP manual (Hewlett-Packard ????).

If Lat_1 = latitude of vector start point
Lon_1 = longitude of vector start point
Lat_2 = latitude of centre point
Lon_2 = longitude of centre point
Lat_3 = latitude of vector end point
Lon_3 = longitude of vector end point

all in degrees, then

Temp_start = Sin(Lat_1) ¤Sin(Lat_2) + Cos(Lat_1) ¤ Cos(Lat_2) ¤
Cos(Lon_1 - Lon_2)
Temp_end = Sin(Lat_3) ¤ Sin(Lat_2) + Cos(Lat_3) ¤ Cos(Lat_2) ¤
Cos(Lon_3 - Lon_2)

and finally:

Radius_start = 60.00 ¤ Arccos(Temp_start) ¤ Conversion_factor _to_km
Radius_end = 60.00 ¤ Arccos(Temp_end) ¤ Conversion_factor _to_km

The conversion factor used is from nautical miles to km and by international definition 1.852.

If any of the vector radii are shorter than the radii of a given frame it is given the weight of that frame. If the end points of a vector are located in different frames the vector gets the weight of the centermost frame. For any vector that is included the meridional and perpendicular component is computed as the difference in latitude and longitude, respectively. The mean latitude and longitude are also computed and the later used to obtain the centre of gravity in the weighted displacement vector field.

Delta_phi = Polemost_phi - Equatormost_phi
Delta_lambda = GM_remote_lambda - GM_close_lambda

Mean_latitude = Delta_phi / 2 + Equatormost_phi
Mean_longitude = Delta_lambda / 2 + GM_close_lambda

Delta_lambda will be negative west of the Greenwich meridian, GM, if the meridians are enumerated negatively to the west. If 360°longitude system is used the formula for Delta_lambda will be reversed. Absolute values are used.

Delta_lambda is normalized using Cos(Mean_latitude). This is valid for a spherical earth as the length of an arc-segment, delta_lambda, at some latitude is equal to delta_lambda ¤ Earth_radius ¤ Cos(that latitude). This is illustrated in fig. 35.The

component values are then multiplied with the frame weight and summed. The mean latitude and longitude are also summed.

The resultant components are computed as the weighed average, i. e. :

$$\text{Phi\_resultant\_component} = \sum(\text{Weight} \times \text{Delta\_phi}) / \sum(\text{Weight})$$

$$\text{Lambda\_resultant\_component} = \sum(\text{Weight} \times \text{Delta\_lambda} \times \text{Cos(Mean\_latitude)} / \text{Cos(Tie\_latitude)} \times \sum(\text{Weight})$$

where

$$\text{Tie\_latitude} = \sum(\text{Weight} \times \text{Mean\_latitude}) / \sum \text{Weight}$$

$$\text{Tie\_longitude} = \sum(\text{Weight} \times \text{Mean\_longitude}) / \sum \text{Weight}$$

The resultant in radians is computed using spherical trigonometry, assuming perpendicular components. The components are also assumed to be in the meridional and perpendicular direction. This gives a right angle between them and simplifies the computations.

$$\text{Resultant\_in\_radians} = \text{Arccos}(\text{Cos}(\text{Phi\_resultant\_component}) \times \text{Cos}(\text{Lambda\_resultant\_component}))$$

$$\text{Angle\_in\_radians} = \text{Arccos}((\text{Cos}(\text{Mean\_longitude}) - \text{Cos}(\text{Resultant\_in\_radians}) \times \text{Cos}(\text{Mean\_latitude})) / (\text{Sin}(\text{Resultant\_in\_radians}) \times \text{Sin}(\text{Mean\_latitude})))$$

The angle is to the left of the right angle in the two quadrants that have equal axis signs and to the right in the two quadrants having opposite axis signs.
The resultant is converted to km using the radius corresponding to the mean curvature (Ussisoo 1977) at the point representing the centre of gravity of the displacement vector field.

$$\text{Mean\_curvature} = \text{Half\_minor\_axis} \times \text{Sqrt}(1 - \text{Eccentricity}^2) / (1 - \text{Eccentricity}^2 \times \text{Sin}^2(\text{Tie\_latitude}))$$

$$\text{Resultant\_length} = \text{Resultant\_in\_radians} \times \text{Mean\_curvature}$$

Half minor axis and eccentricity, above, refers to the earth ellipsoid. Used values are WGS84, 6378137 m and 0.00669438, respectively.

The azimuth is the angle in radians converted to degrees and added 180 (if directed south).

Standard deviation is computed for each component both in the rectangular case and the circular case.

The algorithm for the drift unit:

1. Ask the user for the type of weighing frames, the number of frames, their dimensions and weights.

2. If rectangular frames are chosen transform to UTM coordinate system. Find the frame corners in UTM coordinates.

3. Get the file format from the user. Open the file, if it exists, otherwise give error message. Drift vector coordinates should be in latitude and longitude.

4. Read some header lines

5. Read the data records sequentially.

6. If rectangular frames are chosen transform the vector coordinates to UTM. Check if any end of the vector falls within any of the frames. If circular frames are used, compute the distance from the vector end points to the centre point. Check if any of the distances are shorter than any of the frame radii. If one of the end points of the displacement vector falls within a frame, give it the weight of that frame. If it falls within two, give it the weight of the centermost frame.

7. Add vector components to sums and squared sums. For rectangular frames the components are delta x and delta y, in UTM coordinates and for circular frames the components are delta lambda (longitude) times phi and delta phi (latitude). The longitudinal component is multiplied by phi for normalization.

8. Repeat 5-7 until end of file is reached.

9. Use the computed sums to compute mean displacement, azimuth and component standard deviation. In the rectangular case, plane trigonometry is used and in the circular case, spherical trigonometry is used. The local mean curvature is used for spherical computation.

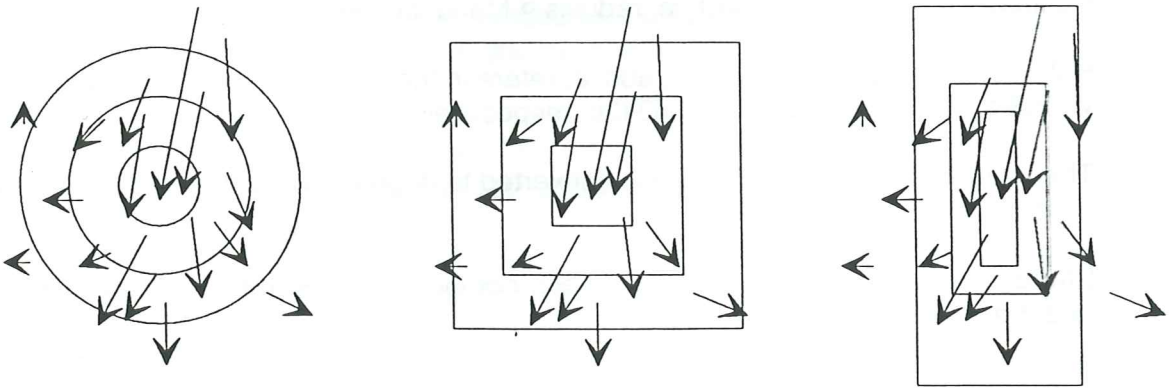

Fig. 34. Examples of frames used for the drift vector averaging.

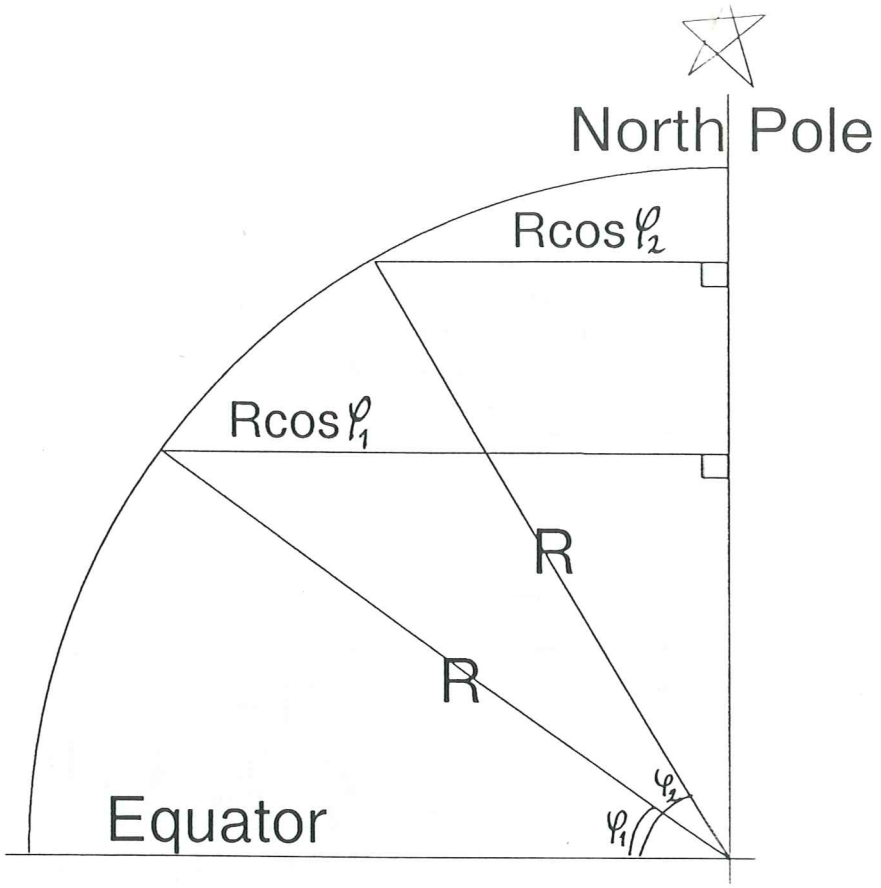

Fig. 35. The perpendicular Earth radius at latitude φ. R = radius of a spherical Earth.

Combination of draft and drift

Both the draft unit and the drift unit were implemented separately first to test performance. Both give an average value for the whole time interval and one value recomputed to yield daily average. The two units have been linked together and the combination value is computed, mean vertical draft times mean horizontal drift. This represents vertical area. It can also be seen as a narrow volume. If the draft average is considered as representative for the selected frame it can be used to assess the ice volume enclosed by the frame. It is anyhow a better estimate than has been possible before. Several ULS bouys with organised locations will give information about the spatial variation of the ice draft and improve the assessment. This kind of investigation is being done 1991-92 in the Greenland Sea, fig 20.

Draft is computed by the developed program, provided the needed files exist. Air pressure information can be digitized from synoptic weather charts, if it does not exist in digital form. To get ice drift vectors the two images must first be registered to each other. This can be done following the procedure described by Brasjö (1990) and by Lauknes (1991), or possibly as described by Hibler III et. al. (1976). It can also be done using ground control points, but they are normally few in the ice images. They are also often difficult to identify. The program described by Schistad et. al. (1991) can be used to get the drift vectors automatically. A landmask is needed, to avoid ice drift on "solid ground". On NOAA AVHRR images also clouds has to be masked. This can be done using the method described by Alm (1991). The program developed by Schistad et. al. (1991) gives the vectors in ARC/INFO generate format. This can be fed into the program, described in this report. The program gives average draft and average drift for the time interval and normalized to daily value. Draft values can be tabulated on a file and combined with the drift per sample.
Preferably the computed values should be stored in a time series for statistical evaluation.

Test and result

Problems with the implementation of the program developed by Schistad et. al. (1990) at NPRI prevented the computation of drift vectors from the selected NOAA AVHRR images during the project period. However, one of the data files supplied by Zhang coincided with one of the periods, 12-13 May. This data has been used for tests and has been combined with draft for that period. Drift recomputed to yield per-sample has been combined with the draft values and plotted, fig 36.

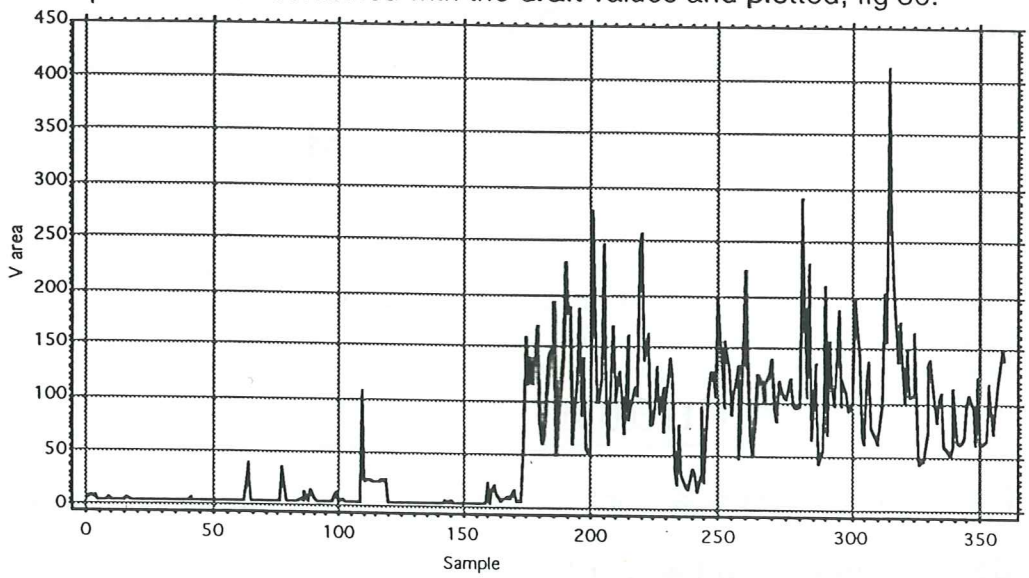

Period 12/5 88 - 13/5 88, vertical area 24 h.

X1 : V area

Mean:	Std. Dev.:	Std. Error:	Variance:	Coef. Var.:	Count:
62,576	67,328	3,548	4533,02	107,593	360
Minimum:	**Maximum:**	**Range:**	**Sum:**	**Sum of Sqr.:**	**# Missing:**
3,526	412,078	408,552	22527,52	3037046,165	0

Descriptive statistics for the above 24 h.

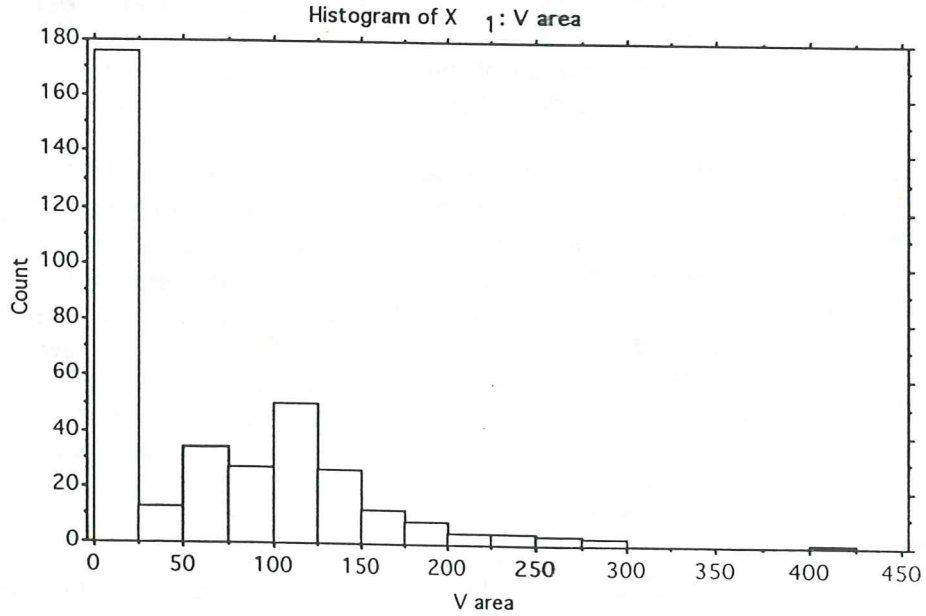

Frequency distribution for the vertical area of the period.

Fig. 36. Example of the combined draft and drift (per sample).

Discussion

Ice conditions influence both climate, ecology and human activities. Human activities influence both climate and ice conditions. That motivates the study of ice conditions. The differing thermal and radiative properties of sea ice and water is important for its role in climate, both at local, regional and hemispherical scale. Feedback effects are important. Global warming will probably not, however, cause an ice-free Arctic Basin.

The ecological effects has been discussed with Birger Ulf Hansen (UoC), with Vidar Bakken (NPRI) and with Dieter Scherer (UoB). It has also been studied by Vibe (1978), who found interesting correlations, for example for the Canadian lynx, the Greenland whale, the musk-oxen, the eider duck and the snowshoe hare. Corbet (1972) gives examples of the influence of the ice on ecology of microscale. The most important period is probably from the end of the melt period in spring and to the late summer. Ice conditions influence for example the establishment and breeding period of arctic birds.

The ice cover affects for example northern ship routes, fishery and oil and gas exploration. New icebreaker technology improves the possibility to penetrate the pack ice. Oden is a good example of that. Operational semi-real-time ice condition charts, based on ERS-1 also improves the possibilities for activity in ice infested waters. The Russians have started icebreaker "charter tours" to the north pole and there are projects going on opening both the northern sea routes. This may have an effect on the stability of the arctic ice cover. Broken leads do freeze up quickly so it may not make any big difference. It is, however, important to monitor the ice contions to see if this activity will have any effect. Oilspills and other dark deposits affect the albedo and the marine wildlife. This can have a noticeable effect on the ice cover, at least locally, and be disastrous for the marine wildlife. Increased arctic resource extraction cause more transports, which is an important factor.

Ice extension monitoring is an established method used in climatic assessment. Normally ocean-wide coverage is used, for example in global change studies. The proposed method of subarea sampling may be informative, though, on a more regional scale. This needs more investigation. The marginal ice zone is an important factor. It is often located near the selected Arctic islands, together with the oceanic polar front. Advection can make the ice conditions at the front unstable. This could be a weakness of the method. Visual inspection of the diagrams, however, seems promising. The major fluctuation of the ice over some years is reflected.

Several authors have emphasized the importance of computing ice volume transport. The sea ice draft and drift program presented here is an effort to accomplish that. It shows one possible way to approach the problem. The program for the draft evaluation also provides a tool for analysing the draft data of an arbitrary time period, less than about ten days. It can be used to produce plots and descriptive parameters for various time resolutions. This can be of interest, for example in the study of ice bottom topography, ice floe dynamics etc.

There are several reasons C has been chosen as the programming language. Most programming today is performed in C. By using C under UNIX (in this case ULTRIX), the program becomes more portable. This is of special interest considering the remarkable rise of interest for the ULS ice thickness series, which the program is primarily intended for. Handling large data sets and images can be

considerably more effective using pointers to addresses, compared to direct addressing of positions. The good possibility of allocating dynamically in C saves space and makes the program more computer economic.

The main sources of error for the draft computation is the lack of salinity values, the precision and averaging of the temperature, damping of the sound energy in the water column, and the averaging effect of the sonar beam footprint. These sources cause draft deviations in the dm scale, or normally less than a dm. The variations have in some aspects a systematic effect, but they cancel out to some degree in the draft averaging. If the first echo is used it will cause a systematic over-estimation of the draft, fig 37. Over-echoes may have some influence. Wave effects can have an influence on the marginal ice zone, fig 38. Wave effects can also be seen in a few of the segments of the 14-day diagrams published in the data report (Vinje & Berge 1989).

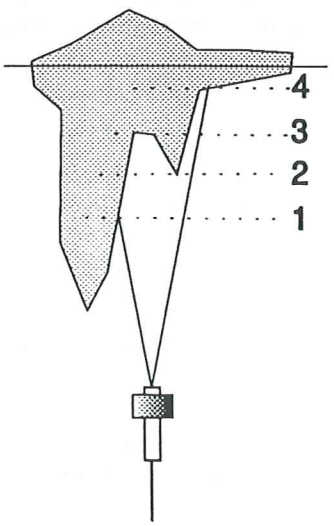

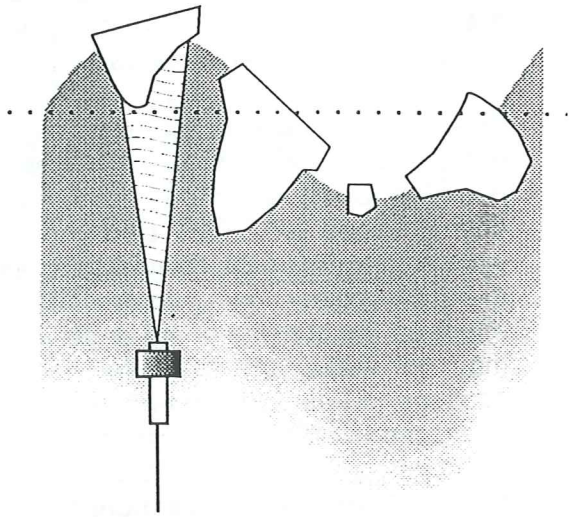

Fig. 37. If a to early echo is used the draft will be over-estimated.
Fig. 38. The effect of waves in the marginal ice zone.

Uncertain accuracy in the displacement vectors cause errors in the mean displacement. If UTM projection is used, controlled, but varying, errors from the projection is also introduced. The accuracy of the displacement vectors is influenced by the positional precision of the geometric transformation of the satellite images. Errors introduced by insensitive frame definition by the user can also be added. This is not so important in the East Greenland Current area, but can be more significant in an area with more diverging currents and drift directions, for example close to the polar front. If an automatic displacement program is used for the generation of the displacement vector field, a land mask is needed. A generalized mask can be used as there is often fast ice close to the coast. On NOAA AVHRR images clouds must be delineated too.

The errors of the displacement field is not so important, as the ice drift in the Greenland Sea is very systematic, compared to the draft. The sizes of the weighing frames depend on the drift situation at the location. Homogeneous drift has been reported for areas of various sizes, from ca 50 km up to 800 km. An often used size appears to be about 100 km.

The projection is important, both for accuracy and for comparability. It can be advantageous to use image pixel-numbers for the computations. It is also faster.

The image must then be properly rectified and resampled. If the pixels can be assigned geographical coordinates it is wise to use spherical computations. Finding the geographical coordinates for the pixels can probably be done using Brasjö's program. There are also unconfirmed rumours that it may accompany more recent NOAA AVHRR images. For the presentation of the drift vector field, or other graphics, it is most appropriate to use the same projection as DNMI uses for the weather and ice forecast charts.

One important factor to be taken into consideration when NOAA AVHRR data are used for generating the displacement vector field, is that on cloudfree occasions the wind direction is normally from the north in the Greenland Sea. This will give a biased data set. Dech (1990) has generated displacement vector fields also on rather cloudy days and the varying directional homogeneity can be seen from his displacement field maps. The use of ERS-1 data would allow independence from the weather and obtaining complementary data to study this effect. The swath width and resolution of ERS-1 is perhaps a bit too small to be optimum for sea ice drift studies with most of the Greenland Sea as an investigation area. About 1 km seems to be a good resolution for assessment of the general background ice displacement. Tests with radar images from USSR with 1 km resolution are to be performed in the near future.

The present program combines average draft with average drift, or displacement. This gives a two-dimensional variable, which can be said to represent vertical area, fig 39. This is itself a good indicator of the ice fluctuations with time. However, combining the variable with some drift perpendicular parameter would give ice volume transport. The simplest way to achieve this is to use the width of the ice stream. This can be collected weekly (retrospectively) from the digital ice charts stored at NPRI or directly from the satellite images. The program developed by Schistad et. al. (1990), for example, gives both the ice displacement and the ice edge position.

Another, more accurate, method would be to use the ice concentration in equalsized units perpendicular to the drift stream as a weighing factor. Each unit could be compared digitally with the centre unit (containing the ULS), thereby obtaining a percentage weighing value. A similar procedure is tested by Ånund Kvambekk (pers. comm). In the long run this can also give a statistical material for a stream cross section. A more elaborate, but most correct, way, would be to have an array of ULSs on a line cross stream and combine the series of 2D time series to a 3D time series. The displacement must then be averaged in narrower frames, with little overlap, to keep the cross stream dynamics. ULSs were positioned along latitudes in the Greenland Sea in 1991.

The vertical area value can very well be a climate monitoring indicator, provided continuous measurements will take place. Some standardized time period each month or year can be stored to generate a time series. Combinations of certain time periods of the year can be used. In any time series it is very important that the parameters are extracted in the same way each time and, that the values of the whole series are comparable. By using one and the same program, like the developed program, comparability is achieved.

The future for this type of ice measurement seems very promising. The ULS concept is very operational and several improvements have been made since the 1987 version. The newer sensors are less depth and shock sensitive (Johannesen

1990). On the new ULSs temperature and signal quality are also recorded (Svein Værholm, CMI, pers. comm.). The interest for this ULS type has grown dramatically, from the one deployed in 1987, used here, to four deployed in 1990 and 16 deployed in 1991. The developed program can, maybe with some minor improvements, be a good operational tool for the generation of time series data, which can be an asset for monitoring ice and climate or for other scientific purposes.

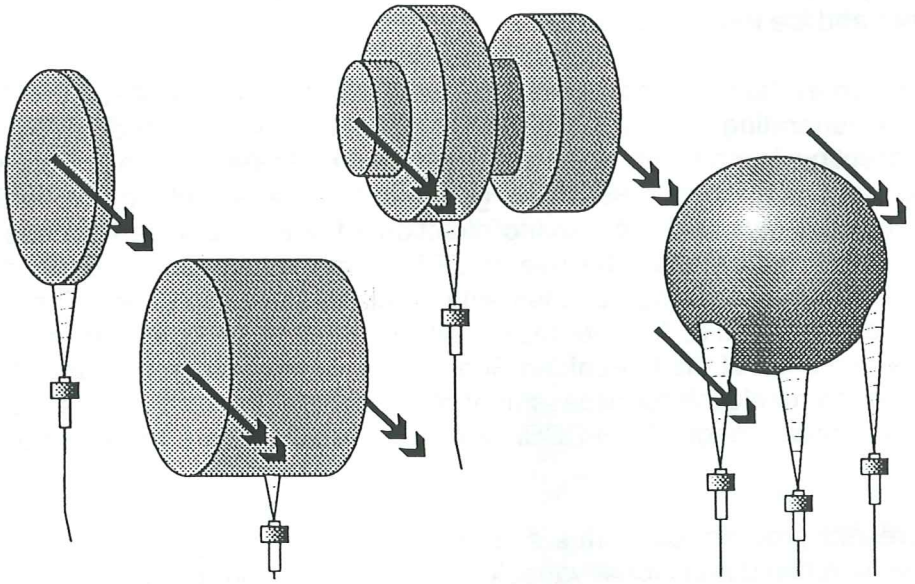

Fig. 39. Symbolic example of vertical area vs. volume. With just one ULS one do not get information about the spatial variation. Average thickness can be assessed or a thickness distribution model can be utilized. Several parallel ULSs give the best information.

Summary

Area sea ice extension as a parameter used for climatic analysis is described. Background and tools needed for ice volume computation is surveyed. A proposed procedure for sea ice volume monitoring is given.

A computer program has been developed for the combination of sea ice draft and drift. The draft data is supplied by upward looking sonar measurements from a moored sonar buoy. The drift data are extracted from a pair of satellite images, preferably not longer apart than three days. Image processing is normally needed before drift vector extraction, based on invariant features, can be done.

Some minor tests have been performed with promising results. The draft part of the program has also been used to extract ice draft data, which has been plotted at a resolution better than earlier. More extensive tests, using ERS-1 and Russian radar data are recommended and foreseen with great interest. The concept of moored upward looking sonars is very operational. Combining the data with ice drift data from weather independent satellites rise great expectations for ice monitoring. This project has clearly shown the feasibility of this combination.

Abbreviations

AIDJEX	Arctic Ice Drift Joint EXperiment
ANSI	American National Standard Institute (?)
AVHRR	Advanced Very High Resolution Radiometer
CMI	the Christian Michelsen Institute
CRT	Catode Ray Tube
DMSP	Defence Meteorological Satellite Program
DNMI	Det Norske Meteorologiske Institutt (the Norwegian Meteorological Institute)
EGC	the East Greenland Current
EGF	East Greenland Front
GECR	Global Environmental Change Report
GM	the Greenwich Meridian
GRID	Global Resource Information Database
GSFC	NASA/Goddard Space Flight Centre, USA
GSG	Greenland Sea Gyre
GSP	the Greenland Sea Project
ICEX	Ice Conditions EXperiment
IAA	Institute for the Arctic and the Antarctic, Russia
IFOV	Instantaneous Field Of View
IIS	Integrated Imaging System
IMLFO	Institute Maurice-Lamontagne, Fisheries and Oceans, Canada
m. b. s. l.	Meters Below Sea Level
MIZEX	Marginal Ice Zone EXperiment
NASA	National Aeronautics and Space Administration, USA
NCC	Norwegian Computing Centre
NERSC	Nansen Environmental Remote Sensing Centre, Norway
NIR	Near InfraRed
NOAA	National Oceanic and Atmospheric Administration
NPRI	the Norwegian Polar Research Institute
SAR	Synthetic Aperture Radar
SMMR	Scanning Multi-channel Microwave Radiometer
SOFAR	SOund Fixing And Ranging
SONAR	SOund Navigation And Ranging
TC	the Transpolar Current
TIR	Thermal InfraRed
TSS	Tromsø Satellite Station
ULS	Upward Looking Sonar
UoB	University of Basel, Schwitserland
UoC	University of Copenhagen, Denmark
UoL	University of Lund, Sweden
UoO	University of Oslo, Norway
UoW	University of Waterloo, Canada
UTM	Universal Transverse Mercator projection
VIS	Visible light, The part of the electromagnetic spectrum we see
V V	Vertically transmitted, Vertically received
WGS84	World Geodetic System 1984

Acknowledgements

Many people have supported me during this project and I want to mention some in particular. I'm grateful for the financial support given to the project by GRID-Arendal, the Norwegian Space Centre and the Norwegian Polar Research Institute (NPRI). Jonas Åkerman, University of Lund, UoL, encouraged me to do it and supplied good planning advice. The working facilities at NPRI have been excellent. I'm grateful that I got the opportunity to work with Torgny Vinje, because of his kindness and his great skills. Terje Løyning, Ånund Kvambekk and Øyvind Finnekåsa, all NPRI, have given good supervision and many pieces of good advice. I'm grateful to Eberhard Fahrbach, Alfred Wegener Institute for Polar and Marine Research, Bremerhaven, Germany, for sending me temperature data from the mooring, and to Hongijang Zhang, Electromagnetics Institute, Lyngby, Denmark, for giving NPRI access to some of his displacement data files for the period 1987-88.
Torgny Vinje, NPRI, Anne Schistad, the Norwegian Computing Centre, NCC, Sindre Langaas, GRID-Arendal, Vidar Hisdal, NPRI, Jim Foster, NASA/Goddard Space Flight Centre, Svein Værholm, the Christian Michelsen Institute, Ellsworth LeDrew, University of Waterloo and Dieter Scherer, University of Basel has contributed with rewarding discussions. Trond Eiken, NPRI, assisted on geodetical questions.
Torstein Berge has given assistance in the use of the NPRI computers and Jostein Amlien in the use of the image processing system, IIS. Anne Schistad, NCC, and Carina Brasjö, UoL, have given advice about their programs. At the end of the project John Thingstad, University of Oslo, has given good assistance in C programming and program improvements. Lars Kullerud at GRID-Arendal assisted on using CorelDraw for some of the figures. Torgy Vinje has kindly read and commented an early version of the report. Mary C Berge, NPRI, has checked the English language for parts of the text. Gerhard Bax, University of Stockholm, has checked the German abstract. Frode Reisnes, Hjelpemiddelsentralen, Arendal, generously gave me access to Macintosh computers.
Susan Barr, NPRI, and Anders Appelquist, UoL, kindly let me stay at their homes during parts of the project. I'm also grateful to all at NPRI and in Lund who have helped in getting a pleasant working and living environment.

Everything is drifting,
the whole ocean moves ceaselessly...
just as shifting and transitory as
human theories.

Fridtjof Nansen

References

Aagaard, K. & Coachman L. K. (1968): **The East Greenland Current North of Denmark Strait**, Part I & II. Arctic Vol 21 No 4, December 1968. part I pp 181-200, part II pp 267-290.

Ahlmann, Hans W:son, Wallèn, C. C., Fristrup, Börge, Thorarinsson, Sigurdur, Liestøl Olaf & Ostrem, Gunnar (1970): **Klimatologiska förändringar omkring Nordatlanten under gammal och nyare tid.** (In Swedish) (Climatological Changes around the North Atlantic Ocean in old times and more recently) Ymer, Årsbok 1970.

Alm, Göran (1988): **Texture Analysis of Drift-Ice in an Arctic NOAA-Scene.** Meddelanden från Naturgeografiska Institutionen vid Stockholms Universitet, Nr A228. University of Stockholm, Department of Physical Geography. 8 pp.

Alm, Göran (1991): **Ice Detection during Cloudy Conditions over the Arctic Region using NOAA AVHRR Satellite Imagery.** Geografiska Annaler 73A (1991) No 3-4. pp155-166.

Arheimer, Berit & Glave, Stefan (1991): **ERS-1 European Remote Sensing Satellite - Ett nytt instrument för global miljöövervakning på 1990-talet.** (In Swedish) (ERS_1 - A new Instrument for Global Environmental Monitoring in the 1990s) Internal report NGE226-91, University of Lund, Department of Physical Geography. 23 pp.

Backman, Anders (1990): **Oden - a New Icebreaker to Challenge Arctic Conditions.** Swedish Polar News, No 2, Feb 1990, Swedish Polar Research Secretariat, Stockholm. pp4.

Barber, David G. & LeDrew Ellsworth F. (1991): **SAR Sea Ice Discrimination using Texture Statistics: A Multivariate Approach.** Photogrammetric Engineering & Remote Sensing, Vol 157, No 4, April 1991. pp 385-395.

Bergdahl, Lars (1977): **Physics of Ice and Snow as Affects Thermal Pressure.** Report Series A:1, Department of Hydraulics, Chalmers University of Technology, Gothemburg.

Bergth'orsson, P'all (1970): **Långtidsprognoser om drivis vid Island.** (In Swedish) (Long time Forcasts on Drifting Ice at the Coasts of Iceland). Proc. Sjunde Nordiska Meterologi mötet, (Seventh Nordic Meteorology Meeting), Helsinki, 9-12 Juni 1970. pp 183.

Bergth'orsson, Pa'll (1972): **Advection of Climate by Ocean Currents,** Sea Ice, Proc. of the Sea Ice Conference in Reykjavik., Karlsson, T. (ed.), National Research Council, Iceland, Reykjavik , pp 94-120.

Brasjö, Carina (1990): **Geometrisk korrektion av NOAA AVHRR data.** (In Swedish) (Geometric Correction of NOAA AVHRR data) Lunds Universitet, Naturgeografiska Institutionen, Seminarie uppsats Nr 18, Report 18, Yellow Series, University of Lund, Department of Physical Geography, Lund, Sweden. 90 pp.

Corbet, Philip S. (1972): **The Microclimate of Arctic Plants and Animals on Land and in Fresh Water.** Acta Arctica, Fasciculus XVIII, Arctic Institute, Charlottenlund, Denmark. 43 pp.

Dech, Stefan Werner (1990): **Monitoring des Meereises in der Ostgrönlandsee im Mai 1988 mit Methoden der Fernerkundung.** (In German) (Monitoring of the Sea Ice in the East Greenland Sea May 1988 using Remote Sensing methods). DLR-Forchungsbericht 90-36 (DLR Research report 90-36) (Ph. D. thesis University of Würzburg). 280 pp.

Del Grosso, V. A. & Mader, C. W. (1972): **Speed of Sound in Sea Water Samples.** Journal of the Acoustic Society of America, No 52. pp 961-974.

Dey, B. (1980): **Applications of Satellite Thermal Infrared Images for monitoring North Water during the Periods of Polar Darkness.** Journal of Glaciology, Vol 25, No 93. pp 425-435.

Edgerton, Harold E (1986): **Sonar Images.** Prentice Hall, Englewood Cliffs, New Jersey 07632. 296 pp.

Eide, Lars Ingolf (1983): **Environmental Conditions in the Barents Sea and near Jan Mayen,** The Norwegian Meteorological Institute, Oslo.

Erlingsson, Bjørn (1991): **On the Temperature Distribution in the Ice Subsurface Water Column.** Unpublished.

Feldman, S I (????): **Make - A program for Maintaining Computer Programs.** Bell Laboratories, Murray Hill, New Jersey. 8 pp.

Fily, M. & Rothrock D. A. (1988): **Fortran Program for Digital Ice Tracking by Cross-correlation,** Informal Document Series, Applied Physics Laboratory, University of Washington, Seattle.

Førland, Eirik J. & Nordli Per Øyvind (1991): **Nye klimanormaler-men er klimaet forandret?.** (In Norwegian) (New Climate Normals, but has the Climate changed?) Dette er meteorologisk institutt...DNMI, Det Norske Meteorologiske Institutt 125 år, 1866-1991.(This is the Norwegian Meteorlogical Institute... DNMI, 125 years, 1866-1991), DMNI, Oslo. pp 36-39.

GECR (1992): **1991 was "Second Warmest" of the Past 140 Years.** Global Environmental Change Report, Vol IV, No 1, 17 Jan 1992, Cutter Information Corporation, Arlington, MA. pp 5-6.

Gloersen, Per & Cambell, William J. (1991): **Recent Variations in Arctic and Antarctic Sea-ice covers.** Nature, Vol 352, 4 July 1991. pp 33-36.

Gordienko, P. (1958): **Arctic Ice Drift,** N. A. S. - N. R. C. Publication 598, pp210-220. (referenced in Häkkinen 1990)

the GSP-group (1990): **Greeland Sea Project - A Venture Toward Improved Understanding of the Oceans Role in Climate.** EOS, Vol 71, No 24, June 1990, transactions, American Geophysical Union. pp750-755.

Hall, Dorothy K. & Martinec, Jaroslav (1985): **Remote Sensing of Ice and Snow.** Chapman and Hall. 189 pp.

Hall, R. T. (1980): **AIDJEX Modelling Group Studies Involving Remote Sensing.** In Sea Ice Processes and Models, Proc. of the AIDJEX International Commision on Snow and Ice Symposium, Pritchard R. S. (ed.), University of Washington Press. pp 151-162

Hansen-Bauer, Inger (1991): **Variationer i temperatur og nedbør i Norge de siste 100 år.** (In Norwegian) (Variations in Temperature and Precipitation in Norway the lat 100 years). Dette er meteorologisk institutt...DNMI, Det Norske Meteorologiske Institutt 125 år, 1866-1991.(This is the Norwegian Meteorlogical Institute... DNMI, 125 years, 1866-1991), DMNI, Oslo. pp34-35.

Heinze, Ch., Schlosser, P., Koltermann, K. -P. & Meincke, J. (1990): **A Tracer Study of the Deep Water Renewal in the European Polar Seas,** Deep Sea Research. (referenced in the GSP-group (1990))

Helland-Hansen, Bjørn & Nansen Fridtjof (1909): **The Norwegian Sea. It´s Physical Oceanography**. Kristiania, Det Mallingske Bogtrykkeri, Report on Norwegian Fishery and Marine Investigations Vol II., 422 pp.

Hewlett-Packard (????): **Instruktionsbok och Programmerings handledning HP-41C/41ev**. (In Swedish) (Manual and Programming Handbook HP41C/41ev)

Hibler III, W. D., Tucker, W. B. & Weeks, W. F. (1976): **Techniques for using Landsat Imagery Without Land References to study Sea Ice Drift and Deformation.** AIDJEX Bulletin, No 31, March 1976. pp 115-134.

Ho, D. & Asem, A. (1986): **NOAA AVHRR Image Referencing,** International Journal of Remote Sensing, Vol 7, No 7. pp 895-904. (referenced in Brasjö 1990))

Hurdle, Burton G. (1986): **The Sound Speed Structure.** In The Nordic Seas, Hurdle, B. G. (ed.), Springer Verlag - New York (777pp). pp 155-181.

Häkkinen, Sirpa (1990): **Models and Their Applications to Polar Oceanography,** In Polar Oceanography, Part A, Physical Science, Smith Jr., Walker, O. (ed.), Academic Press. (406 pp) pp 335-384.

Iizuka, K., Freunddorfer, A., Wilson, D., Tsang, G. & Haras W. (1988): **Measurements of Saline Ice Thickness using a Step Frequency Radar.** Cold Regions Science and Technology, No 15(1988), Elsvier Science Publishers BV, Amsterdam. pp 23-32

Jayaweera, K. O. L. F. (1976): **Use of Enhanced Infrared Satellite Imagery for Ice and Oceanographic Studies.** Ocean Engineering, No 3:1976. pp 293-298.

Johannessen, Atle A (1990): **CMI ES-300 Series User´s Guide. Special applicablefor Model V.** CMI report 10124, the Christian Michelsen Institute, Department of Science and Technology, Bergen, Norway. 21 pp.

Johansson, Bengt, M. & Liljeström, Göran, C. (1989): **Oden - A-State-of-the-Art Icebreaker**, POAC89, Proc. of the 10:th International Conference on Port and Ocean Engineering under Arctic Conditions, Luleå, Sweden, 12-16 June 1989, Axelsson, K. B. E. & Fransson, L. Å. (eds.), Research report TULEA 1989:08, Luleå University of Technology.Proc. POAC 1989. pp 1229-1265.

Johnsen, Ånund S (1989): **Relations between Top and Bottom Ice Topography using a Scanning Sonar**, POAC89, Proc. of the 10:th International Conference on Port and Ocean Engineering under Arctic Conditions, Luleå, Sweden, 12-16 JUne 1989, Axelsson, K. B. E. & Fransson, L. Å. (eds.), Research report TULEA 1989:08, Luleå University of Technology.Proc. POAC 1989. pp 77-86.

Johnsen, Ånund, S. & Vinje, Torgny (1987): **Havisundersøkelser i Barentshavet, Utkast til Sluttrapport,** (In Norwegian) (Sea Ice Investigations in the Barents Sea, Draft) AKUP-prosjekt, Deloppgave 01.03.5, the Norwegian Polar Research Institute, 103 pp.

Kinsler, Lawrence E., Frey, Austin , Coppens, Alan B & Sanders, James V. (1982): **Fundamentals of Acoustics**. 3:d ed. Wiley. 480 pp.

Korsnes, Reinert (1991): **Statistical Description and Estimation of Ocean Drift Ice Environments,** Doktor Ingeniør avhandling, Ph D thesis, 1991:24, The Norwegian Institute of Technology, Division of Structural Engineering, Trondheim, NTH-tryck.

Kovacs, Austin & Holladay, J. Scott (1989): **Airborne Sea Ice Thickness Sounding.** POAC89, Proc. of the 10:th International Conference on Port and Ocean Engineering under Arctic Conditions, Luleå, Sweden, 12-16 June 1989, Axelsson, K. B. E. & Fransson, L. Å. (eds.), Research report TULEA 1989:08, Luleå University of Technology. pp 1042-1052.

Kozo, Thomas L. & Diachok, Orest I. (1973): **Spatial Variability of Topside and Bottomside Ice Roughness and its relevance to Underside Acoustic Reflection Loss.** AIDJEX Bulletin 19. pp113-121

Kristensen, Monica (1983): **The Fram Strait Monitoring and modelling Project. Draft** Internal report, The Norwegian Polar Research Institute.

Kverndal, A.-I., Elvebakk, A. Jaworowski, Z & Hansson R. (1990): **Virkninger av klimaendringer i polarområdene.** (In Norwegian) (Influence of Climatic Change in the Polar Areas), Bidrag til den interdepartementale klimautredningen, NP rapport serie nr. 62, (Norwegian Polar Research Institute report series No 62), the Norwegian Polar Research Institute, Oslo. 118 pp.

Lamb, H. H. & Mörth, H. T. (1978): **Arctic Ice, Athmospheric Circulation and World Climate.** The Geographical Journal, Vol 144, Part I, March 1978. pp 1-22.

Langaas, Sindre (1992): **Temporal and Spatial Distribution of Savanna Fires in Senegal and the Gambia, West-Africa 1989-90, derived from Multi-Temporal AVHRR Night-Images.** International Journal of Wildland Fire. In print.

Larsen, J. & Lu, Q.-M. (1986): **Sea Ice Modelling in the East Greenland Area.** Ice Technology: Proc. of the 1:st International Conference on Ice Technology, Cambridge, Mass, USA, Murthy, T. K. S., Connor, J. J. & Brebbia, C. A. (eds.), Springer Verlag, Computational Mechanics Publication. pp147-156.

Lauknes, Inge (1990): **NOAA Ouick Look** (In Norwegian). Foredrag fra NOBIM-konferansen 1990 (Proc. from the NOBIM conference 1990), Report IR0409 FORUT, University of Tromsø. 118 pp.

Lillesand, Thomas M. & Kiefer Ralph W (1979): **Remote Sensing and Image Interpretation.** Wiley & sons. 615 pp.

Loeng, Harald (1983): **Strømmålinger i tidsrommet 1979-1982 i de sentrale deler av Barentshavet,** (In Norwegian) (Current measurements in the Barents Sea 1979-1982), In Eide, Lars Ingolf (1983): Environmental Conditions in the Barents Sea and near Jan Mayen, The Norwegian Meteorological Institute, Oslo.

Mackenzie, K. V. (1981): **Nine-Term Equation for Sound Speed in the Oceans.** Journal of the Acoustic Society of America. No 170. pp 807-812.

Massom Robert A. (1991): **Satellite Remote Sensing of Polar Regions,** Bellhaven, 288 pp.

Mellen, R. H. (1984): **Sound Absorption in Sea Water.** In Edgerton, Harold E (1986): Sonar Images. Prentice Hall, Englewood Cliffs, New Jersey (296 pp). pp36-37.

Moritz, Richard E (1988): **Ice Budget of the Greenland Sea.** Ph. D. dissertation, Yale University. 180 pp.

Munk, Walter (1991): **Refraction of Sound Waves at Polar Latitutde.** Journal of Geophysical Research, Vol 96, No C4, April 15 1991. pp 7015-7022.

Nakayama, Hiroshi, Sone, Mitsuo & Takagi, Mikio (1987): **Meterological Satellite Image Analysis using Fractal Dimension and Lower-Order Statistics.** Image Analysis, Proc. of the 5th Scandinavian Conference on Image Analysis, Stockholm June 1987, Svenska Sällskapet för automatiserad Bildanalys (Swedish Society for Automated Image Analysis). pp 261-269.

Nansen, Fridtjof (1897): **Fram over Polhavet, Den norske Polarfærd 1893-1896. Med tillægg av Otto Sverdrup. Band I.** (In Norwegian) ([Drift of] Fram over the Polar Ocean, The Norwegian Polar Voyage 1893-1896. With appendix by Otto Sverdrup. Vol I). Kristiania, H. Aschehoug & co's førlag. 526 pp (+ 553 pp in Vol. II).

NOAA (1988): **Data Extraction and Calibration of TIROS-N/NOAA Radiometers.** NOAA Technical Memorandum NESS 107-Rev. 1, US Department of Commerce, NOAA, National Environmental Satellite Data and Information Service, Washington DC 20233. 97 pp.

Novitskiy, V. P. (1967): **Postoyannyye Techeniya Severnoy Chasti Barentseva Morya** (In russian) (Permanent Currents of the Northern Barents Sea). Trudy Gosudarstvennogo Okeanografich'eskogo Instituta, Vol. 64, Leningrad. pp 1-32.

Nutile, D. A. (1976): **Computer Programs for Obtaining Sound Speeds from Digitized Environmental Data.** NRL Report 7993, Naval Research Laboratory, Washington DC. (referrenced in Hurdle (1986)).

Olsson, Kjell B.-E. (1992): **A Computer Program for Combining Sea Ice Draft and Drift.** Technical report, NP rapport serie nr. 76, (Norwegian Polar Research Institute report series No 76), the Norwegian Polar Research Institute, Oslo. 143 pp.

Parkinson, Claire L. & Washington Warren M. (1979): **A Large-Scale Numerical Model of Sea Ice,** Journal of Geophysical Research, Vol 184, No C1, Jan 20 1979. pp 311-337.

Pohl, Peter., Eriksson, Gerd & Dahlquist Germund (1984): **Lärobok i numeriska metoder.** (In Swedish) (Schoolbook on Numerical Methods). 6:th ed. Liber. 261 pp.

Pratt, William, K. (1991): **Digital Image Processing,** (2:nd ed.), John Wiley & Sons Inc., 689 pp.

Press, William H., Flannery, Brian P., Teukolsky, Saul A. & Vetterling William T. (1990): **Numerical Recipes in C. The Art of Scientific Computing**. Cambridge University Press. 735pp.

Quadfasel, Detlef (1991): **Das Eis wird Dünn am Pol.** (In German) (The Ice is getting Thin at the Pole) Geoskop (Engeln H. (ed.), GEO, No 6 C2498E, May 1991. pp188.

Saull, R. (1985):**Land Applications of the Advanced Very High Resolution Radiometer (AVHRR): A U.K. example.** In: Remote Sensing: data, aquisition, management and applications, Remote Sensing Society and CERMA, London. pp 57-67.

Schistad, Anne, Holbæk-Hanssen, Erik & Råheim Erlend (1990): **Ice Monitoring based on SAR Images, Task 1016: Test of Algorithms for the ERS-1 Application Project**. NCC-Note Bild/02/90, Norwegian Computing Center, Limited availability. 29 pp.

Schowengerdt, Robert A (1983): **Techniques for Image Processing and Classification in Remote Sensing.** Academic Press. 249 pp.

Stewart, Robert, H. (1985): **Methods of Satellite Oceanography,** University of California Press. 360 pp.

Stringer, William J. (1984): **Handbook for Sea Ice Analysis and Forecasting,** Naval Environmental Prediction Research Facility, Monterey, California.

Sverdrup, H. U., Johnson, Martin W. & Fleming Richard H (1970): **The Oceans. Their Physics, Chemistry and general Biology**. Prentice Hall, Engelwood Cliffs, N. J. 1087 pp.

Swithinbank, Charles (1972): **Arctic Pack Ice from Below.** Sea Ice, Proc. of the Sea Ice Conference in Reykjavik., Karlsson, T. (ed.), National Research Council, Iceland, Reykjavik pp 246-254.

Thompson, Thomas (1986): **Ymer-80, Satellites, Arctic Sea Ice and Weather.**SMHI rapport RO2, Mars 1986, SMHIs tryckeri, (the Swedish Meterological and Hydrological Institute), Norrköping. 36 pp.

Thorndike, A. S. (1980): **Tests of the Ice Thickness Distribution Theory,** In Sea Ice Processes and Models, Proc. of the AIDJEX International Commision on Snow and Ice Symposium, Pritchard R. S. (ed.), University of Washington Press. pp 144-150.

Tryde, P. (1986): **East Greenland Current-Ice Studies.** In Ice Technology: Proc. of the 1:st International Conference on Ice Technology, Cambridge, Mass, USA, Murthy, T. K. S., Connor, J. J. & Brebbia, C. A. (eds.), Springer Verlag, Computational Mechanics Publication. pp 129-156.

Ussisoo, Ilmar (1977): **Kartprojektioner**. (In Swedish) (Map projections) Teknisk skrift 1977/6, LMV, (Professional Paper 1977/6, National Land Survey, Sweden), Gävle.

Vibe, Christian (1978): **Arctic Climatic and Ecological Changes, the Spring-tide and the Declination of the Sun,** Proc. of the Nordic Symposium on Climatic Changes and Related Problems, Copenhagen 24-28 April 1978, Frydendahl, Knud (ed.), Climatological Papers No 4, Danish Meteorological Institute, pp 154-161.

Vinje, Torgny (1977): **Sea Ice Studies in the Spitsbergen-Greenland Area, Investigation No 28 540.** Landsat report E77-10206, U. S. Department of Commerce, National Technical Information Service, Springfield, USA. 45 pp

Vinje, Torgny (1981): **Frequency Distribution of Sea Ice in the Greenland and Barents Seas, 1971-80,** the Norwegian Polar Research Institute, Year Book 1980.

Vinje, Torgny (1982): **The Drift Pattern of Sea Ice in the Arctic with particular reference to the Atlantic Approach,** In The Arctic Ocean - the Hydrographic Environment and the Fate of Pollutants, Rey Louis (ed.) (433 pp) pp 83-96.

Vinje, Torgny & Finnekåsa, Øyvind (1986a): **The Ice Transport through the Fram Strait.** Norsk Polarinstitutt Skrifter Nr. 186, Norwegian Polar Research Institute, Oslo, Norway. 39 pp.

Vinje, Torgny & Finnekåsa, Øyvind (1986b): **Norwegian Ice Drift Experiment, Bouy Drift Data 1976-1979,** Data report, NP Rapportserie Nr 28, (Norwegian Polar Research Institute report series No 28), the Norwegian Polar Research Institute, Oslo, Norway. 57 pp.

Vinje, Torgny (1988): **Ice Borders in the Barents Sea. Final report, ESSO Norge a/s on behalf of OKN's Subcommitee for R & D coordination from the Norwegian Polar Research Institute.** The Norwegian Polar Research Institute, Limited availability. 17pp.

Vinje, Torgny E. (1989): **An Upward Looking Sonar Ice Draft Series,** POAC89, Proc. of the 10:th International Conference on Port and Ocean Engineering under Arctic Conditions, Luleå, Sweden, 12-16 JUne 1989, Axelsson, K. B. E. & Fransson, L. Å. (eds.), Research report TULEA 1989:08, Luleå University of Technology. pp178-187.

Vinje, Torgny & Berge Torstein (1989): **Upward Looking Sonar Recordings at 75N - 12W from June 1987 to June 1988.** Data report, NP Rapportserie Nr 51, (Norwegian Polar Research Institute report series No 51), the Norwegian Polar Research Institute, Oslo, Norway. 24 pp.

Vinje, Torgny (1991): **Arctic Ice Thickness Monitoring Project (AITMP). Status and Implementation.** Unpublished.

Vinje, Torgny (1992): **Sea Ice Variability in the Nordic Seas.** Proc. of the International Conference on the Role of the Polar Regions in Global Change, Fairbanks, June 11-15, 1990. In print.

Wadhams Peter (1980): **A Comparison of Sonar and Laser Profiles along Corresponding Tracks in the Arctic Ocean.** In Sea Ice Processes and Models, Proc. of the AIDJEX International Commision on Snow and Ice Symposium, Pritchard R. S. (ed.), University of Washington Press. pp34-45. pp 283-299.

Wadhams, P. & Horne R. J. (1980): **An Analysis of Ice Profiles obtained by Submarine SONAR in the Beaufort Sea.** Journal of Glaciology, Vol 25, No 93. pp 401-424.

Walsh, John E. (1991): **The Arctic as a Bellwether.** Nature, Vol 352, 4 Jul 1991. pp 19-20.

Washington, W. M. & Meehl, G. A. (1989): **Climate Sensitivity due to Increased CO_2. Experiments with a Coupled Atmosphere and Ocean General Circulation Model.** Climatic Dynamics, No 4. pp 1-38. (Referenced in Kverndal 1991).

Westhall, V. H. & Li, H. (1976): **An Analysis of Sea Ice Bottomside data in the Denmark Strait.** AIDJEX Bulletin No 31, March 1976. pp 101-113.

Weydahl, Dan Johan (1991): **Change Detection in SAR Images,** Proc. from the NOBIM Conference, Olavsgaard, 17-18 June 1991, Bildbehandlingslaboratoriet, Institutt for Informatikk, Universitetet i Oslo, Rapport Nr 55, (Report 55, Institute of Informatics, University of Oslo). pp 73-76.

von Wiese, W. (1922): **Die Einwirkung das Polareises in Gronlandischen Meere auf die Nord-Atlantische Zyklonale Tätigkeit.** (In German) (The influence of the Polar Ice on the Cyclonic activity in the North Atlantic ocean). Annaler der Hydrographie 50, 1922. pp 271-280.

Williams, Elizabeth, Swithinbank Charles & Robin G. de Q. (1985): **A Submarine Sonar Study of Arctic Pack Ice.** Journal of Glaciology, Vol 15, No 73, 1975. pp349-362.

Zhang, Hongjiang (1988): **Greenland Sea Ice Motion determined from Satellite Imagery.** Internal report Greenland Sea Project No 7, Electromagnetics Institute, Technical University of Denmark, Lyngby, Denmark. 19 pp.

Zhang, Hongjiang (1989): **Ice Motion Fields in the Greenland Sea derived from AVHRR Imagery, MIZEX 87.** Internal report Greenland Sea Project No 30, Electromagnetics Institute, Technical University of Denmark, Lyngby, Denmark. 36 pp.

Zhang, Hongjiang (1990): **Ice Motion Tracking Algorithms.** Internal report Greenland Sea Project No 33, Electromagnetics Institute, Technical University of Denmark, Lyngby, Denmark. 46 pp.

Lunds Universitets Naturgeografiska institution. Seminarieuppsatser.

Uppsatserna finns tillgängliga på Naturgeografiska institutionens bibliotek, Sölvegatan 13, 223 62 LUND.

1. **Pilesjö, P.** (1985): Metoder för morfometrisk analys av kustområden.
2. **Ahlström, K. & Bergman, A.** (1986): Kartering av erosionskänsliga områden i Ringsjöbygden.
3. **Huseid, A.** (1986): Stormfällning och dess orsakssamband, Söderåsen, Skåne.
4. **Sandstedt, P. & Wällstedt, B.** (1986): Krankesjön under ytan - en naturgeografisk beskrivning.
5. **Johansson, K.** (1986): En lokalklimatisk temperaturstudie på Kungsmarken, öster om Lund.
6. **Estgren, C.** (1987): Isälvsstråket Djurfälla-Flädermo, norr om Motala.
7. **Lindgren, E. & Runnström, M.** (1987): En objektiv metod för att bestämma läplanteringars läverkan.
8. **Hansson, R.** (1987): Studie av frekvensstyrd filtringsmetod för att segmentera satellitbilder, med försök på Landsat TM-data över ett skogsområde i S. Norrland.
9. **Matthiesen, N. & Snäll, M.** (1988): Temperatur och himmelsexponering i gator: Resultat av mätningar i Malmö.
10. **Nilsson, S.** (1988): Veberöd. En beskrivning av samhällets och bygdens utbyggnad och utveckling från början av 1800-talet till vår tid.
11. **Tunving, E.** (1989): Översvämning i Murciaprovinsen, sydöstra Spanien, november 1987.
12. **Glave, S.** (1989): Termiska studier i Malmö med värmebilder och konventionell mätutrustning.
13. **Mjölbo, Y.** (1989): Landskapsförändringen - hur skall den övervakas?
14. **Finnander, M-L.** (1989): Vädrets betydelse för snöavsmältningen i Tarfaladalen.
15. **Ardö, J.** (1989): Samband mellan Landsat TM-data och skogliga beståndsdata på avdelningsnivå.
16. **Mikaelsson, E.** (1989): Byskeälvens dalgång inom Västerbottens län. Geomorfologisk karta, beskrivning och naturvärdesbedömning.
17. **Nilén, C.** (1990): Bilavgaser i gatumiljö och deras beroende av vädret. Litteraturstudier och mätning med DOAS vid motortrafikled i Umeå.
18. **Brasjö, C.** (1990): Geometrisk korrektion av NOAA AVHRR-data.
19. **Erlandsson, R.** (1991): Vägbanetemperaturer i Lund.
20. **Arheimer, B.** (1991): Näringsläckage från åkermark inom Brååns dräneringsområde. Lokalisering och åtgärdsförslag.
21. **Andersson, G.** (1991): En studie av transversalmoräner i västra Småland.

22. **Skillius, Å.** (1991): Water havesting in Bakul, Senegal.

23. **Michelson, D.** (1991): Land Use Mapping of theThat Luang – Salakham Wetland, Lao PDR, Using Landsat TM-Data.

24. **Malmberg, U.** (1991): En jämförelse mellan SPOT- och Landsatdata för vegetationsklassning i Småland.

25. **Mossberg, M. & Pettersson, G.** (1991): A Study of Infiltration Capacity in a Semiarid Environment, Mberengwa District, Zimbabwe.

26. **Theander, T.** (1992): Avfallsupplag i Malmöhus län. Dränering och miljöpåverkan.

27. **Osængius, S.** (1992): Stranderosion vid Löderups strandbad.

28. **Olsson, K.** (1992): Sea Ice Dynamics in Time and Space. Based on upward looking sonar, satellite images and a time series of digital ice charts.